INVESTIGATION INTO THE BASIS OF PROTEIN-LIPID INTERACTIONS FOR ATP-BINDING (ABC) TRANSPORTERS, USING NOVEL POLYMER-BASED SOLUBILISATION.

Olivia Paige Hawkins

Doctor of Philosophy

Aston University

September 2024

Thesis Abstract

ABC transporters such as BmrA are key targets for structural and functional characterisation due to their role in multi-drug efflux and the resulting development of multi-drug resistance. While a wealth of knowledge is available regarding the structure of some of these membrane proteins thanks to developments in techniques such as cryo-EM, functional study remains limited. Using the traditional detergent solubilisation method, concerns are raised regarding the stability and integrity of studied membrane proteins due to the non-native nature of detergent micelles. Due to this, novel alternatives such as amphipols, membrane scaffold proteins and co-polymers were introduced, but each method displays their own advantages and disadvantages.

Solubilisation of membrane proteins using co-polymers has been studied here as they have the unique ability to retain the native phospholipid environment resulting in the production of highly stable nanodiscs with intact protein-lipid interactions. However, co-polymers such as SMA2000 display a sensitivity to divalent cations which is a concern for ABC transporter study due to the requirement of magnesium as a co-factor for ATPase activity. To overcome this issue, a range of co-polymers have been tested in the solubilisation of ABC transporters BmrA and MRP4 in bacterial and insect membrane models.

In this project, SMA variants and Glyco-DIBMA were relatively unsuccessful at solubilising BmrA. However, DIBMA and AASTY co-polymers solubilised BmrA at a good purity and yield with nanodiscs displaying a lower sensitivity to magnesium. Further experimentation found BmrA to be capable of substrate binding in selected co-polymer nanodiscs, but while SMA2000 and DIBMA solubilised BmrA did not display ATPase activity, 6-50 and 11-50 solubilised BmrA did. Nanodiscs characteristics such as size, polydispersity and lipid composition were also investigated. DIBMA appears to produce larger nanodiscs with a wider distribution when compared to SMA2000, 6-50 and 11-50, but all nanodiscs displayed an enrichment of PE when compared to crude membranes.

Co-polymer solubilisation has been shown to be effective in the study of membrane proteins, with characterisation in this project finding AASTY 6-50 and 11-50 to be superior polymers for the functional study of BmrA.

Acknowledgments

This thesis would not have been possible without the help and guidance of numerous individuals who in one way or another contributed to the completion of my PhD.

To my supervisors Dr Alice Rothnie and Professor Alan Goddard, your never-ending willingness to help, share and build will not easily be forgotten, and I shall forever be indebted for your support and patience over the last four years.

I would also like to thank Dr Philip Kitchen and Ophelie Langlois for the wonderful collaborations conducted as part of this thesis. Your expert knowledge was enlightening, and I thank you for your help with mass photometry and mass spectrometry.

I am also most grateful to Midlands Integrative Bioscience Training Partnership (MIBTP) and Biotechnology and Biological Science Research Council (BBSRC) for providing financial support and ultimately gifting me the opportunity to undertake a PhD. Thank you to Professor Roslyn Bill and Gill Pilford who not only helped to develop MIBTP at Aston University but encouraged me every step of the way.

My gratitude is also extended to colleagues of Aston University who have become good friends, particularly those based in MB331, MB347, Health and Life Sciences and AMPL research group. The wealth of knowledge across our team is outstanding, and I wish you all the best for your future endeavours.

A special mention to my soul sister Cristina Croitoru. Words cannot express how much I miss having your face around the lab. Without your encouragement, words of advice and occasional distraction, I truly do not know where I would be. You completed my experience, and I cannot thank you enough.

To my family – I hope you are proud. Without your support and unwavering encouragement, I doubt I would ever have pushed myself to apply for this opportunity, never mind make it to the other end. To Nan and Grandad Steve, you did not get to see this stage of my life come to completion, but I know you are up there cheering me on every step of the way.

Finally, to my life partner Nabeel. You have been absolutely instrumental to my success and your constant enthusiasm for life and uplifting words meant I always found a way though hardships.

They say it takes a village to raise a child…. I'd say it takes a village to raise a PhD student. Thank you all.

List of Contents

Abbreviations

Aβ -	Amyloid beta
$A_{2A}R$ –	Adenosine A2A Receptor
AASTY –	Acrylic Acid Styrene
ABC –	ATP Binding Cassette
AD –	Alzheimer's Disease
AMP –	Adenosine Monophosphate
Apo A-I –	Apolipoprotein A-I
ATP –	Adenosine Triphosphate
BmrA –	*Bacillus subtilis* Multidrug Resistance ABC transporter
BSA –	Bovine Serum Albumin
BV –	Bed Volume
cAMP –	Cyclic Adenosine Monophosphate
CF –	Cystic Fibrosis
CFTR –	Cystic Fibrosis Transmembrane Conductance Regulator
CGRP –	Calcitonin Gene Related Peptide
CH –	Carbon-Hydrogen
CL –	Cardiolipin
Cl –	Cardiolipin
CMC –	Critical Micelle Concentration
DAGK –	Diacylglycerol Kinase
DDM –	N-Dodecyl-β-D-Maltoside
DDM –	n-Dodecyl-β-D-Maltoside
DIBMA –	Diisobutylene Maleic Acid
DIBMALPs –	DIBMA Lipid Particles
DMPC –	Dimyristoylphosphatidylcholine
DMSO –	Dimethylsulfoxide
DTT –	Dithiothreitol
DTT –	Dithiothreitol
ECF –	Energy Couple Factor
ER –	Endoplasmic Reticulum
FBS –	Foetal Bovine Serum
G-protein –	GTP-Binding Protein

GLUTS – Glucose Transporters

Glyco-DIBMA – DIBMA Glucamine

GPCR – G-Protein Couple Receptor

HDL – High Density Lipoprotein

hTRPM4 - human Transient Receptor Potential Melastatin type 4

IPTG – Isopropyl β-D-1-Thiogalactopyranoside

LB – Luria Broth

LPS – Lipopolysaccharides

LSB – Laemmlli Sample Buffer

MATE – Multidrug and Toxin Extrusion

MDR – Multi-Drug Resistance

MRP4 – Multidrug Resistance Protein 4

MRSAE – Multidrug Resistant StaphylococcI

MSPs – Membrane Scaffold Proteins

MTBE – Methyl-Tert-Butyl Ether

NATA – N-Acetyltryptophanamide

NBD – Nucleotide Binding Domain

OATPs – Organic Anion Transporting Polypeptides

OEP – Outer Membrane Efflux Protein

OmpLA - Outer Membrane Phospholipase A

P-gp – P-Glycoprotein

PBS – Phosphate Buffered Saline

PC – Phosphotidylcholine

PDB – Protein Data Bank

PE – Phosphatidylethanolamine

PG – Phosphatidylglycerol

PI – Protease Inhibitor

PMSF – Phenylmethylsulfonyl Fluoride

PS – Phosphotidylserine

PSI – Pounds per Square Inch

Pt – Pellet

PVDF – Polyvinylidene Fluoride

RAAS – Renin-Angiotensin-Aldosterone System

RAFT – Reversible Addition Fragmentation Chain Transfer

SBPs –	Substrate Binding Proteins
SDS –	Sodium Dodecyl Sulfate
SDS-PAGE –	Sodium Dodecyl Sulfate Polyacrylamide Gel Electrophoresis
SEC –	Size Exclusion Chromatography
SLC –	Solute Carrier
SMA –	Styrene Maleic Acid
SMA-EA –	SMA Ethanolamine
SMA-ED –	SMA Ethylenediamine
SMA-QA –	SMA Quaternary Ammonium
SMA-SH –	SMA Solvent Exposed Sulfhydryls
SMAd-A –	SMA Dehydrated Ethylenediamine
SMALPs –	SMA Lipid Particles
SMAnh –	Styrene Maleic Acid Anhydride
Sol –	Supernatant
TEMP –	Type III Endosome Membrane Protein
TLC –	Thin Layer Chromatography
TMD –	Transmembrane Domain
TolC –	Trimeric Outer Membrane Channel
UV –	Ultraviolet
VRE –	Vancomycin Resistant Enterococci

List of Figures

List of Tables

1. Introduction

1.1 The Significance of Membrane Proteins

Membrane proteins are a group of diverse and complex molecules associated with or attached to the plasma membrane at the cell surface or within cytosolic compartments such as mitochondria. They are found across all species of life, with an estimated 20-30% of all genomes encoding for membrane proteins (Krogh, *et al.,* 2001). The number of membrane proteins can vary across organisms based on cell type, but more complex cells tend to exhibit higher numbers (Yang, *et al.,* 2015). One study identified over 600 membrane proteins by topology analysis of *E. coli* (Daley, *et al.,* 2005), while another group found 6,718 different membrane proteins in the human proteome (Almén, *et al.,* 2009). In plants, *Aradopsis* is generally considered complex while having a relatively small genome of ~ 135 megabase pairs, but studies conducted using green tissue found 232 membrane proteins (Alexandersson, *et al.,* 2004).

Alongside an immense number, membrane proteins also display considerable variation in size, structure and function. Some are smaller than 100 amino acids such as SARS-CoV-2 E protein, while others are over 700 amino acids in length such as the Cadherin group. Located at the plasma membrane, endoplasmic reticulum (ER) and Golgi apparatus in viral cells, E protein plays multiple roles in the viral life cycle. It has been found to be involved in protein trafficking and is known to form pores to augment virulence (Zhou, *et al.,* 2023). Members of the Cadherin group are split into four types based on distribution – epithelial (E), neuronal (N), placental (P) and vascular (V) but all primarily function in cell-cell adhesion (Maître, *et al.,* 2012) with roles in morphogenesis through mediation of cell polarity (Bosveld, *et al.,* 2012), proliferation (Nelson, *et al.,* 2003) and fate specification (Sarpal, *et al.,* 2012).

The structure of membrane proteins can also vary widely and can be grouped based on their location and association with the plasma membrane as shown in Figure 1.1. Integral membrane proteins are directly associated with the plasma membrane and can either partially span the membrane (monotopic) or span the entire width of the membrane (transmembrane). Transmembrane proteins can also be grouped based on how many transmembrane loops are present. They may contain a single transmembrane loop (bitopic)

such as receptor-activated tyrosine kinase (Cournia, *et al.,* 2020) or multiple transmembrane loops (polytopic) such as the transporter lactose permease (Nagamori, *et al.,* 2004).

Transmembrane proteins can display two structural motifs – alpha helices (α-helices) and/or beta barrels (β-barrels) also shown in Figure 1.1. These directly correlate to location with the highly hydrophobic α-helical bundles often found in receptors and ion channels (Galdiero, *et al.,* 2007), while the rigid structure of β-barrels are associated with the outer membrane of Gram-negative bacteria, mitochondria and chloroplasts (Galdiero, *et al.,* 2007).

A smaller subset of membrane proteins (peripheral) are only temporarily associated with the membrane, binding to integral membrane proteins or directly to lipids as shown in Figure 1.1. The majority of monotopic membrane proteins that are structurally characterised display extensive soluble domains (Allen, *et al.,* 2019), are biologically active as dimers (Mattevi, *et al.,* 2006) and share homology with soluble proteins of known function (Nam, *et al.,* 2013).

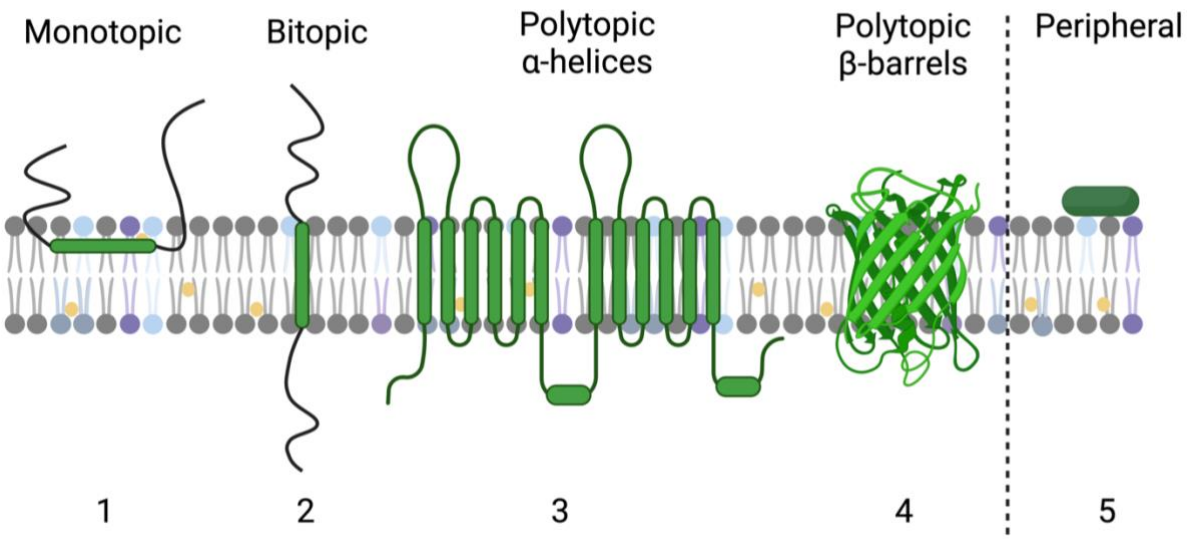

Figure 1.1 : Schematic representation of membrane associated protein structures. 1 – Monotopic proteins span a single layer of the plasma membrane. 2 – Bitopic proteins span the entire width of the plasma membrane only once. 3 - α-helical polytopic proteins span entire width of the plasma membrane multiple times in α-helical structures. 4 - β-barrel polytopic proteins span entire width of the plasma membrane multiple times in β-sheet structures. 5 – Peripheral proteins are only temporarily associated with the plasma membranes. Created with BioRender.

While transmembrane proteins have become increasingly studied with many now structurally solved (Shimizu, *et al.,* 2018), they remain to be underrepresented in the Protein Data Bank (PDB) when compared to soluble proteins due to the difficulty in extraction. Maintaining protein structure and function is problematic and so computational modelling is commonly used. However, while bitopic proteins exhibit high sequence homology and simple architecture, polytopic proteins exhibit significant variation in shape, size and function which highlights the requirement for *in vitro* study.

Polytopic proteins are typically large and more structurally complex than bitopic proteins. They commonly exhibit highly ordered re-entrant helices, are hydrophobic in nature and contain the aromatic amino acids tryptophan and tyrosine (Moosmann, *et al.,* 2000). Many have also been structurally solved in multiple conformations (Zhou, Lewis and Lu, 2023). While some polytopic proteins have multiple transmembrane domains in single polypeptide such as the Type III Endosome Membrane Protein (TEMP) (Aturaliya, Kerr and Teasdale, 2012), others are expressed in separate polypeptides which dimerise to produce oligomers containing multiple transmembrane domains such as the trimeric outer membrane channel (TolC) in *E. coli* (Koronakis, *et al.,* 2004).

The function of polytopic transmembrane proteins can also vary widely, with roles in signal transmission, energy conversion and transport of nutrients and drugs to name a few. One major superfamily of transmembrane proteins involved in signal transduction are G Protein Coupled Receptors (GPCRs). These proteins act as receptors which bind extracellular signals and undergo conformational changes, initiating a signal transduction cascade in the associated GTP-binding protein (G protein). β1-adrenergic receptor (ADRB1) is a GPCR found in cardiac myocytes that is activated by the binding of adrenaline and noradrenaline. This leads to an increase in cAMP production, contraction strength, cardiac output and blood pressure (Sun, *et al.,* 2021). It also plays a role in renin-angiotensin-aldosterone system (RAAS), which regulates blood pressure and sodium transport in the kidneys (Kelley, *et al.,* 2019).

Energy conversion is critical for the maintenance of life and is achieved with the presence of the mitochondrial respiratory chain. This is a series of polytopic protein complexes found in the inner membrane of mitochondria, which functions to maintain electrochemical gradients for the consistent production of adenosine triphosphate (ATP) – the primary energy source in cells (Guan, *et al.,* 2022). The proton gradient is maintained by three large complexes, complex

I (NADH/ubiquinone oxidoreductase), III (cytochrome c reductase) and IV (cytochrome c oxidase). Complex I transfers electrons from the soluble NADH to membrane bound quinol, where complex III then transfers from quinol to cytochrome *c* contributing a single proton. Complex IV then transfers from cytochrome c to oxygen resulting in the production of 4 protons per molecule of oxygen consumed (Kühlbrandt, 2015).

Perhaps the most common function of polytopic membrane proteins is transport. The majority of transporters display high substrate promiscuity with the ability to transport a diverse range of substrates that vary in size, shape and chemistry, including nutrients such as sugars, amino acids and metal ions.

Glucose transporters (GLUTs) are passive transporters of glucose that are found in all phyla due to the universal requirement of glucose as an energy source (Alexander, *et al.,* 2023). All members of the GLUT family are ~ 500 amino acids in length, with 12 α-helical transmembrane loops and a single N-linked oligosaccharide (Joost, *et al.,* 2002), with 14 GLUTs expressed in humans. GLUT1 is found in the brain blood capillaries where it allows for the distribution of glucose across the blood-brain barrier and into the cerebral tissue (Pragallapati and Manyam, 2019). GLUT11 is also found in skeletal and cardiac muscle and is overexpressed in slow-twitch but not fast-twitch fibres (Gaster, *et al.,* 2004). It functions to maintain nutrient homeostasis in the energy demanding muscle tissue by providing glucose. It shares 42% homology to GLUT5 (Navale and Paranjape, 2016) – which is a fructose transporter – but appears to be inhibited by fructose (Doege, *et al.,* 2001).

GLUTs are considered to be uniporters – functioning passively with substrate transported across the membrane using a concentration gradient. But other types of transporters have also been identified that require ATP hydrolysis for function - primary and secondary transporters. While both are involved in the transport of substates across the membrane against a concentration gradient, secondary transporters require the co-transport of a second substrate for function – otherwise known as antiporters or symporters.

The Na^+/K^+ pump is an electrogenic transmembrane ATPase protein that actively pumps three Na^+ out of the cell for every two K^+ that enters the cell, per ATP consumed (Pivovarox, Calahorro and Walker, 2018) functioning as an antiporter. This results in a cellular increase in net negative charge, hyperpolarising the cell membrane against the increasing net positive

charge extracellularly – contributing to muscle contraction and neuronal communication (Gagnon and Delphire, 2021). This protein is critical for the maintenance of the proton gradient and energy production and the requirement for rapid transport is met by the presence of a channel. Unlike transporter proteins which require conformational change to transport substrate, channel proteins have the ability to rapidly transport substrates across the membrane without the need for conformational change.

While transporters are slower when compared to channels, they are also a major cellular defence against drugs, contributing to drug absorption, distribution and excretion (Roberts, 2021). Three major subfamilies of transmembrane proteins are known to transport multiple drugs including the Solute Carrier (SLC) family, the SLCO family of organic anion transporting polypeptides (OATPs) and the ATP-Binding Cassette (ABC) transporters.

The SLC superfamily comprises of 55 gene families, with a minimum of 362 functional protein-coding genes (He, Vasiliou and Neber, 2009). In 2005, a human multidrug and toxin extrusion (MATE) protein was identified as a homolog to the bacterial NorM (Otsuka, *et al.,* 2005). It functions as a H+/organic cation antiporter and is highly expressed in the kidney, adrenal gland, liver and skeletal muscle (Masuda, *et al.,* 2006) with localisations in proximal tubule membranes, suggesting a role in renal secretion of cationic drugs. MATE 1 is able to transport drugs such as metformin, procainamide and cimetidine, all of which are pharmacologically relevant in the treatment of type II diabetes (Flory and Lipska, 2019), arrhythmia (Toniolo, *et al.,* 2021) and gastric ulcers (Brogden, et al.,1978).

There are over 300 members of the OATP superfamily with 11 currently known to be expressed in humans (Hagenbuch and Stieger, 2013). All are 643 – 722 amino acid polypeptides with 12 transmembrane segments and both C and N – terminus in the cytosol. They primarily function in the intestinal-hepatic circulation of bile (Li, *et al.,* 2019) playing a role in absorption metabolism and excretion of bile. OATPs substrates are mainly large hydrophobic organic anions such as bile acids, thyroid hormones, prostaglandins and testosterone (Li, *et al.,* 2019). However, OATPs have also been found to transport drugs such as pentamidine, HIV protease inhibitors (PIs) and fexofenadine – as in the case of OATP1A2 which is highly expressed in the brain, liver and kidneys (Schulte, *et al.,* 2019). Pentamidine is utilised as an anti-protozoa agent in the treatment leishmaniasis (Piccica, *et al.,* 2021), PIs are

the primary anti-viral cocktail for the treatment of HIV (Weber, Wang and Harrison, 2021) and fexofenadine is an antihistamine used to treat the symptoms of allergy (Howarth, *et al.,* 1999).

ABC transporters are the largest class of drug transporters that function as either exporters or importers in an ATP-dependent manner. They exhibit a high level of substrate promiscuity, able to transport substrates that vary widely in size, shape and chemistry (Steinfels, *et al.,* 2004). P-glycoprotein (P-gp) is a human 170kDa polypeptide chain ABC transporter which folds into two pseudo-symmetric halves to form a functional protein (Ward, *et al.,* 2013). It acts as a drug efflux pump for xenobiotic compounds such as colchicine, digoxin, tacrolimus and doxorubicin. All of which are pharmacologically relevant in the treatment of gout (McKenzie, *et al.,* 2021), heart failure (Parikh, *et al.,* 2022), prevention of organ rejection (Pernin, *et al.,* 2023) and chemotherapy in response to sarcomas (Pautier, *et al.,* 2022). The overexpression or mutation of P-gp confers multi-drug resistance (MDR) by decreasing the bioavailability of drugs intracellularly, reducing efficiency of the treatments previously described.

One of the first identified ABC transporters involved in drug efflux in Gram-negative bacteria is MacB (Kobayashi, Nishino and Yamaguchi, 2001). MacB has four transmembrane helices, an N-terminal transmembrane domain (TMD) and a large periplasmic domain (Okada, *et al.,* 2017). Similarly to other ABC transporters, MacB requires dimerization for function, but these dimers are fairly rigid and contains no transmembrane cavities (Crow, *et al.,* 2017). In order to function as a transporter, MacB dimers must form the MacAB-TolC complex, with the outer membrane efflux protein (OEP) TolC acting as the efflux pathway to expel xenobiotic compounds such as the macrolide class of antibiotics (Lu and Zgurskaya, 2013). Increased expression of MacAB has also been found to result in resistance to the tetracycline antibiotic eravacycline (Zheng, *et al.,* 2018).

1.2 The Significance of ABC Transporters

ABC transporters have also been linked to health disorders – with mutations in vital ABC genes leading to the development of conditions such as Alzheimer's disease (AD) and cystic fibrosis (CF). AD is a neurodegenerative disorder characterised by the increasing presence of amyloid-beta (Aβ) peptides in the cerebral tissue and the progressive formation of plaques in grey matter. Mutations of ABC transporters ABCB1 AND ABCA1 have been found to cause impaired

clearance of Aβ peptides, resulting in the development of amyloid plaques and disease progression (ElAli and Rivest, 2013).

CF is a respiratory disorder caused by the mutation of the cystic fibrosis transmembrane conductance regulator (CFTR) gene. 1,480 amino acids in length. While CFTR is actually an ion channel rather than a transporter, it functions to maintain the balance of water and salt (Liou, 2019). Mutation and dysfunction of CFTR causes an imbalance in salt homeostasis, leading to an overproduction of thick mucus and persistent respiratory infections (Lyczak, Cannon and Pier, 2002). While many ABC transporters can interact with drugs prescribed for different conditions, CFTR is the only ABC transporter with clinically approved targeted drug treatment known as trikafta (Zaher, *et al.,* 2021).

Due to the role of ABC transporters in drug transport, they have become increasingly utilised in drug trials for pharmacokinetic safety and efficacy testing (Giacomini, *et al.,* 2010). While many ABC transporters are structurally well characterised – functional study remains difficult due to their tendency to aggregate once removed from the cell membrane. As one of the largest subfamilies of membrane proteins that is commonly linked to human health and MDR – the structural and functional study of ABC transporters is critical to further our understanding.

The human genome contains 48 ABC genes encoding for seven different subfamilies – each of which contain a different number, expression level and combination of ABC genes (Vasiliou, Vasiliou and Nerbert, 2009). However, they all exhibit similar key structural characteristics with two nucleotide binding domains (NBDs), where ATP is bound and hydrolysed, and two transmembrane domains (TMDs), which facilitate the substrate translocation. They also all share the structural motifs Walker-A, Walker-B and LSGGQ, which are critical for facilitating nucleotide binding (Aktar and Turner, 2022). While NBDs are generally well conserved across all ABC transporters, the TMDs exhibit a level of sequence variety with differences in TMD folding (Beek, Guskov and Slotboom, 2014). The four domains of ABC transporters are generally expressed as a single polypeptide in eukaryotes, or as two 'half-transporters' comprising one NBD and one TMD that dimerise, while it is more common in prokaryotes for the domains to be expressed as separate polypeptides (Davidson, *et al.,* 2008). The seven subfamilies of ABC transporters can be grouped based on their TMD fold and function as

shown in Figure 1.2. Type I, II and III ABC transporters are importers, Types IV and V are exporters and types VI and VII are considered mechanotransducers.

Type I and II ABC transporters depend on soluble substrate-binding proteins (SBPs) to capture substrate and deliver to the transmembrane domain (Quiocho and Ledvina, 1996) – as is the case for ModABC and BtuCDF (Figure 1.2). First characterised in *Archaeoglobus fulgidis* (Hollenstein, Frei and Locher, 2007), ModABC imports molybdate, an important co-factor in microbial metabolism (Kisker, Schindelin and Rees, 1997) and enzyme synthesis (Zang, Rump and Gladyshev, 2011). The transmembrane region ModB contains 6 transmembrane helices per TMD – with a total of 12 helices contributing to an inward-facing conformation. Structural comparison against the maltose transporter ($MalFGK_2$) - which is considered a model system for this class - suggests an alternating access and release mechanism of function for type I ABC transporters (Chen, 2013).

Type II importers are generally larger, containing 20 TMDs and exhibit a higher binding affinity when compared to type I - accepted to reflect the abundance of substrate (Locher, 2016). BtuCDF imports vitamin B_{12}, an important co-factor in amino acid synthesis (Sultana, *et al.,* 2023) and gene regulation (Degnan, *et al.,* 2014). This complex contains 10 transmembrane helices per TMD totalling 20 helices and displays a very high binding affinity for vitamin B_{12} (Lewinson, *et al.,* 2010). But its high basal activity (Borths, *et al.,* 2005) and low substrate-binding stimulation (Lewinson, *et al.,* 2010) suggests an alternative mechanism of action when compared to the reported alternating access and release of type I (Rice, Park and Pinkett, 2014).

The type III importer group are energy-coupling factor (ECF) proteins first discovered in the 1970s (Henderson, Zevely and Huennekens, 1979). The architecture of folate ECF transporter is strikingly different to other members of the ABC transporter family - as shown in Figure 1.2. In place of SBPs, ECFs use secondary integral membrane proteins (S components) to bind its substrates. For folate ECF in Lactococcus, the S component binds riboflavin with nanomolar affinity (Duurkens, *et al.,* 2007). It then undergoes substantial conformation change (Xu, *et al.,* 2013) in a lipid-dependent toppling-based mechanism (Faustino, *et al.,* 2020) to allow for transport of substrates, crucial for nucleic acid and amino acid synthesis (Kok, *et al.,* 2020).

Type VI and VII are considered mechanotransducers (Figure 1.2), referring to their mechanism of action whereby there is significant conformational changes transmitted from one side of the membrane to the other (Crow, *et al.,* 2017). This facilitates the transport of substrates without the presence of a central cavity. While they have similar structures to type V exporters, they exhibit distinct differentiating features including a lack of amphipathic 'elbow' helices and re-entrant TM5/6 helices (Thomas, *et al.,* 2020).

Type VII MacB - as previously explored – is a multi-drug efflux transporter with 4 helices per TMD, totalling 8 per homomeric complex. Type VI LptBFG however, has 6 transmembrane helices – forming a total of 12 per heterodimeric complex (Dong, *et al.,* 2017). LptBFG is a lipopolysaccharide (LPS) transporter that extracts LPS from the inner membrane of Gram-negative bacteria and deposits to the periplasmic domain of the inner membrane protein LptC. This helps to maintain the asymmetric outer membrane of bacteria, critical for drug resistance and pathogenesis (Bryant, *et al.,* 2010).

The final group and perhaps the most clinically significant are the type IV and V exporters (Figure 1.2). While bacteria can employ both importer and exporter ABC transporters, eukaryotes mostly express exporters (El-Awady, *et al.,* 2016) and type IV and V encompass all human ABC transporters. However, there are exceptions in type V with examples such as retina-specific importer ABCA4 that functions as an importer (Quazi, Lenevich and Molday, 2012).

Both type V and IV exporters display classical ABC architecture, with highly conserved NBDs and six helices per TMD totalling to twelve. However, type IV proteins also feature cytosolic extended TMDs which dimerise via domain swapping (Mascarenhas and Gosavi, 2017). This mediates larger conformational changes promoting a widely open central cavity, allowing for increased substrate access. However, Type V ABC exporters possess much shorter TMDs and therefore have restricted substrate access (Hou, *et al.,* 2022).

Type V exporter ABCG5 (Figure 1.2) plays a role in cholesterol homeostasis through mediation of plant sterol excretion from the liver and intestines when in heterogenous complex with ABCG8 (Zhang, *et al.,* 2021). Although sterol binding sites in ABCG5/8 are similar to another type V member (ABCG1), which requires cholesterol acceptors for transport, ABCG5/8 is able to export cholesterol independently (Hou, *et al.,* 2022).

The first type IV transporter characterised was Sav1866 (Figure 1.2) from Staphylococcus *aureus* (Dawson and Locher, 2006). Like many type IV transporters, Sav1866 has a very broad substrate spectrum including Hoechst 33342, verapamil and tetraphenylphosphonium (Velamakanni, Gutmann and van Ween, 2008) and is believed to function in an alternating access mechanism (Immadisetty, Hettige and Moradi, 2019).

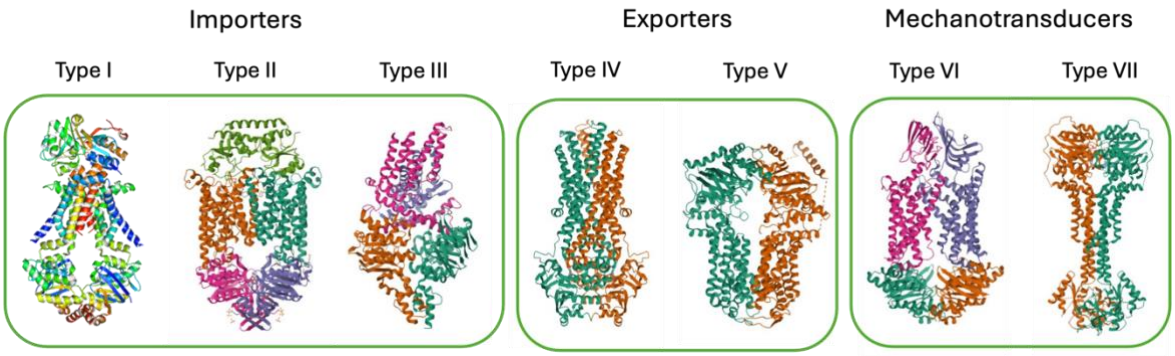

Figure 1.2 : Schematic representation of the seven ABC transporters superfamilies. ABC transporter types I – VII structures grouped based on mode of function. From left to right; Type I – ModABC (molybdate transporter), Type II – BtuCDF (vitamin B12 transporter), Type III – FolT (Folate energy-coupled micronutrient transporter), Type IV – Sav1866 (multi-drug exporter), Type V – ABCG5 (sterol exporter), type VI – LptBFG (LPS transporter), Type VII – MacB (multi-drug exporter).

Type IV ABC transporters are those most commonly linked with the development of MDR and are the group of interest for this research. However, their study is hampered by hurdles experienced during expression, extraction, and purification due to their large size, hydrophobicity and lack of stability once removed from the cell membrane (Carpenter, 2008). In order to study them, we must first solubilise them and many methods exist with their own advantages and disadvantages.

1.3 BmrA

Bacillus subtilis Multidrug Resistance ABC transporter (BmrA) is a 64.5kDa type IV ABC transporter (Figure 1.3) studied as a model membrane protein in this research due to its link with Cervimycin C resistance in *Bacillus subtilis* (Krügel, *et al.,* 2010). Produced by *Streptomyces tendae*, Cervimycin C is an antibiotic with bactericidal activity against Gram-positive bacteria (Hoffmann, *et al.,* 2024) and is one of the few antibiotics currently available for the treatment of clinically significant infections such as multidrug-resistant staphylococci (MRSA) and vancomycin-resistant enterococci (VRE) (Herold, *et al.,* 2004). Understanding the function of BmrA may help to develop proactive defences against the development of MDR.

BmrA – also known as YvcC (Steinfels, *et al.,* 2004) - shares close sequence homology to other type IV ABC transporters including *Lactococcus lactis* multi-drug resistance protein (LmrA) and mammalian P-gp (van Veen, *et al.,* 1996, Ward, *et al.,* 2013) at 41.5% and 28% identity coverage respectively. While bacterial BmrA and LmrA are considered half-size ABC transporters – meaning dimerisation is required to for a functional unit – P-gp is expressed as a single polypeptide that folds into two pseudo-symmetrical halves (Ward, *et al.,* 2013). All three have been linked to MDR in prokaryotic and eukaryotic models (Krügel, *et al.,* 2010, van Veen, *et al.,* 1998 and de Graaf, *et al.,* 1996), highlighting the clinical significance and the necessity for structural and functional characterisation of this group.

Since the first identification of BmrA in genomic analysis of *Bacillus subtilis* (Kunst, *et al.,* 1997), a wealth of research has been conducted to structurally and functionally characterise it. BmrA is a homomeric ABC transporter, with each monomer consisting of one TMD covalently linked at the C-terminal end of one NBD (Chami, *et al.,* 2002). Each functional unit of BmrA also contains twelve transmembrane helices – all typical characteristics of type IV ABC transporters (Thomas, *et al.,* 2020).

BmrA displays two carbon-hydrogen (CH) moieties, important for TMD and NBD interactions which mediate the transmission of conformational changes from ATP binding/hydrolysis in the NBDs to the TMDs (Thomas and Tampé, 2020). BmrA also contains three tryptophan residues at positions W104, W164 and W413 (Oepen, Mater and Schneider, 2023). W104 is localised in the TMD, W164 is found in the extracellular short loop between TM3 and TM4 and

W413 is found at the C-terminus of the cytosolic NBD. The intrinsic fluorescent properties of tryptophan can be utilised in functional study, as environmental polarity changes shift fluorescent emissions, therefore indicating substrate binding based on conformational changes (Eftink, 1994). This method has been applied in previous studies with BmrA exhibiting conformational changes upon binding known substrates doxorubicin and Hoescht 33342 (Morrison, *et al.,* 2016) and is further investigated in this study.

Advances in techniques such as cryo-EM has uncovered a wealth of BmrA structures in multiple conformations. This includes inward and outward facing conformations in complex with a range of different ligands and/or substrates (Chaptal, *et al.,* 2022).This information has helped illuminate mechanistic understanding of BmrA transport, which in turn provides critical information by which pharmacological agents may be able to mediate ABC transporter transport in clinically relevant cases.

The generally accepted mechanism of action for multi-drug exporters is the alternating access theory in which the catalytic cycle of ATP drives the switch between inward and outward facing conformations. Upon ATP binding, a tight dimer is formed between the Walker A motif from one NBD and the LSGGQ motif of the other NBD, resulting in an outward facing state that is responsible for substrate release (Kim, *et al.,* 2018). ATP hydrolysis then causes NBD dimer disassociation, resetting transporter conformation back to an inward facing state (Lewinson, *et al.,* 2020).

While BmrA is able to transport a diverse range of substrates that differ in size, shape and chemistry, there is limited information about how this transport is mediated. Theoretically, larger substrates require a larger TMD pore to be able to pass through the membrane, and this is probed in recent studies. In one study, BmrA mutant A582C was created by a cysteine substitution at the NBD c-terminus, producing a disulfide bond which restrains NBD separation during the catalytic cycle. While this mutation did not affect the transport of doxorubicin and Hoechst 33342, it reduced the transport of 7-amino-actinomycin – a large DNA binding dye - suggesting the transport of larger molecules requires a higher degree of freedom in the NBDs during the transport cycle (Di Cesare, *et al.,* 2024). This highlighted a new inward facing state of BmrA, in which the NBDs conduct a ‘tweezer-like’ motion to allow for a wider opening to larger drugs (Di Cesare, *et al.,* 2024).

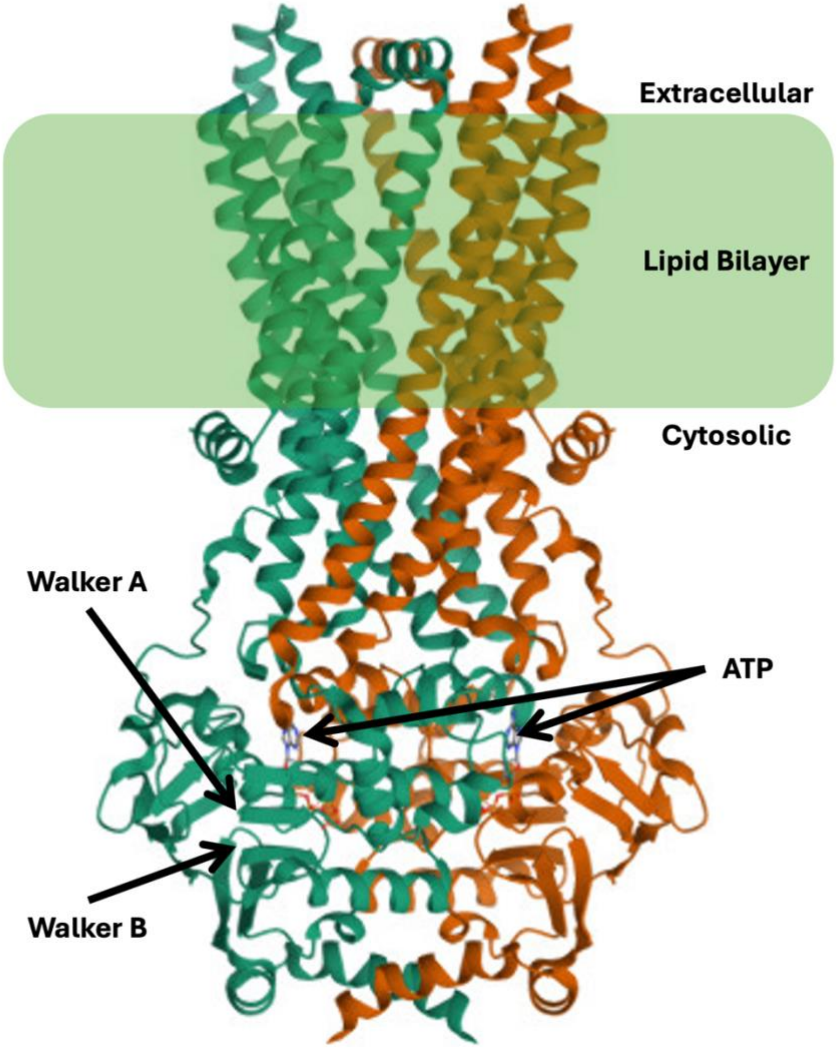

Figure 1.3 : Cryo-EM structure of the ABC transporter BmrA in complex with ATP-Mg. Homomeric BmrA with nucleotide binding domains at the cytosolic surface and membrane spanning regions across the lipid bilayer with extracellular extensions. Bound ATP and Walker A and B motifs highlighted. PDB ID : 7OW8, https://doi.org/10.2210/pdb7OW8/pdb (Chaptal, *et al.,* 2022).

1.4 MRP4

The mammalian multidrug resistance protein 4 (MRP4) is another type IV ABC transporter used as a comparative membrane protein model in this project (Figure 1.4). It has been successfully solubilised using co-polymers in multiple expression models including insect, yeast and mammalian cell lines (Hardy, *et al.,* 2019) and is utilised in this study to probe if co-polymers exhibit lipid-class dependencies and how expression models with differential lipid composition may play a role co-polymer solubilisation efficiency.

MRP4 is a 170kDa monomeric complex with classical ABC transporter architecture of two TMDs and two NBDs with each TMD comprised of six transmembrane helices – similar to BmrA. These helices undergo large conformational changes during the transport cycle in an alternating access and release mechanism as previously explored (Huang, *et al.,* 2023).

It is endogenously expressed in high levels in the kidney and prostate (Lee, Klein-Szanto and Kruh, 2000) and low levels in other tissue sites such as the liver, testes and adrenal gland (Borst, de Wolf and van de Wetering, 2007) and functions in compliance with other type IV ABC transporters as a multi-drug exporter of a wide range of substrates. This includes hormones such as prostaglandins (Reid, *et al.,* 2003) which play key roles in the female oestrous cycle (Lacroix-Pépin, *et al.,* 2011). MRP4 also exports cyclic nucleotides adenosine monophosphate (AMP) and cyclic adenosine monophosphate (cAMP) (Ritter, *et al.,* 2005). Both are important metabolic messengers which drive biochemical processes such as lipid and sugar mobilisation and breakdown (Patra, *et al.,* 2023).

The MRP4 gene expression is highly variable with mutations linked to differential transport of xenobiotics including methotrexate (Lee, Klein-Szanto and Kruh, 2000) and azidothymidine (Abla, *et al.,* 2008). The overexpression of MRP4 has also been linked to MDR as witnessed in patients with adenocarcinoma (Gancedo, *et al.,* 2024).

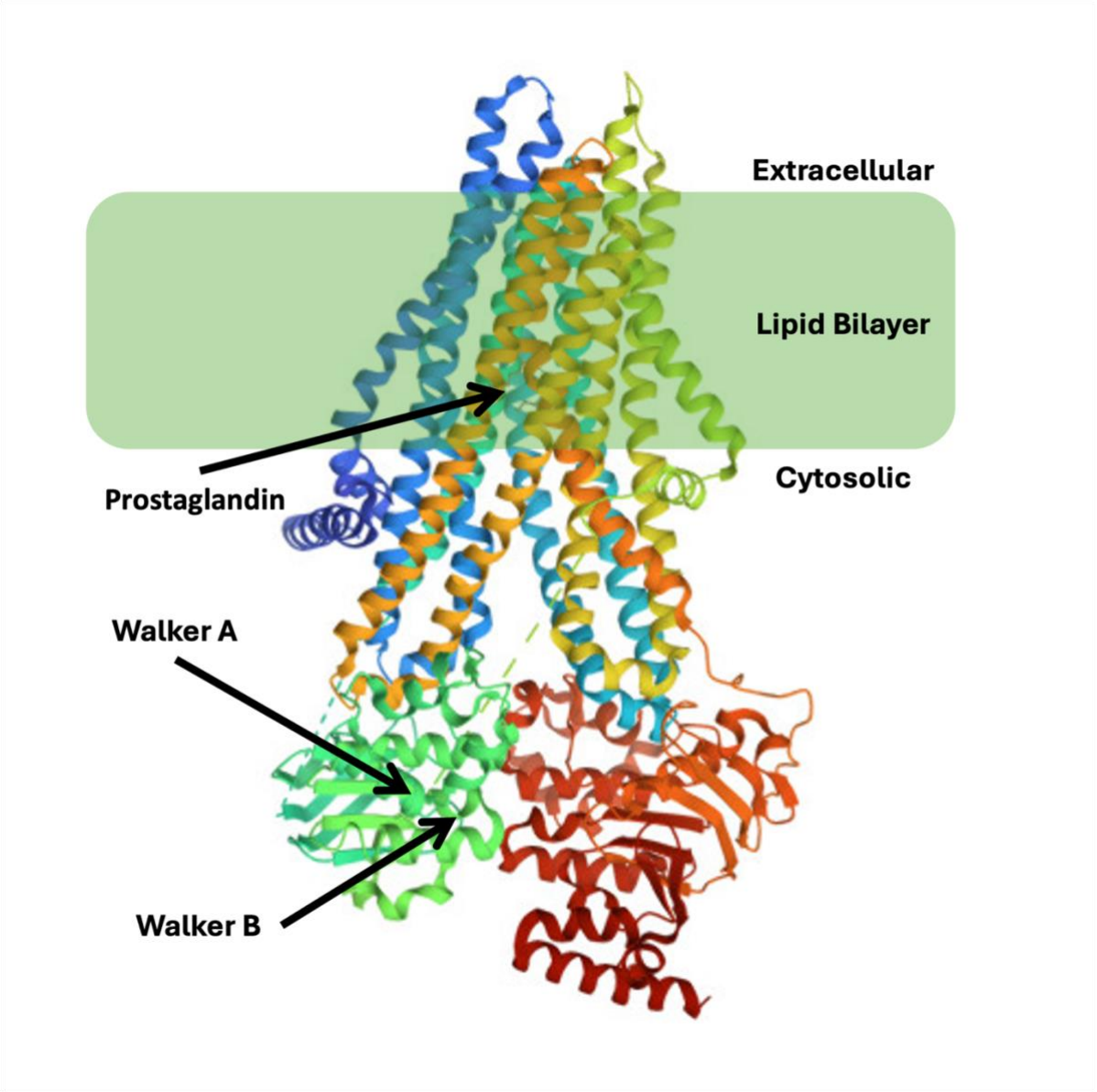

Figure 1.4 : Cryo-EM structure of the ABC transporter MRP4 in complex with prostaglandin E2 in MSP lipid nanodisc. Monomeric MRP4 with nucleotide binding domains at the cytosolic surface and membrane spanning regions across the lipid bilayer with extracellular extensions. Prostaglandin E2 and Walker A and B motifs highlighted. PDB ID : 8SXB, https://www.rcsb.org/structure/8SXB (Pourmal, *et al.,* 2024).

1.5 Methods of Solubilisation

1.5.1 Detergents

The first and most commonly utilised method of membrane protein solubilisation involves the use of detergents to produce micelles in a four-step process (Figure 1.5). First, detergent is added to a membrane sample with detergent monomers able to integrate into the outer layer of the membrane, where it interferes with polar interactions causing curvature and mechanical strain. This results in the disruption of membrane structure, leading to the formation of pores which in turn allows for further integration of detergent monomers. Once the critical micelle concentration (CMC) is achieved, detergent micelles are formed containing a mixture of detergent and membrane proteins.

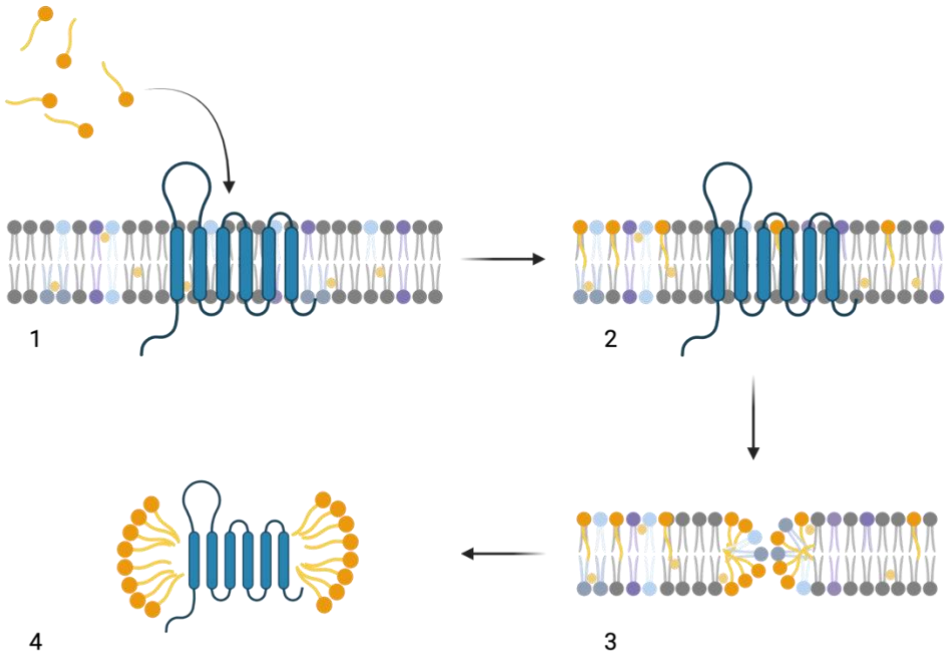

Figure 1.5 : Schematic representation of detergent micelle formation. 1 : Detergent is added to native membrane samples. 2 : Detergent monomers protrude into the outer layer of the plasma membrane, inducing curvature and mechanical strain. 3 : Pores are formed with detergent monomers continuing to integrate into the membrane. 4 : Detergent micelles containing membrane proteins are formed when CMC is achieved. Created with BioRender.

The CMC value is defined as the minimum concentration at which a detergent is capable of producing micelles and is determined by the level of hydrostatic interactions between detergents and membranes. Higher CMC values generally indicate weak protein binding and lower micelle stability while low CMC values indicate strong protein binding and higher micelle stability (Kapse, *et al.,* 2020, Francis, *et al.,* 2004). While reported CMC values are useful to

begin studies, the value can differ based on factors such as temperature, detergent chain length and concentration so optimisation is required.

Studies have found that by increasing the temperature from 15°C to 30°C, CMC values are decreased, with more intense decreases at lower temperatures (Kroll, *et al.,* 2022). This is due to weakened hydrogen bonds between detergent ethylene chains and surrounding water molecules leading to dehydration (Crook, *et al.,* 1964). This increases detergent hydrophobicity and lowers the CMC values (Kroll, *et al.,* 2022). Increasing temperature has also been linked to the formation of much larger micelles (Naous, Molina-Bolívar and Ruiz, 2014).

There are three major classes of detergents grouped according to their structure and head group charge (Table 1.1). Ionic detergents contain charged head groups that are either cationic or anionic and also display a hydrocarbon or steroidal backbone. Interestingly, the formation of micelles using ionic detergents can be modulated by size depending on the utilisation of counter ions at varying concentrations, with higher concentrations of counter ions resulting in larger micelle sizes (Molina-Bolívar and Ruiz, 2012). Longer alkyl chain detergents also produce larger micelles (Molina-Bolívar, Hierrezuelo and Ruiz, 2013). This modulation is useful in various applications such as drug delivery with different sizes of micelles able to permeate different tissue sites. Larger micelles tend to accumulate in permeable tumours, while smaller micelles are able to penetrate poorly permeable tumours (Cabral, *et al.,* 2011).

Ionic detergents such as sodium dodecyl sulfate (SDS) exhibit high solubilisation efficiencies in membrane protein solubilisation (Hjertén, Sparrman and Liao, 1988, Arachea, *et al.,* 2012) but is considered to be one of the most denaturing detergents available. In fact, SDS is commonly used in polyacrylamide gel electrophoresis (SDS-PAGE) for its activity against protein-protein interactions, whereby it breaks down tertiary structure to linearise the protein and produce high resolution protein separation (Nowakowski, Wobig and Petering, 2014).

Non-ionic detergents are considered to be less denaturing as they have a limited effect on protein-protein interactions and as such are the most commonly utilised for membrane protein solubilisation (Seddon, Curnow and Booth, 2004). These contain uncharged hydrophilic head groups consisting of either polyoxyethylene or glycosidic groups and

hydrophobic acyl tails. Due to their reduced electrostatic repulsion, non-ionic detergents are able to integrate into the membrane with ease, and as such generally display much lower CMC values when compared to ionic (Tadros, 2013). They are also less affected by the presence of ions in regard to micelle size.

Non-ionic detergents such as n-dodecyl-β-D-maltoside (DDM) have been shown to solubilise a wide range of membrane proteins (Kotov, *et al.,* 2019) including ABC transporters (Hawkins, *et al.,* 2021, Hardy, *et al.,* 2019) and their utilisation accounts for over half of all unique protein structures between 2010 and 2019 (Choy, *et al.,* 2021). However, it is reported that non-ionic detergents display a lower solubilisation efficiency when compared to ionic.

In order to maintain solubilisation efficiency while reducing the level of denaturation, a third class of detergents was identified. Zwitterionic detergents display characteristics of both ionic and non-ionic detergents. Similarly to non-ionic detergents, zwitterionic detergents have no net charge as they contain both positively and negatively groups. However, they retain the ability to interfere with protein-protein interactions much like ionic detergents.

Zwitterionic detergents lack conductivity and do not bind to ion-exchange resins making downstream purification of target proteins more accessible without the requirement of separate surfactant removal stages (Hjelmeland, 1980). FOS-Choline 12 is an example of a zwitterionic detergent that has been shown to solubilise membrane proteins (Pustovalova, *et al.,* 2023).

Table 1.1 : Information regarding detergents utilised for membrane protein solubilisation. Detergent class, examples of each class with CMC values and associated advantages and disadvantages.

Detergent Class	Examples	CMC (mM)	Advantages	Disadvantages
Non-ionic	DDM	0.17-0.18	Mild and non-denaturing.	Low efficiency.
Ionic	SDS	8.2	High solubilisation efficiency.	Highly denaturing.
Zwitterionic	FOS-Choline 12	1.5	Often used in crystallisation studies.	More denaturing than non-ionic.

While detergents have been critical for the structural determination of a wide range of membrane proteins, representing 77% of all structures solved (Lee, *et al*., 2022) there are some major disadvantages to their application. The first is the limited structural diversity of detergents which is in contrast with the diversity observed in membrane proteins (Ratkeviciute, Cooper and Knowles, 2021). There is no 'one-case-fits-all' and the majority of membrane protein studies begin with detergent screens to determine suitability.

Detergents can also be fairly expensive which limits some applications, especially considering the requirement for the sustained presence of detergent at CMC concentrations in subsequent buffers to limit loss of solubility during purification (Linke, 2009). On the other hand, high concentrations of detergents can also interfere with downstream processing such as spectroscopy leading to the requirement of detergent removal (Seddon, Curnow and Booth, 2004).

However, the major disadvantage of detergent utilisation is the progressive loss of native phospholipids during solubilisation and purification and the selective nature of detergents (Ilgü, *et al.,* 2014). While proteins are typically the subject of study, they only account for ~50% of the membrane biomass (Cooper, 2000). Other membrane components such as phospholipids, cholesterol, carbohydrates and glycolipids account for the other ~50%. Twenty of the forty-eight human ABC transporters have also been linked to lipid or lipid-related transport (Tarling, de Aguair Vallim and Edwards, 2013), and protein-lipid interactions are increasingly evidenced to support membrane protein structure and function (Sych, Levental and Sezgin, 2022).

In some cases, membrane proteins have been found to selectively bind lipids (Laganowsky, *et al.,* 2014) which can modulate substrate binding affinity and efflux in the mechanosensitive channel MscL (Powl, East and Lee, 2008). Lactose permease of *Escherichia coli* has also been shown to exhibit dynamic conformational switching in different lipid environments, with a total loss of phosphatidylethanolamine (PE) resulting in the protrusion of TMD seven into the periplasm (Vitrac, *et al.,* 2015).

Phospholipids also play a key role in the maintenance of membrane thickness, fluidity and lateral pressure – all key components affecting membrane permeability. Phospholipids with longer acyl tail lengths increases the hydrophobic thickness of the membrane (Frallicciardi, *et*

al., 2022) which can decrease permeability and therefore modulate protein activity as shown with Tolaasin II (Steigenberger, *et al.,* 2022). Membrane lateral pressure has also been shown to affect protein structure and function (Cantor, 1999).

Detergents may therefore provide a poor membrane mimic (Seddon, Curnow and Booth, 2004) and in order to further study membrane proteins and probe protein-lipid interactions, the search for alternative methods was stimulated.

1.5.2 Amphipols

Amphipols were introduced in the 1990s as a response to the protein instability exhibited in detergent micelles (Tribet, Audebert and Popot, 1996). Synthesised from polyacrylic acid precursors and octylamine, these amphipathic molecules bind to protein surfaces encompassing their hydrophobic segments (Figure 1.6). They have been shown to maintain protein solubility following dilution of the detergent used for solubilisation to below CMC (Popot, 2010). Unlike detergents, they are unable to solubilise directly from the cell membrane and are utilised to extend the time in which the protein remains stable, allowing for downstream study that may otherwise have been inaccessible. However, novel amphipols introduced retain the ability to directly solubilise as shown in recent studies with a cycloalkane modified amphipol able to solubilise AcrB from *Escherichia coli* (Higgins, *et al.,* 2021).

Another benefit of amphipols is the relatively low mass requirement for protein solubility when compared to detergents (Popot, *et al.,* 2003). Cytochrome B was found to bind ~260 molecules of DDM but only ~100 molecules of amphipol (Tribet, Audebert and Popot, 1997), which helps to reduce the interference with crystallography studies witnessed with detergents. Amphipols may also be utilised as novel delivery systems with amphipol packaged diacylglycerol kinase (DAGK) – an integral membrane protein – inserted into pre-formed lipid vesicles and exhibiting activity (Nagy, *et al.,* 2001). Unlike detergents, amphipols are safe up to excessive concentrations of 0.1g and remain stable once injected into different mediums until interaction with membranes (Popot, *et al.,* 2003).

However, amphipols are still considered a non-bilayer mimetic in the fact that they fail to retain lipids and associated interactions. They also display sensitivities to changes in pH and

the presence of divalent cations with exposure causing protein precipitation and aggregation (Zoonens and Popot, 2014).

1.5.3 Membrane Scaffold Proteins (MSPs)

In 2002, another novel method was introduced in the form of Membrane Scaffold Proteins (MSPs) (Bayburt, Grinkova and Sligar, 2002). This method involves the use of truncated forms of the naturally occurring α-helical protein apolipoprotein A-I (Apo A-I), a major component of high-density lipoprotein (HDL). Due to its intrinsic amphipathic nature (Brouillette, *et al.,* 1984), Apo A-I is able to wrap around phospholipids, encompassing hydrophobic segments in a double belt configuration with or without the presence of membrane proteins into discoidal nanoparticle– otherwise known as an MSP nanodisc (Figure 1.6).

MSP nanodisc diameter can be modulated depending on the form of MSP used with some studies reporting sizes of 6 – 18 nm (Schuler, Denisov and Sligar, 2013) while others report 9.5 – 12.8 nm (Denisov, Grinkova and Lazarides, 2004) and 16 – 17 nm (Grinkova, Denisov and Sligar, 2010). However, MSP nanodisc thickness appears to be independent to nanodisc diameter at a thickness reported between 4.5 – 5.5 nm (Bayburt, Grinkova and Sligar, 2002, Denisov, Grinkova and Lazarides, 2004).

Unlike detergents and amphipols, MSPs are able to reconstitute membrane proteins in association with phospholipids (Bayburt, Grinkova and Sligar, 2002), providing the opportunity to study membrane proteins in a more representative bilayer environment. They are also more consistent, monodisperse and stable when compared to micelles and amphipols (Nath, Atkins and Sligar, 2007) and have been shown to successfully reconstitute a range of membrane proteins including GPCRs such as β2-adrenergic receptor (Leitz, *et al.,* 2006), bacterial chemoreceptors (Boldog, *et al.,* 2006), bacteriorhodopsin trimers (Bayburt, Grinkova and Sligar, 2006) and ABC transporters such as P-gp (Ritchie, *et al.,* 2009).

However much like traditional amphipols, MSPs are unable to directly solubilise from native membranes and require an initial detergent solubilisation step. While MSP nanodiscs provide a good representation of a bilayer system, the phospholipids found within are non-native and are selectively added to detergent: protein: MSP mixtures during reconstitution. Because of

this, native protein-lipid interactions are lost, exposing membrane proteins to brief periods whereby structure and function can degrade. The lipid: MSP ratio also requires optimisation on a case-by-case basis and the production of MSPs can be time consuming and requires specialist equipment to produce consistently good yields (Ritchie, *et al.,* 2009).

1.5.4 Styrene Maleic Acid

To address the concerns raised with solubilisation methods explored previously, Styrene Maleic Acid (SMA) was introduced (Knowles, *et al.,* 2009). SMA is an amphipathic co-polymer that has the ability to self-insert into the membrane bilayer, encompassing sections of phospholipids with membrane proteins embedded (Figure 1.6). While the exact method of formation is yet to be elucidated, the resulting nanodiscs are known as SMA lipid particles (SMALPs) or co-polymer nanodiscs (Figure 1.7). SMALPs are generally ~10 nm in diameter, but reported values range from 5 – 30 nm depending on the preparation and membrane protein extracted (Dörr, *et al.,* 2016).

SMA is composed of repeating units of hydrophobic styrene and hydrophilic maleic acid moieties and is easily synthesised in the lab environment by hydrolysis of anhydride precursors. Co-polymer solubilisation is easily accessible and less time consuming when compared to other methods of solubilisation, and SMALPs provide a good mimic of a bilayer membrane. However, SMA is unique in its ability to retain protein associated phospholipids following direct protein extraction from the plasma membrane without the requirement for detergent. This provides a rare opportunity to study native protein-lipid interactions alongside membrane protein structure and function, including studies such as the analysis of SMA co-extracted lipids. While SMA appears to show no lipid extraction preference, SMA solubilised ZipA nanodiscs exhibit an enrichment in PE and a depletion of cardiolipin (CL) while SMA solubilised FtsA nanodiscs contained higher proportions of longer chain phosphatidylglycerol (PG) (Teo, *et al.,* 2019).

SMA solubilisation is considered to be milder when compared to detergents and therefore have fewer denaturing effects on protein structure and function. It remains a popular choice in membrane protein solubilisation and is widely considered as the industry standard, with SMA2000 continuing to show promise in the solubilisation of a wide range of membrane

proteins including GPCRs such as calcitonin gene related peptide (CGRP) and adenosine A2a receptor ($A_{2A}R$) (Gulamhussein, *et al.,* 2020) and ABC transporters such as BmrA, P-gp and bacteriorhodopsin in different expression models (Gulati, *et al.,* 2014, Cao, *et al.,* 2022, Broecker, Eger and Ernst, 2017).

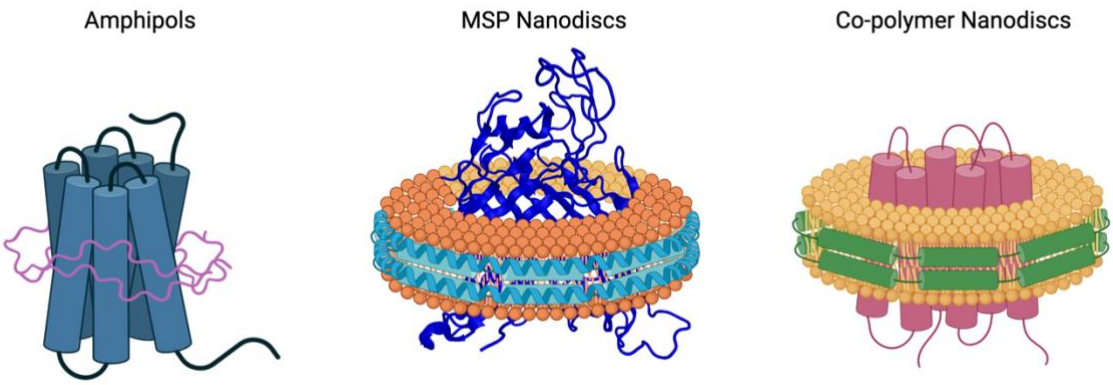

Figure 1.6 : Representation of nanoparticle structures formed using alternative solubilisation agents. From left to right ; Amphipols, MSP nanodiscs, Co-polymer nanodiscs. Created with BioRender.

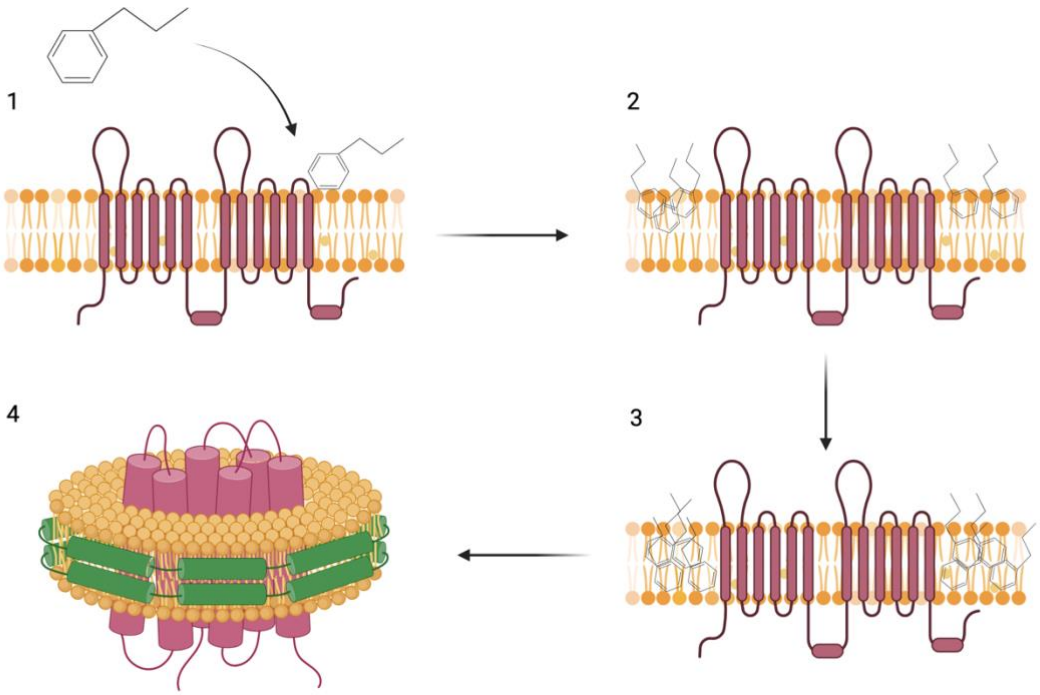

Figure 1.7 : Schematic representation of co-polymer nanodisc formation. 1 : Co-polymer is added to native membrane samples where it adheres by hydrophobic interactions. 2 : Co-polymer hydrophobic head groups bury into the acyl core of the bilayer cause local membrane undulation. 3 : Co-polymers continue to saturate the membrane, leading to pore formation. 4 : Segments of membrane with protein embedded are encapsulated into co-polymer nanodiscs. Created with BioRender.

However, there are still disadvantages in the application of SMA for membrane protein solubilisation. While protocols for the synthesis of SMA are widely available, conditions must be optimised on a case-by-case basis to ensure a good yield (Klumperman, 2010) and the process may still yield heterogenous co-polymer populations. Styrene maleic anhydride (SMAnh) hydrolysis can be controlled by changing the feed monomer ratio but resulting SMA exhibit a random distribution including polymeric length and composition, introducing issues with batch variance (Dörr, *et al.,* 2016). SMA also interferes with spectroscopic analysis with styrene absorbing at a wavelength of 260 nm, partially obscuring the ultraviolet (UV) absorption range of some proteins (Oluwole, *et al.,* 2017).

Perhaps mostly importantly, SMALPs display a sensitivity to divalent cations such as magnesium (Gulamhussein, *et al.,* 2020). This sensitivity is believed to the result of cationic chelation by the exposed carboxyl groups in maleic acid moieties (Pollock, *et al.,* 2017, Hawkins, *et al.,* 2021) and is a concern for the functional investigation of ABC transporters as magnesium is an essential cofactor for ATPase hydrolysis. This makes the measurement of ATPase activity as an indicator for ABC transporter functionality difficult.

Another concern is co-polymer nanodisc size, as the reported ~10 nm diameter is much too small for larger proteins and multi-complex proteins (Pollock, *et al.,* 2018). It is also hypothesised that SMALPs hold ABC transporters too tightly for full conformational flexibility during substrate transport (Pollock, *et al.,* 2018). While native lipids are retained in SMALPs, studies into co-polymer nanodisc lipid packing found increased headgroup packing in dimyristoylphosphatidylcholine (DMPC) SMALPs when compared to DMPC liposomes (Hernandez and Levental, 2023). To overcome some of the issues presenting with SMA-based solubilisation, a range of new polymers have been developed and introduced to the market.

1.5.5 SMA Variants

Due to the continued success of SMA2000 in membrane solubilisation and developments in synthesis – a range of SMA variants have been developed. New synthesis methods such as reversible addition fragmentation chain transfer (RAFT) polymerisation has fine-tuned co-polymer production. Utilising RAFT, co-polymer distribution is narrowed with more defined molecular weights, chain length and compositions (Cheng, *et al.,* 2023).

This includes SMA variants with different apolar: polar ratios such as SMA1000 and SMA3000 which have ratios of 1:1 and 3:1 respectively. The balance of hydrophobic and hydrophilic moieties is known to be the driving force behind co-polymer association and integration with plasma membrane, with less hydrophobic polymers expected to exhibit lower solubilisation efficiencies. In one study, SMA1000 exhibited a lower solubilisation efficiency when compared to SMA2000, but interestingly SMA3000 did not provide a higher efficiency (Morrison, *et al.,* 2016).

SMA is also commonly chemically modified to functionalise the co-polymer for specific applications. This includes SMA solvent-exposed sulfhydryls (SMA-SH) which unlike SMA covalently binds to thiol-reactive species such as biotin and fluorophores (Lindhoud, *et al.,* 2016).

In an attempt to reduce the sensitivity of SMA to magnesium, partial monoesters SMA1440 and SMA2625 were introduced. By esterifying SMA and reducing the number of exposed carboxyl groups from two to one, interactions with divalent cations are reduced resulting in a lower co-polymer sensitivity. SMA1440 and SMA2625 have been shown to solubilise thylakoid membranes to a high efficiency (Cherepanov, 2020, Olena, *et al.,* 2019) and were tested for the solubilisation of *Escherichia coli* membranes where SMA1440 was found to provide lower yields of protein and an unexpectedly higher magnesium sensitivity (Hawkins, *et al.,* 2021).

A more recent introduction to the field are SMA variants SMA -EA, SMA-ED, SMAd-A and SMA-QA (Figure 1.8). They are reported to display reduced magnesium sensitivity (Ravula, *et al.,* 2017a, Ravula, *et al.,* 2017b, Ravula, *et al.,* 2018) and were tested in this study.

All are variants of SMAnh, with SMA-EA synthesised via a nucleophilic ring opening reaction using ethanolamine (Table 3.2). It was reported that SMA-EA exhibited an increased tolerance to magnesium when compared to SMA2000 (Ravula, *et al.,* 2017a) and therefore more variants were produced. SMA-ED is a zwitterionic analogue of SMA2000 synthesised via ethylenediamine before creation of a maleimide group by dehydration into acid stable SMAd-A (Table 3.2). SMA-QA was then synthesised via aminoethyltrimethylammonium to form a polymer with a pH independent hydrophilic group (Table 3.2). SMA-ED, SMA-d-A and SMA-QA were also reported to exhibit some degree of magnesium tolerance (Ravula, *et al.,* 2017b and Ravula, *et al.,* 2018).

1.5.6 DIBMA Variants

Other co-polymers showing promise for membrane protein solubilisation is Diisobutylene Maleic Acid (DIBMA) and Glyco-DIBMA, which contain aliphatic diisobutylene moieties in place of the aromatic styrene moieties found in SMA - in a 1:1 ratio with maleic acid (Figure 1.8). This exchange results in a polymer with lower hydrophobicity but similar hydrophobic: hydrophilic balance, which is hypothesised to result in less sensitive DIBMA lipid particles (DIBMALPs). It also does not absorb in the region of 260 nm, making them more applicable for spectroscopic study of membrane proteins.

DIBMA has been successful in the solubilisation of many membrane proteins across multiple membrane models including $A_{2A}R$ and CGRP (Gulamhussein, *et al.,* 2020) and outer membrane phospholipase A (OmpLA) (Oluwole, *et al*., ,2017). It also consistently displays a higher tolerance to magnesium when compared to SMA2000. DIBMALPs are also reported to be between 10 – 50 nm in diameter (Oluwole, *et al.,* 2017), which is bigger than reported values for SMALPs, potentially making them more applicable for larger membrane protein or protein complex studies. However, DIBMALP size distribution is wider than SMALPs (Oluwole, *et al.,* 2017) and displays a reduced solubilisation efficiency and yield of ABC transporter BmrA (Gulamhussein, *et al.,* 2020).

In response to the reported lower solubilisation efficiencies, DIBMA was functionalised by partial amidation with sugar residue meglumine into Glyco-DIBMA. This modification reduces polymer charge, increases hydrophobicity and is expected to maintain solubilisation efficiency. Glyco-DIBMA has been shown to successfully solubilise BmrA (Gulamhussein, *et al.,* 2020) and so both DIBMA and Glyco-DIBMA were selected for study.

1.5.7 AASTY Variants

The third co-polymer group explored in this project are the acrylic acid styrene (AASTY) co-polymers 6-45, 6-50, 6-55, 11-45, 11-50 and 11-55 (Figure 1.8), which were introduced in response to the high polymer heterogeneity of existing co-polymers available. Produced by RAFT, AASTY polymers have a highly alternating structure and are more monodisperse producing nanodiscs with lower heterogeneity when compared to SMA and DIBMA.

While the structures of the six AASTY co-polymers tested in this study are identical, they differ by molecular weight at either 6kDa or 11kDa and the ratio of apolar: polar moieties with 45%, 50% or 55% acrylic acid – providing the opportunity to probe the effect of polymeric weight and ratio in areas such as efficiency, protein yield and functionality.

While a more recent introduction to membrane protein solubilisation, AASTY has been successfully applied in the solubilisation of human transient receptor potential melastatin type 4 (hTRPM4) into co-polymer nanodiscs of ~18 nm (Smith, *et al.,* 2020) – a slightly bigger diameter than SMALPs. AASTY has also been shown to exhibit an increased tolerance to magnesium (Timcenko, *et al.,* 2022). The six studied AASTY co-polymers also provide an interesting study due to the exchange of maleic acid to acrylic acid – which is uncommon among all other co-polymers tested in this research.

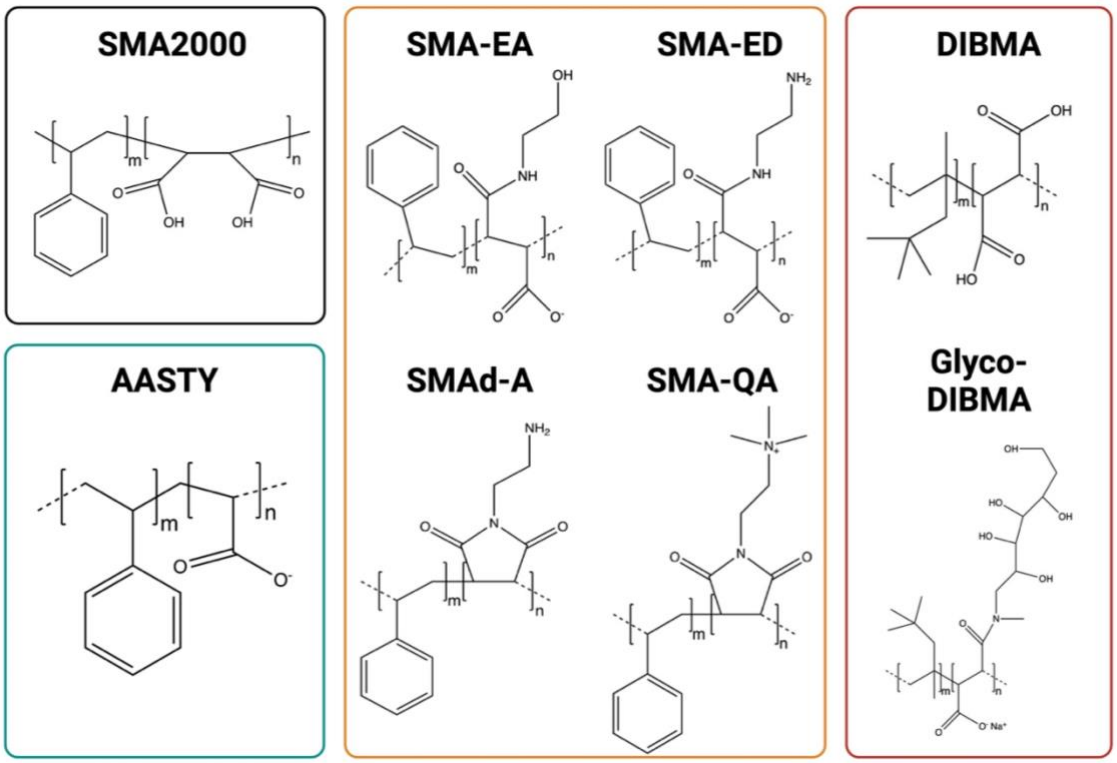

Figure 1.8 : Representation of the chemical structures of co-polymer variants tested. 'm' represents the number of repeating apolar moieties, while 'n' represents the number of repeating polar moieties. From top left to bottom right ; SMA2000, SMA-EA, SMA-ED, DIBMA, AASTY, SMAd-A, SMA-QA and Glyco-DIBMA. Coloured boxes represent classes of co-polymers ; Black : SMA2000, Orange : SMA variants, Red : DIBMA variants, Aqua : AASTY variants. Created using ChemDraw v21.0.0 and BioRender.

1.6 Aims & Objectives

The aims of this project were to identify co-polymers suitable for the functional study of BmrA, while probing nanodisc characteristics and solubilisation agent 'switching'.

Objectives included:

- Express, prepare and purify BmrA from *E. coli* membranes to investigate ABC transporter functionality in a range of co-polymer solubilised nanodiscs.
- Probe nanodisc characteristics such as size/mass, lipid environment and fluidity, and define co-polymer suitability application for ABC transporter study.
- Investigate solubilisation agent 'switching' utilising co-polymers, detergent and proteoliposomes to overcome methodological challenges and highlight co-polymer application to a wide range of targets.

2. Methods and Materials

2.1 Polymer Preparation

SMA2000 was provided as a kind gift from Cray Valley, supplied as SMAnh powder which required conversion into active SMA form. This was carried out as previously described (Morrison, *et al.,* 2016) with 25g of SMAnh hydrolysed by reflux in 250ml 1M NaOH for 2 hours at 120°C before leaving to cool to room temperature. The solution was then transferred to two 500ml centrifuge tubes with 50ml concentrated HCl and 300ml dH_2O added before centrifugation (11000 *x g*, 15 minutes, 5°C). The supernatant was carefully discarded with the precipitated polymer in the pellet resuspended in dH_2O before a second centrifugation step (11000 *x g*, 15 minutes, 5°C). This was repeated once again before resuspending the pellet in 125ml 0.6M NaOH and freezing at -20°C. The polymer was then freeze dried into a dry powder for room temperature storage.

Polymers purchased from Cube Biotech and Anatrace including SMA variants, DIBMA, Glyco-DIBMA and AASTY variants were supplied in a powdered active form, which required reconstitution with purification buffer (20mM Tris and 150mM NaCl, pH 8) to a working concentration of 10%.

2.2 BmrA Expression, Culture and Membrane Preparation

C41 *E. coli* BmrA overexpressing cells were utilised for this study, transformed with the vector pET23b-BmrA (Morrison, *et al.,* 2016). To inoculate an overnight culture, a 10µl tip was pushed into the surface of glycerol stocks stored in 1.5ml centrifuge tubes at -80°C and ejected into 5ml of Luria Broth (LB [Formedium™]) supplemented with 5µl 100mg/ml ampicillin. Following incubation overnight at 37°C 200rpm, the overnight sample was added to 1L LB and returned to incubation. Once OD_{600} of 0.6 was achieved, protein synthesis was induced using 1ml 0.5M isopropyl β-D-1-thiogalactopyranoside (IPTG) [Fisher Bioreagents] and left to incubate overnight at 25°C, 200rpm. Cells were then harvested by centrifugation (6000 *x g*, 10 minutes) with pellet retained.

Cell pellets were resuspended in homogenisation buffer (50mM Tris, 0.25mM $CaCl_2$ and 250mM Sucrose) up to a total volume of 20ml. 200µl of protease inhibitors [Sigma] was then added to samples before being processed through a French Press (3 x 16,000 pounds per square inch (PSI)). The resulting cell lysate was centrifuged (650 *x g*, 10 minutes, 4°C) with the supernatant further ultracentrifuged (100000 *x g*, 20 minutes, 4°C). The resulting pellet was then resuspended at a wet membrane weight of 60mg/ml with purification buffer and stored at -20°C.

2.3 Sf9 Expression, Culture and Membrane Preparation

Sf9 MRP4 overexpressing cells were also utilised in this study, transformed using a baculovirus expression system with pFastBac-MRP4-his_6 construct as previously described (Gulati, *et al.,* 2014). 1ml of transformed stocks were added to T25 flasks with 9ml growth media (ESF 921 insect cell culture medium, 10% foetal bovine serum (FBS) and 1% penicillin-streptomycin) and incubated overnight at 28°C. Once cells reach 80% confluency, cells were passaged by gently knocking the flask bottom and transferred to 125ml shaker flasks supplemented with 20ml growth media. This was then incubated at 28°C on a shaker plate set to 100rpm. For further passages, cells are counted with a haemocytometer before transfer to new 125ml shaker flasks diluted to a density of 0.5 x 10^6 cells/ml before returning to incubation at 28°C, 100rpm.

Cells were harvested by centrifugation (7000 *x g*, 10 minutes, 4°C) with the pellet retained and resuspended in 10ml phosphate buffered saline (PBS). The sample was then centrifuged once more (3220 *x g*, 10 minutes, 4°C) before resuspension in 20ml homogenisation buffer with protease inhibitors added. To harvest membranes, nitrogen cavitation was utilised with cell suspension transferred to a precooled cell disruption vessel with 500 PSI pressure applied. The vessel was left on ice for 15 minutes before the sample was transferred to 50ml falcon tubes before repeating nitrogen cavitation another two times. The samples were then centrifuged (750 *x g*, 10 minutes, 4°C), with supernatant retained and centrifuged again (100000 *x g*, 20 minutes, 4°C). The pellet was then resuspended at a wet membrane weight of 60mg/ml with purification buffer and stored at -80°C.

2.4 Protein-Lipid Nanodisc Production

5% (SMA, SMA variants, DIBMA and Glyco-DIBMA) or 1% (AASTY) w/v polymer in purification buffer was added in equal volume to 60mg/ml $BmrA^+$ C41 or $MRP4^+$ Sf9 membrane stocks and mixed for 1 hour at room temperature. Samples were then ultracentrifuged (100000 *x g*, 20 minutes, 4°C) with the supernatant containing soluble membranes captured for further study. 20µl samples of the supernatant and pellet fractions were also collected and stored at -20°C with 5µl 5 x laemmli sample buffer (LSB) for SDS-PAGE analysis.

2.5 Protein-Lipid Nanodisc Purification

0.4ml of HisPur resin [ThermoFisher] was pre-equilibrised with purification buffer before centrifugation (500 *x g*, 10 minutes, 4°C). Solubilised membrane samples were then added to the washed resin and mixed overnight at 4°C using a rotary mixer. The following day, loaded resin samples were loaded onto a gravity column and washed five times with 10 x bed volume (BV) of purification buffer containing 20mM imidazole. This was followed by another two washes with 10 x BV of purification buffer containing 40mM imidazole. Elution fractions were then taken using 0.5 x BV of purification buffer containing 200mM imidazole solution. 20µl samples of flow-through (Ft), wash one (W1), wash seven (W7) and each elution fraction (E1, E2, …) were taken for SDS-PAGE analysis and stored with 5µl 5 x LSB at 4°C.

2.6 Detergent Micelle Production

DDM was also tested as a conventional detergent solubilisation agent. This was carried out using a protocol as previously mentioned (Steinfels, *et al.,* 2004) Briefly, 1ml of 60mg/ml membrane stocks were mixed with detergent solubilisation buffer (100mM potassium phosphate, 100mM NaCl, 15% glycerol, 10mM imidazole, 1% DDM, 5mM β-Mercaptoethanol and 1mM phenylmethylsulfonyl fluoride (PMSF)) for one hour at 4°C. Sample was then ultracentrifuged (220000 *x g*, 1 hour, 4°C) with supernatant containing soluble membrane captured for further study. 20µl samples of the supernatant and pellet fractions were also collected and stored at -20°C with 5µl 5 x LSB for SDS-PAGE analysis.

2.7 Detergent Micelle Purification

0.4ml of HisPur resin [ThermoFisher] was washed with equilibration buffer (100mM potassium phosphate, 100mM NaCl, 15% glycerol and 5mM β-Mercaptoethanol) and centrifuged (500 *x g*, 10 minutes, 4°C). Solubilised membrane samples were then added to the washed resin and mixed overnight at 4°C. Sample was loaded into a gravity column and washed five times with 20 x BV of 20mM imidazole solution, followed by another two washes with 10 x BV of 40mM imidazole solution. 10 elutions were then captured using 0.5 x BV 200mM imidazole solution. Samples of Ft, W1, W7 and each elution fraction were taken for SDS-PAGE analysis and stored with 5µl 5 x LSB at 4°C.

2.8 Western Blot

Supernatant (Sol) and pellet (Pt) samples collected during solubilisation were analysed by Western Blot to determine polymer efficiency. To do this, 10µl supernatant and pellet samples with 2.5µl 5 x LSB were loaded on SDS-PAGE with pre-stained molecular weight ladder [FisherScientific] and ran at 100v for 1 hour. Protein samples were then transferred to polyvinylidene fluoride (PVDF) membranes using Trans-Blot® [Bio-Rad] system, running at 100v for 1 hour. Membranes were then probed with 1:4000 mouse α-his primary antibody [R&D Systems] and 1:10000 α-mouse-HRP secondary antibody [Cell Signalling] for BmrA, or 1:100 rat α-MRP4 primary antibody and 1:3000 α-rat-HRP secondary antibody for MRP4. Membranes were then visualised using West Pico Plus [ThermoFisher] chemiluminescent substrate and C-Digit scanner [LI-COR] imaging system and analysed by densitometry. Bands associated with BmrA in Sol and Pt lanes are quantified and compared to calculate solubilisation efficiency with unpaired t-test and one-way ANOVA statistical tests applied.

2.9 Mass Spectrometry

Mass spectrometry of SDS-PAGE bands for identification purposes was carried out with thanks to Ophelie Langlois (Aston University). To begin, samples were prepared by in-gel trypsin digestion of Coomassie stained proteins cut from SDS-PAGE gel elution lanes. Gel bands were excised in a sterile manner, cut into smaller pieces and placed into a 1.5ml Eppendorf tube.

This was washed with 500µl 100mM ammonium bicarbonate for 1 hour on a shaker before a second wash with 500µl of acetonitrile/ammonium bicarbonate for a further 1 hour. To reduce the sample, 150µl of 100mM ammonium bicarbonate and 10µl of 45mM dithiothreitol (DTT) was added and incubated at 60°C for 30 minutes. Sample was then cooled to room temperature before 10µl 100mM iodoacetamide was added and incubated for 30 minutes under darkness. Solvent was then discarded, and sample washed again with 500µl acetonitrile/ammonium bicarbonate for 1 hour. Sample was then dried in a vacuum centrifuge for 10 minutes 30°C before rehydration with 10µl of 100µg trypsin at a time. 25mM ammonium bicarbonate was then added to cover gel pieces before incubation overnight at 37°C. The following day, sample was centrifuged to pellet gel pieces with 20µl formic acid then added before incubation at 37°C for 20 minutes. 40µl acetonitrile was then added before further incubation at 37°C for 20 minutes. Samples were then dried down in a vacuum centrifuge for 1 hour and analysed by mass spectrometry using an ESI-QUAD-TOF system. Mascot search against peptide samples were established, with protein matches and sequence coverage highlighted.

2.10 Lipid-Only Nanodisc Production and Purification

DMPC lipid stocks stored at -20°C were weighed out and rehydrated with 1:1 chloroform: methanol before drying under nitrogen. DMPC was then further dried using a vacuum pump for 1 hour before reconstituting at a concentration of 4% in purification buffer. Equal volumes of 4% DMPC and 5% (SMA2000 and DIBMA) or 1% (AASTY) was then mixed before loading into Akta Pure superdex 200 increase 10/300 column for size exclusion chromatography (SEC). Peaks associated to lipid-only nanodisc populations identified on SEC trace with associated 0.5ml fractions pooled and stored at 4°C.

2.11 Protein-Lipid Sensitivity Assay

Pooled purified BmrA nanodiscs produced with SMA2000, DIBMA and AASTY co-polymers were mixed with varying concentrations of $MgCl_2$ (0-10mM) ensuring good mixing. Following brief incubation at room temperature, solutions were ultracentrifuged (100000 *x g*, 20 minutes, 4°C) with the supernatant harvested, and pellet resuspended in equal volume purification buffer supplemented with 10% SDS. 20µl sol and pt samples were then taken and

mixed with 5µl 5 x LSB and stored at -20°C for SDS-PAGE analysis. Densitometric analysis was then carried out to determine the percentage of soluble BmrA remaining at each magnesium concentration to establish co-polymer sensitivity. Sol and Pt BmrA bands were quantified and compared with non-linear inhibitor vs response curves applied.

2.12 Lipid-Only Sensitivity Assay

SEC purified lipid-only nanodiscs produced with SMA2000, DIBMA and AASTY co-polymers were mixed with varying concentrations of magnesium (0-50mM) in a 96 well plate up to a total volume 100µl per well ensuring good mixing. Following brief incubation at room temperature, light scattering was read at 390nm using a plate reader [Multiskan GO] with data normalised to 0mM magnesium controls. Data plotted with non-linear agonist vs response curves fitted.

2.13 Sf9 Light Scattering Assay

A scattering clearance assay was utilised to study the solubilisation kinetics of co-polymers for insect membranes prepared by Dr David Hardy. To do this, 100µl of purification buffer was pipetted into a black quartz cuvette with scattering measured at 390nm to set reference. Buffer was then removed and discarded. Following this, 50µl samples of Sf9 membranes at 60mg/ml were added to the cuvette with 50µl 5% SMA2000, DIBMA, Glyco-DIBMA and AASTY co-polymer rapidly mixed with scattering profile over 5 minutes recorded by video. Experiments were repeated in triplicate for each co-polymer with buffer control also tested to account for dilution factor. Data plotted with two-phase decay lines plotted.

2.14 Tryptophan Quenching Assay

The binding activity of BmrA was determined using a tryptophan quenching assay, based on the shift of the intrinsic fluorescence of BmrA in response to addition of known substrate Hoechst 33342. To prepare samples for analysis, pooled purified BmrA produced using SMA2000, DIBMA, 6-50 and 11-50 were buffer exchanged using 500µl filter concentrators with a 30kDa cut-off [Amicon Ultra]. Samples were added to filter and centrifuged (20000 *x g*,

10 minutes) with flow-through discarded and supernatant topped up with 400µl purification buffer before spinning again. This was repeated a further two times to remove imidazole with protein diluted to original volume. Following this, 100µl buffer exchanged BmrA is pipetted into a black quartz cuvette with fluorescence measured five times by spectrophotometer [Perkin Elmer LS55] with an excitation wavelength of 280nm and emission wavelength spectra between 310 – 400nm, 15nm slit widths, 1500nm/min and medium gain. Hoechst 3342 was then successively added to the cuvette at final concentrations of 0.99, 1.97, 4.83, 9.54, 14.22, 18.85, 27.94 and 49.68 µM with fluorescence measured at each concentration five times. The same experiment was also carried out using N-acetyltryptophanamide (NATA) in place of BmrA to normalise data against inner filter and dilution effects.

To analysis, fluorescence values at 335nm for each attempt was averaged with percentage quenching calculated by $100-((S_{385nm}/C_{385nm})*100)$, with S representing fluorescence of selected data points and C representing fluorescence of 0mM Hoechst 33342 control. Data was NATA normalised by subtraction and plotted with non-linear regression one site binding curves fit and Kd and maximal quenching calculated. One-way ANOVA statistical tests applied where appropriate.

2.15 ATPase Assay

The ATPase activity of purified BmrA in nanodiscs produced with SMA2000, DIBMA, 6-50 and 11-50 and micelles produced with DDM was measured using a modified colorimetric 96-well plate assay as previously described (Chifflet, *et al.,* 1988), which is based on the detection of inorganic phosphate released during ATP hydrolysis. To do this, a range of phosphate standards (0,1,2,3,4,5,6,8,10,12,16 and 20 nmoles) were added to wells up to a volume of 50µl. 30µl samples of BmrA nanodiscs and micelles were then added to separate wells with ATP (0,0.2,0.4,0.8,1.5 and 2 mM) and dH_2O up to a volume of 40µl. A row with no protein is also plated as a control. The plate was the incubated for 20 minutes at 37°C before 40µl 12% SDS was added. 100µl of equal volume 1% ammonium molybdate and 6% ascorbic acid was then applied with plate incubated for 5 minutes at room temperature. Following this, 100µl of equal volume 2% sodium citrate, 2% metaarsenite and 2% acetic acid was applied to each well before final incubation at 37°C for 15 minutes. Absorbance was then measured at 750nm

using a microplate reader [Multiskan GO] with activity presented as nanomoles of P_i liberated per minute per milligram of pure protein with Michaelis-Menten curves fitted.

2.16 Mass Photometry

Mass photometry of protein-lipid and lipid-only nanodiscs to define mass, binding activity and homogeneity was carried out with thanks to Dr Philip Kitchen (Aston University) using Refyn Two MP equipment. To set up, equipment was switched on to allow for thermal equilibration at a minimum of 1 hour before readings were taken and coverslips were well washed with repeated dipping into dH_2O and ethanol to remove any dust particles. A 6-well reusable gasket was then applied to the coverslip and loaded into position following application of immersion oil on microscope objective. Acquire MP software was opened and calibration undertaken with 20µl of purification buffer added to a gasket to focus the microscope lens before being removed and disposed. To produce a mass calibration curve, 47.5µl of purification buffer was mixed with 2.5µl of NativeMark [Thermofisher LC0725] with 2µl of this mixture added to 18µl of purification buffer. This was then pipetted into the gasket with data rapidly collected. To measure nanodisc mass, 18µl of purification buffer was loaded into a fresh gasket with 2µl nanodiscs rapidly added while ensuring good mixing before data was collected. This was repeated with fresh gaskets for each sample.

Mass photometry data is then processed using installed analysis software with DiscoverMP programme opened. Protein standard distribution peaks and gaussian functions were fitted with nanodisc samples analysed by correlation to the calibrant set. Figures were produced using Discover MP with mass (kDa) and counts of identified peaks highlighted.

2.17 Lipid Extraction

Lipids co-solubilised in protein-lipid nanodiscs and crude membrane samples from bacterial and insect cells (prepared by Dr David Hardy) were extracted for analysis by thin layer chromatography (TLC). Nanodiscs were produced as described previously, with the supernatant mixed with 300µl of methyl-tert-butyl ether (MTBE) and methanol in a 10:3 ratio. This is incubated at room temperature on a shaker plate for 1 hour, after which 50µl dH_2O

was added. The sample was then centrifuged (1000 *x g*, 10 minutes, 4°C) with solvent layer retained and dried down to a powder form using nitrogen before storing at -20°C.

2.18 Thin Layer Chromatography

Lipid extracts were analysed by TLC using a chloroform:methanol:dH_2O (65:25:4) solvent system with silica gel 60 F254 plates. To set up for TLC, solvent is added to a TLC tank to an appropriate level with sample line on TLC plate marked above the solvent level. Lipid extracts were rehydrated using chloroform: methanol (1:1) and successively dotted onto the sample line alongside 25µg lipid controls (phosphotidylserine (PS), phosphotidylcholine (PC), PG, CL and PE). Plate was then transferred to the TLC tank and left for ~1 hour or until the solvent line reaches the top of the TLC plate. It was then rapidly removed from the tank with solvent running line marked at the top of the plate, before staining with molybdenum blue which binds compounds containing phosphate esters such as phospholipids.

To quantify and compare the lipid composition of protein-lipid nanodiscs, densitometric analysis of TLC plates was carried out. Bands associated with PE and PG for bacterial membranes and PE and PC for insect membranes were isolated and quantified with lipid ratio calculated. One-way ANOVA statistical tests applied.

2.19 Laurdan Assay

To measure membrane fluidity, a laurdan assay was employed. To begin, 5µl 1mM laurdan in dimethylsulfoxide (DMSO) was mixed with 500µl 0.1% DMPC liposomes at room temperature in a 1.5ml centrifuge tube. Sample was then transferred to a cuvette with fluorescence measured in triplicate using a spectrophotometer [Perkin Elmer LS55] with an excitation wavelength of 350nm and emission wavelength spectra of 380 – 600nm, 15nm slit widths, 750nm/min and medium gain. The sample was then transferred back into a 1.5ml centrifuge tube and incubated for five minutes at 4°C using a heat block. The chilled sample was then transferred back to cuvette with triplicate measurements taken before being returned to incubation. This was repeated up to temperatures of 60°C with fluorescence measured at 4°C, 20°C, 25°C, 30°C, 35°C, 40°C, 50°C and 60°C. This protocol was repeated when testing lipid-only nanodiscs produced using SMA2000, DIBMA, 6-50 and 11-50.

The average fluorescence reading between triplicates at 435nm and 490nm were utilised in analyses, with GP value calculated by : ((435nm-490nm)/(435nm+490nm)). Data plotted as mean ± SD with non-linear inhibitor vs response curves fitted.

2.20 Reconstitution from Nanodiscs to Proteoliposomes

To reconstitute BmrA from co-polymer nanodiscs to proteoliposomes, pooled purified BmrA nanodiscs produced with 2.5% SMA2000 were mixed with 4% *E. coli* lipids – produced as previously described using *E. coli* total lipid extract [Avanti] – at a ratio of 1:100 protein to lipid. This mixture was incubated at 37°C for 5 minutes before 10mM $MgCl_2$ or an equal volume of purification buffer was added and briefly sonicated. Mixtures were then returned to incubation at 37°C for either 30 or 5 minutes with gentle mixing. Samples were then centrifuged (20000 *x g*, 10 minutes) with 20µl supernatant (S) sample taken. For samples without magnesium, the pellet (Pt) was resuspended with purification buffer to a concentration of 10mg/ml with 20µl taken for SDS-PAGE analysis. For samples with magnesium, the pellet was resuspended up to a volume of 500µl with 20µl sample taken for SDS-PAGE analysis before another two rounds of centrifugation (20000 *x g*, 10 minutes). S and Pt samples were then loaded onto SDS-PAGE and analysed by densitometry with bands associated with BmrA quantified, allowing for the calculation of reconstitution efficiency with unpaired t-test statistical tests utilised.

2.21 Reconstitution from Nanodiscs to Micelles

To reconstitute BmrA from co-polymer nanodiscs to detergent micelles, pooled purified BmrA nanodiscs produced with 2.5% SMA2000 and DIBMA and 0.5% AASTY 6-50 and 11-50 were mixed with different concentrations of DDM (10%, 1% and 0.1%) in the presence of 10mM $MgCl_2$ in ultracentrifuge tubes up to a volume of 100µl. Controls were also established with negative representing no detergent or magnesium, and positive representing no detergent but containing magnesium. All tubes were well mixed and incubated briefly at room temperature before centrifugation (100000 *x g*, 20 minutes, 4°C) with supernatant (Sol) harvested. Pellets (Pt) were resuspended with 100µl purification with 20µl samples of Sol and

Pt taken for SDS-PAGE analysis with densitometric analysis of bands associated with BmrA quantified, allowing for the calculation of soluble BmrA (%) remaining at defined detergent concentrations.

2.22 Densitometric and Statistical Analysis

All densitometric analysis was carried out using Image J software v1.51 with data plotting and statistical analysis performed by GraphPad Prism Software v10.2.0 (335).

2.22.1 BmrA Purity

To calculate percentage protein purity, SDS-PAGE purification gels were analysed with the elution lane showing the highest BmrA presence selected. Peaks associated with BmrA were isolated and quantified alongside all other identifiable peaks, with BmrA density and total density calculated and unpaired t test and one-way ANOVA statistical tests conducted.

2.22.2 BmrA Yield

To calculate BmrA yield, bovine serum albumin (BSA) standards (0.25, 0.5, 0.75, 1, 1.25 and 1.5µg/ml) along with pooled purified BmrA were run on SDS-PAGE. The band associated with BSA at each concentration was quantified and plotted to produce a standard curve. The line equation of the curve was then utilised to calculate the concentration of protein following the isolation and quantification of bands associated with BmrA. Following conversion to µg/ml, the yield is normalised against batch effects and compared to SMA2000, presented as mean $\pm$ SD with unpaired t test and one-way ANOVA statistical tests applied.

3. Results Chapter One : Polymer Trials

Section One : Solubilisation of an ABC transporter from Bacterial Cells

3.1.1 SMA2000 and DDM

SMA2000 was the first amphiphilic polymer utilised for direct solubilisation of MPs. It is comprised of hydrophobic styrene groups and hydrophilic maleic acid groups in a 2:1 ratio (Figure 3.1, Table 3.1). It has remained a popular choice for polymer solubilisation screening and has become commonplace in both academic and industrial research groups. SMA2000 has previously been utilised for the solubilisation of BmrA (Gulamhussein, *et al.,* 2019, Hawkins, *et al.,*2021) and was selected for initial solubilisation trials of BmrA alongside DDM, which is the most commonly used detergent for membrane protein solubilisation (Choy, *et al.,* 2021).

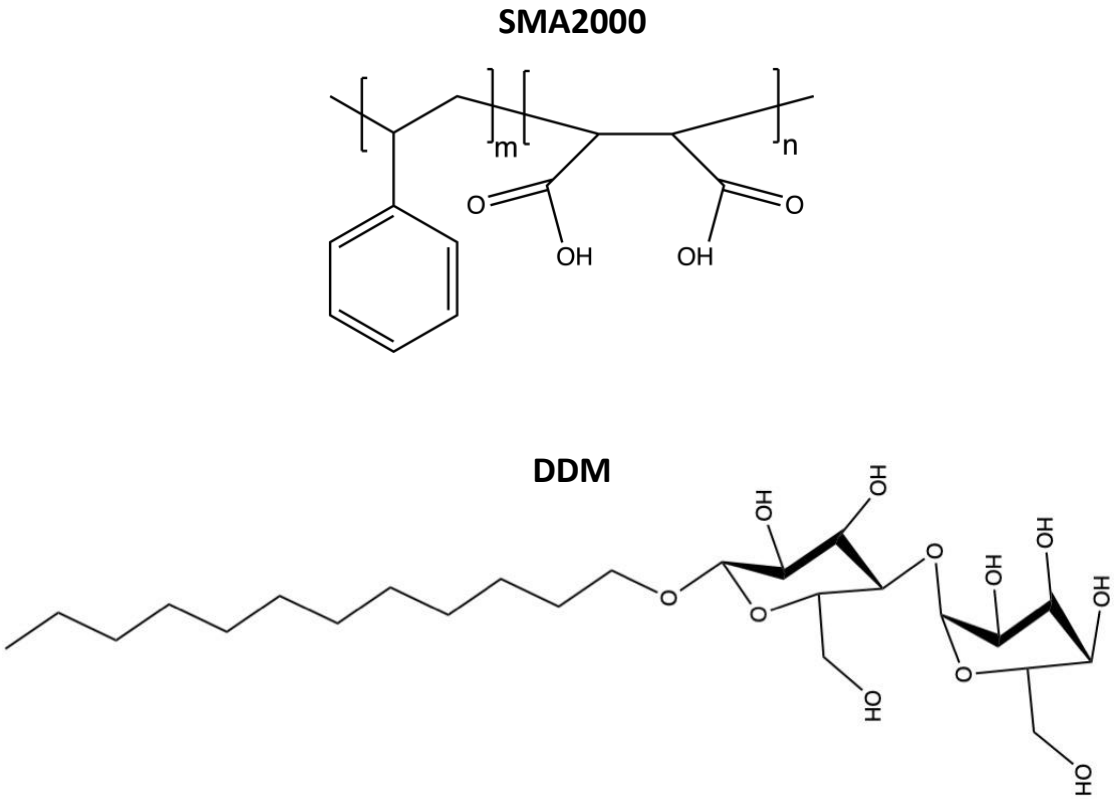

Figure 3.1 : Representation of the chemical structure of SMA2000 and DDM. 'm' represents the number of repeating apolar styrene moiety, while 'n' represents the number of repeating polar maleic acid moiety. DDM is a non-ionic detergent consisting of a hydrophobic 12 carbon acyl group tail and a hydrophilic maltose head. Created using ChemDraw v21.0.0.

Table 3.1 : Co-polymer information. Chemical and structural characteristics of SMA2000 as per manufacturer. Ratio, styrene to maleic acid; Mw, weight average molecular weight; Mn, number average molecular weight.

Name	Manufacturer	Apolar Subunit	Polar Subunit	Chemical Modifications	Ratio (S:M)	Mw (kDa)	Mn (kDa)
SMA2000	Cray Valley	Styrene	Maleic acid	N/A	2:1	7.5	3

3.1.2 BmrA Solubilisation Efficiency

The efficiency of SMA2000 and DDM to extract BmrA which was recombinantly overexpressed in *E. coli* was first tested in small scale solubilisation trials. Supernatant and pellet samples were investigated by western blot (Figure 3.2 A and B) and analysed by densitometry of western blots (Figure 3.2 C).

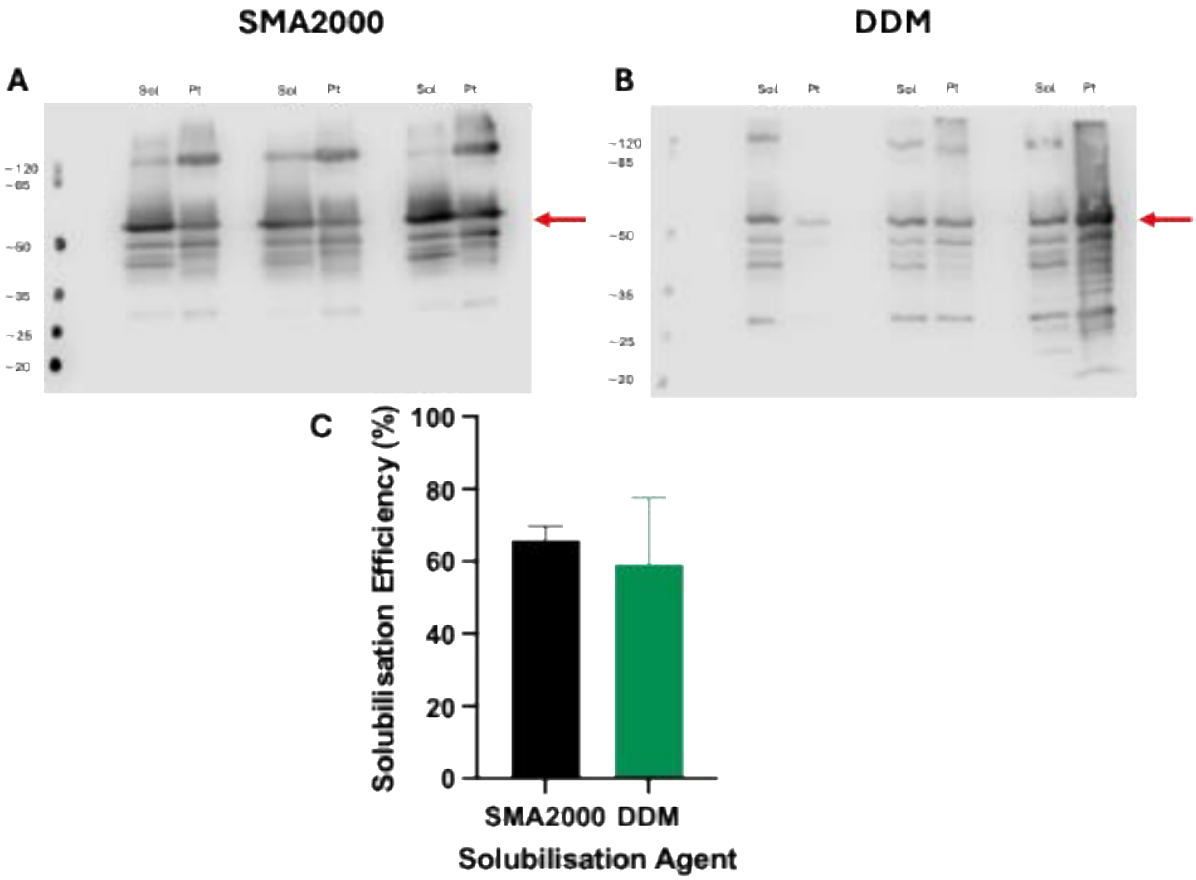

Figure 3.2 : SMA2000 and DDM are both able to solubilise BmrA. BmrA and *E. coli* membranes (60mg/ml) were mixed with equal volume of 5% (w/v) SMA2000 (A) or 1% DDM (B) for 1 hour at room temperature. Samples were then centrifuged (100,000 x g, 20 min, 4℃) with supernatant (Sol) and pellet (Pt) samples collected. 10µl samples were analysed by western blot, probed with 1:4000 mouse α-his Ab and 1:10000 α-mouse-HRP Ab. Membrane visualised using West Pico Plus and LI-COR imaging system with BmrA bands highlighted. Solubilisation efficiency calculated by densitometry using ImageJ (C) with data shown as mean ± SD, n ≥3. Data analysed by unpaired t-test with no significance found.

Both SMA2000 and DDM can successfully solubilise bacterial BmrA from *E. coli* cells as shown in figure 3.2 A and B, with highlighted bands representing BmrA seen in both Sol and Pt samples across repeats. The efficiency of SMA2000 and DDM is comparable as shown in figure 3.2 C with SMA2000 solubilising 66±3.9% compared to DDM solubilising 59±18.4%.

3.1.3 BmrA Purity

After confirming both SMA2000 and DDM were capable of solubilising BmrA, the next step was to purify the extracted protein. BmrA was expressed with a C-terminal his tag and was purified using Ni-affinity chromatography with purification samples run on SDS-PAGE. To

quantify the level of BmrA purity, the elution lane with the highest BmrA presence on SDS-PAGE gels (Figure 3.3 A and B) was analysed by densitometry (Figure 3.3 C).

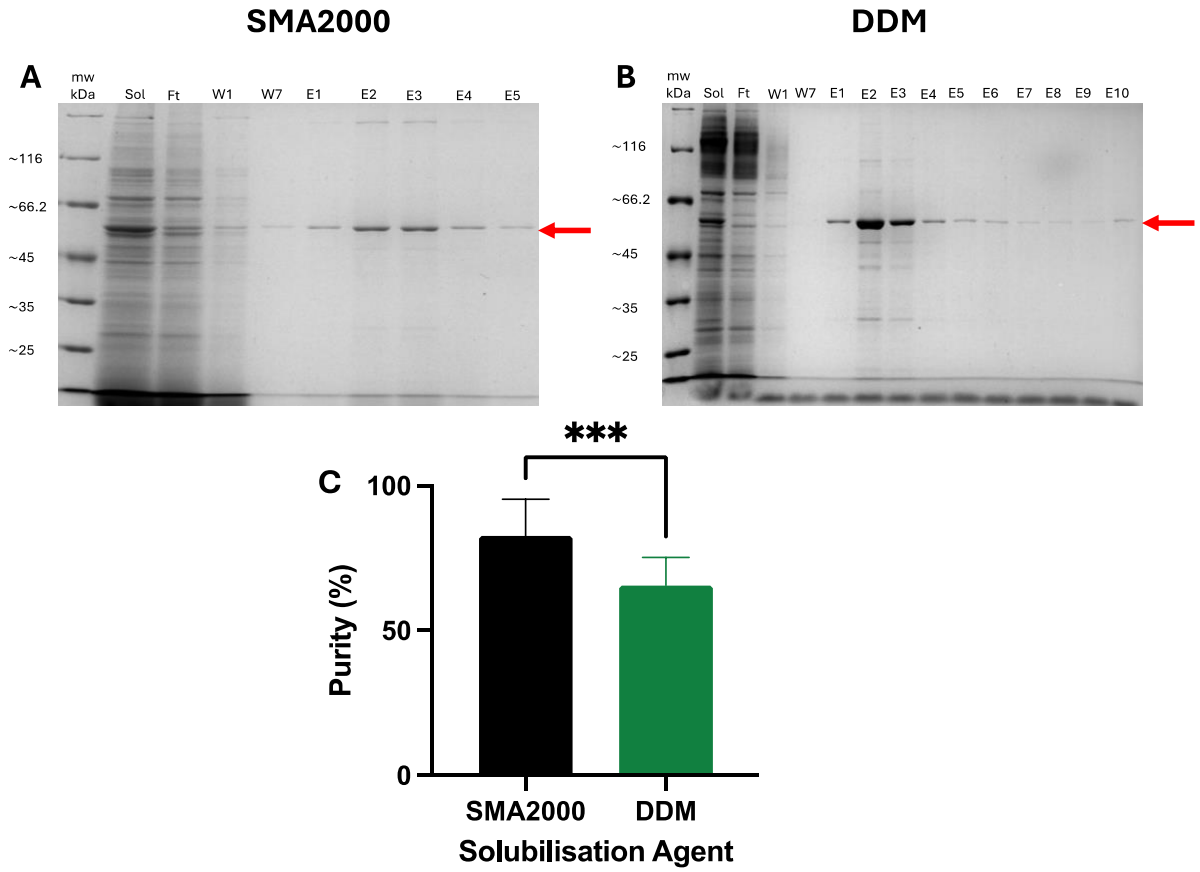

Figure 3.3 : SMA2000 provides a higher level of BmrA purity compared to DDM. A) Purification SDS-PAGE gel of SMA2000 solubilised BmrA$^+$ *E. coli* membranes (60mg/ml). 20µl samples of solubilised (Sol), pellet (Pt), washes one and seven (W1 and W7) and elutions one to five (E1-5) loaded and stained with Instantblue. B) Purification SDS-PAGE gel of DDM solubilised BmrA$^+$ *E. coli* membranes (60mg/ml). 10µl samples of solubilised (Sol), pellet (Pt), washes one and seven (W1 and W7) and elutions one to ten (E1-10) loaded and stained with Instantblue. C) BmrA purity calculated by densitometry and presented as mean ± SD, n ≥11. Data analysed by unpaired T-test with ***p ≤ 0.001.

BmrA was successfully purified by Ni-affinity chromatography following solubilisation into SMA2000 nanodiscs and DDM micelles, as shown by the highlighted bands in elution fractions E1 to E5 in figure 3.3 A and elution fractions E1 to E10 in figure 3.3 B. The purity of BmrA was also maintained to a good level, but SMA2000 presents with a significantly higher purity level with a mean of 83±12.6% when compared to DDM with a mean of 66±9.7% in figure 3.3 C.

3.1.4 LSB Dimer Check

The presence of a higher molecular weight band in the elution fractions on SDS-PAGE and western blots was consistently observed. As BmrA is known to function as a homodimer at a size of ~130kDa, this upper band may represent dimeric BmrA and prompted further investigation. LSB can deteriorate over time and exhibit a reduced ability to break down complex forming disulphide bonds. To quickly probe this, LSB was freshly prepared and mixed with purification samples and ran on SDS-PAGE (Figure 3.4).

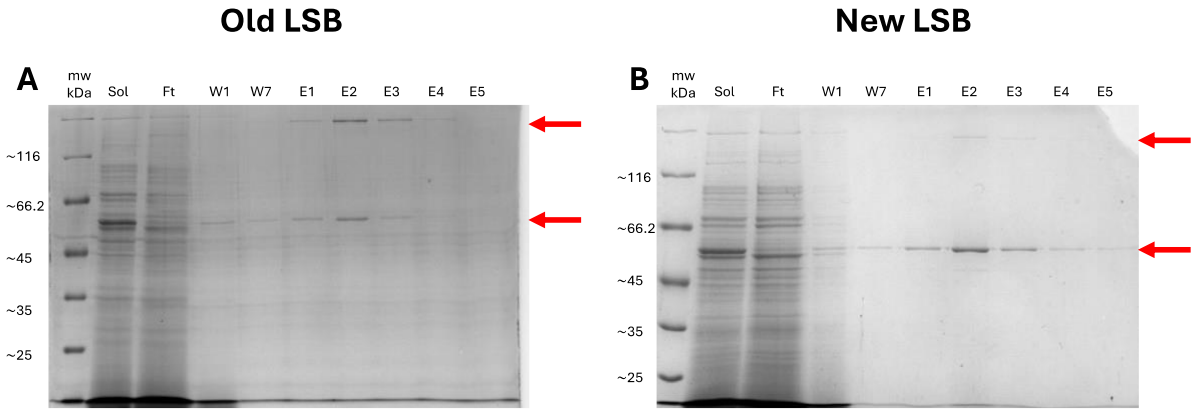

Figure 3.4 : The use of freshly prepared LSB reduces the presence of the higher molecular weight band. Purification SDS-PAGE gel of SMA2000 solubilised BmrA^{+} *E. coli* membranes (60mg/ml). 20µl samples of solubilised (Sol), pellet (Pt), washes one and seven (W1 and W7) and elutions one to five (E1-5) loaded with old LSB (A) or freshly prepared LSB (B).

The use of freshly prepared LSB in Figure 3.4 appears to reduce the presence of the higher molecular weight band at ~130kDa, while increasing the presence of the BmrA band at ~65kDa. This provides evidence to suggest that the upper band represents a BmrA dimer.

3.1.5 BmrA Mass Spectrometry

To further confirm identity, mass spectrometry was utilised – with upper and lower bands from a purification SDS-PAGE of SMA2000 solubilised BmrA excised and analysed (Figure 3.5).

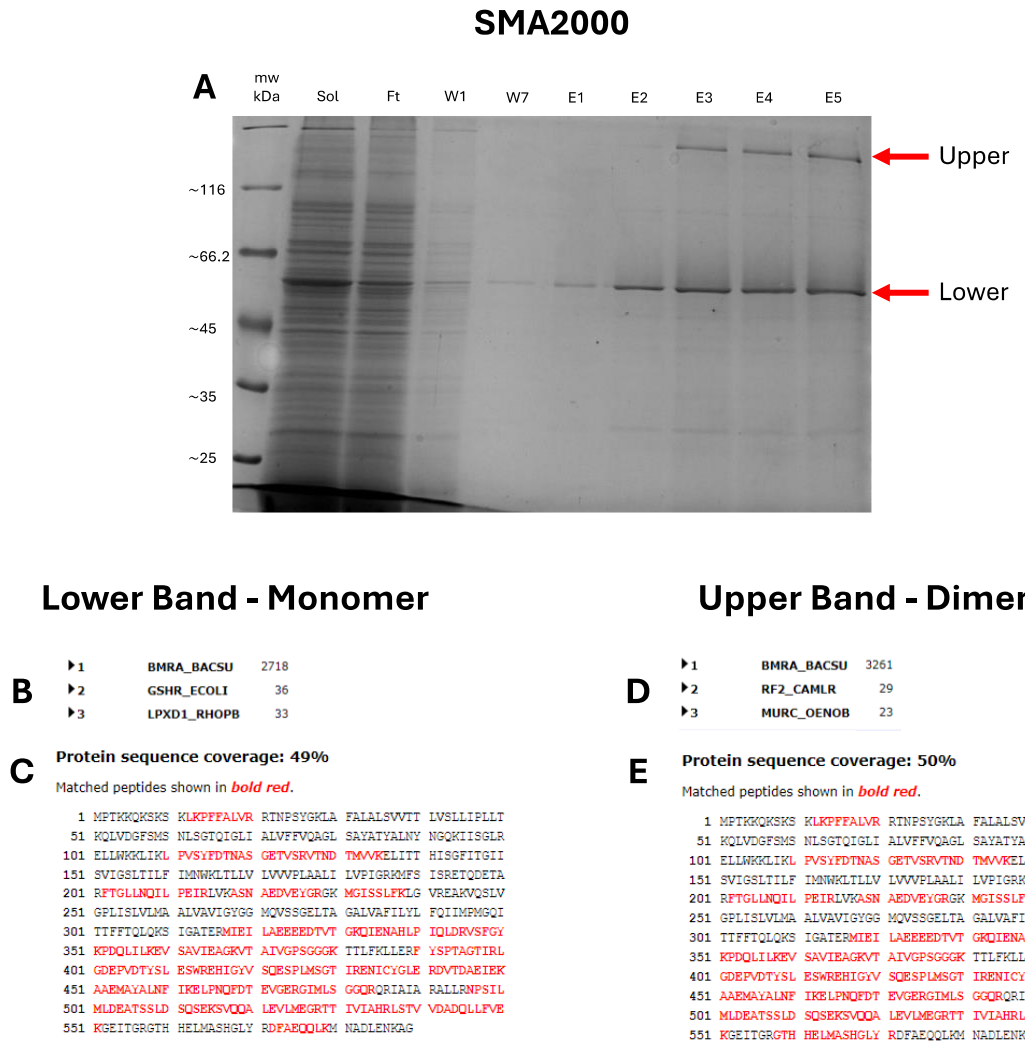

Figure 3.5 : Mascot results for mass spectrometry analysis of upper and lower bands in SDS-PAGE. A) Purification SDS-PAGE gel of SMA2000 solubilised BmrA^{+} *E. coli* membranes. Upper and lower bands which were cut out and analysed highlighted. B) The top three protein matches and total score for lower band. C) Protein sequence coverage for lower band. D) The top three protein matches and total score for upper band. E) Protein sequence coverage for upper band. Data provided courtesy of Dr Ophelie Langlois, Aston University.

Utilising older LSB stocks to induce higher presence of the upper band in Figure 3.5 A resulted in clean bands for analysis by mass spectrometry. Results shown in Figure 3.5 B and D confirms the identification of both the lower (monomer) and upper (dimer) bands as BmrA, with the sequence coverage highlighted in Figure 3.5 C and E. Both bands were therefore utilised in all purity and yield analyses going forward.

3.1.6 BmrA Yield

The yield of purified BmrA was next investigated by running samples on SDS-PAGE alongside BSA controls (Figure 3.6 A and B) and analysed by densitometry (Figure 3.6 C).

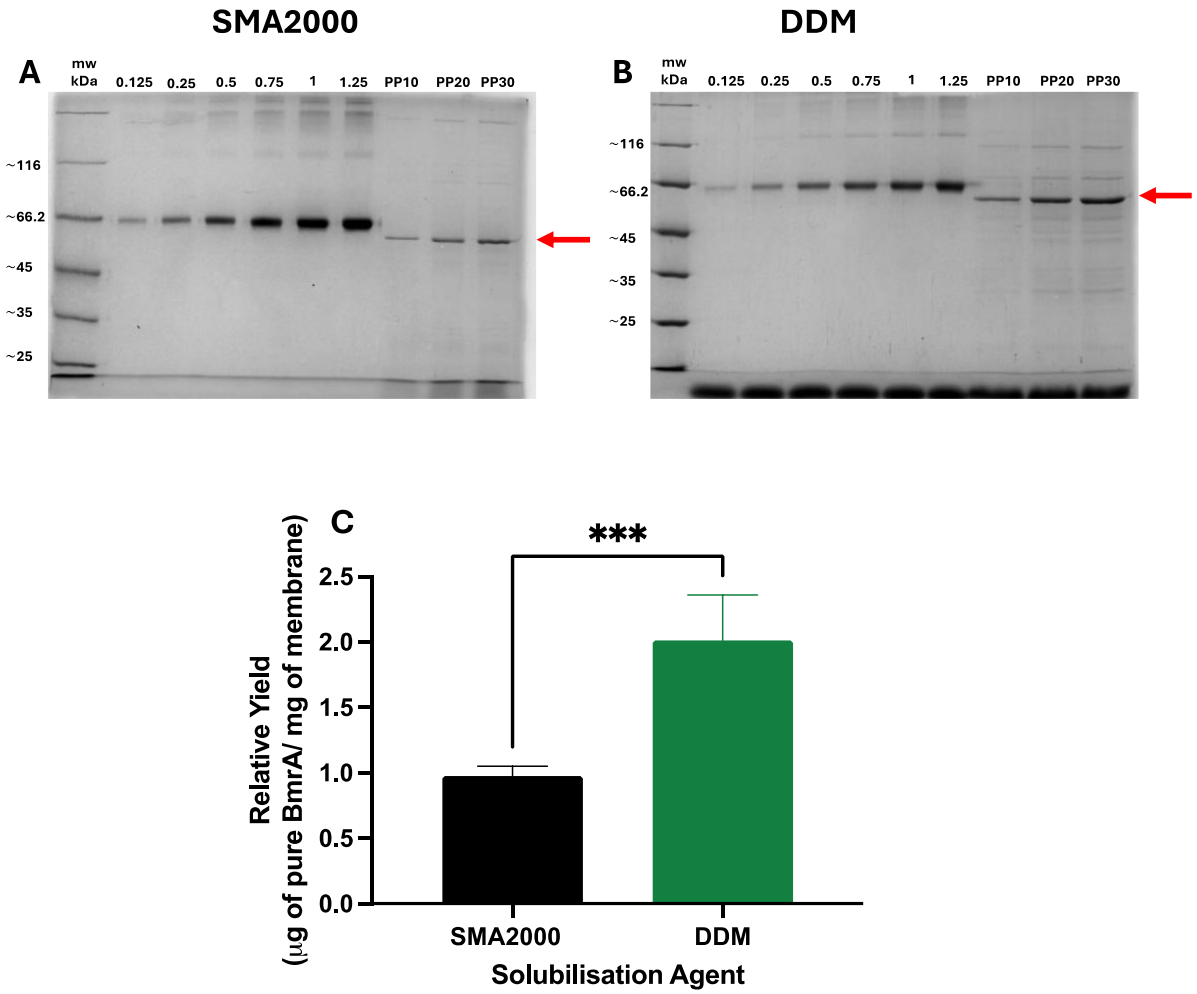

Figure 3.6 : DDM solubilisation produces a significantly higher yield of BmrA when compared to SMA2000. Quantification SDS-PAGE gel of SMA2000 (A) and DDM (B) solubilised BmrA. 20µl samples of a standard range of BSA (0.125-1.25µg/ml) loaded alongside 10µl , 20µl and 30µl of pooled purified protein (PP10, PP20 and PP30). C) BmrA relative yield was calculated by densitometry and presented as mean ± SEM, n ≥8. Data analysed by unpaired t-test with ***p ≤0.001.

Pooled purified BmrA in SMA2000 and DDM presents well in SDS-PAGE in figure 3.6 A and B. However, DDM clearly shows a higher level of contaminating band, supporting previous results. Regardless, the use of SMA2000 significantly reduces the yield of purified BmrA when compared to DDM in figure 3.6C. While DDM gives a yield of 2±1µg/mg, SMA2000 produces just 0.975±0.4µg/mg.

3.1.7 Sensitivity

One of the major drawbacks of SMA2000 suitability for ABC transporter functional study is the sensitivity to divalent cations. This is because of the requirement of Mg^{2+} as a co-factor for ATP hydrolysis and ATPase activity. To quantify this sensitivity, purified protein-lipid and lipid-only nanodiscs were tested using a centrifugation and SDS-PAGE based assay (Figure 3.7 A and B) and a light scattering assay (Figure 3.7 C). While a negative axis represents the loss of soluble BmrA in protein-lipid samples, a positive axis for lipid-only samples represents an increase in scattering as soluble BmrA is lost.

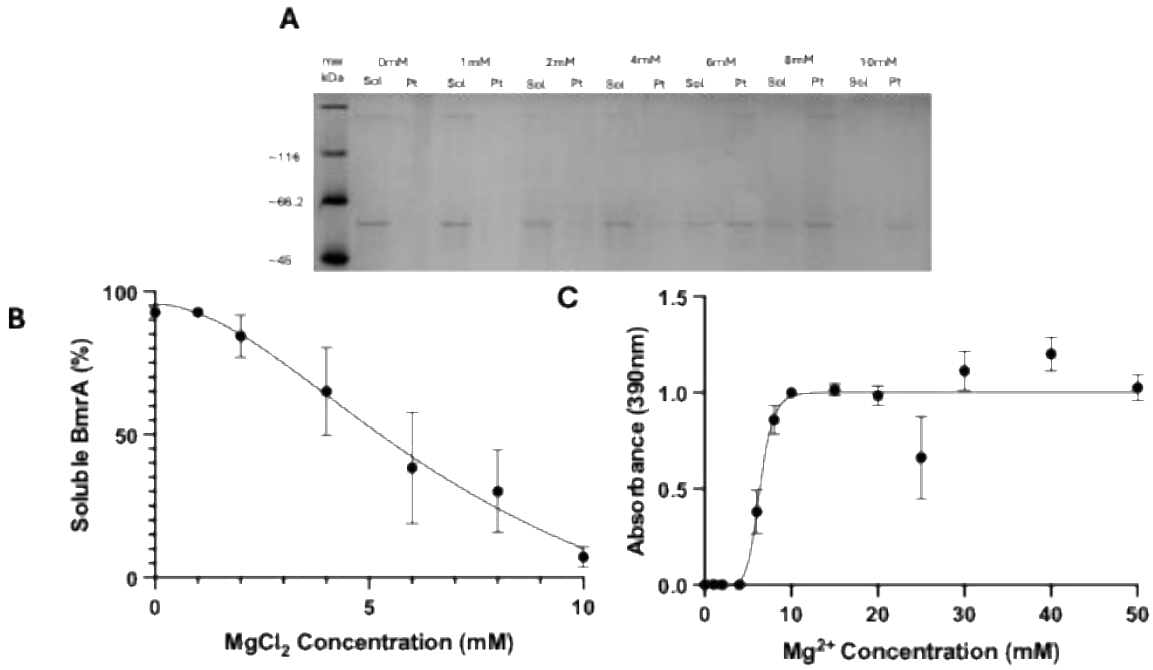

Figure 3.7 : SMA2000 solubilised protein-lipid and lipid-only discs exhibit a sensitivity to magnesium. A) SDS-PAGE gel of SMA2000 solubilised and purified BmrA mixed with different concentrations of magnesium (0-10mM) and centrifuged (100,000 x g, 20 min, 4°C) with supernatant (Sol) and pellet (Pt) samples taken and loaded onto SDS-PAGE and stained with Instantblue. B) Graph showing loss of soluble BmrA as magnesium concentration increases. Percentage of soluble BmrA (%) calculated by densitometry and presented as mean ± SEM, n ≥3. C) Graph showing an increase in scattering of lipid-only nanodiscs as magnesium concentration increases. Purified lipid-only nanodiscs are mixed with different concentrations of magnesium (0-50mM) in a 96 well plate format and scanned at 390nm. Data presented as mean ± SEM, n ≥3 where error bars are shown.

As the concentration of magnesium increases from 0mM to 10mM, there is a visible shift of protein from the soluble (sol) to the insoluble (pt) fractions as seen in figure 3.7 A. This relationship was quantified in figure 3.7 B, with SMA2000 displaying a dose-dependent sensitivity with around half of total soluble BmrA precipitating at 5mM magnesium. This is

supported in lipid-only scattering study in figure 3.7 C, with SMA2000 displaying a rapid increase in scattering between 0mM to 10mM magnesium and an EC_{50} of 6mM.

3.1.8 SMA variants

To try an overcome some of the reported limitations of SMA2000, a range of modified SMA polymers were developed (Figure 3.8) and made commercially available. SMA-EA was the first variant synthesised from styrene anhydride via a nucleophilic ring opening reaction using ethanolamine (Table 3.2). It was reported that SMA-EA exhibited an increased tolerance to magnesium when compared to SMA2000 (Ravula, *et al.,* 2017a) and therefore more variants were produced. SMA-ED - a zwitterionic analogue of SMA2000 – was synthesised using ethylenediamine before further modifying into the acid stable SMAd-A by dehydration reactions creating a maleimide group (Table 3.2). SMA-QA was also synthesised using aminoethyltrimethylammonium to form a polymer with a pH independent hydrophilic group (Table 3.2). SMA-ED, SMA-d-A and SMA-QA were also reported to exhibit some degree of magnesium tolerance (Ravula, *et al. ,*2017b and Ravula, *et al.,* 2018), and all four SMA variants – SMA-EA, SMA-ED, SMAd-A and SMA-QA were therefore tested in the solubilisation of BmrA.

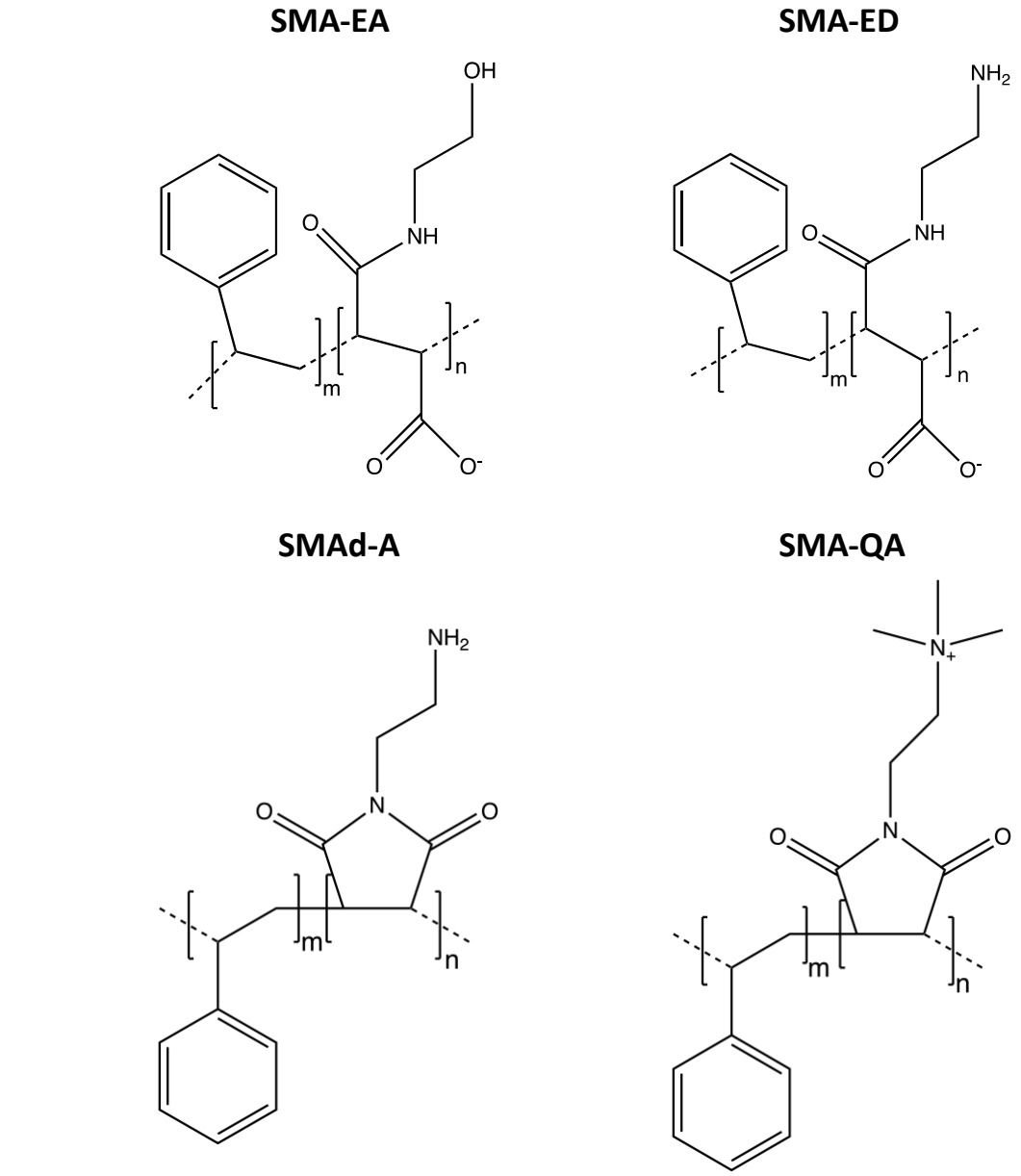

Figure 3.8 : Representation of the chemical structure of SMA variants SMA-EA, SMA-ED, SMAd-A and SMA-QA. 'm' represents the number of repeating apolar styrene moiety while 'n' represents the number of repeating polar maleic acid/maleimide moiety. Created using ChemDraw v21.0.0.

Table 3.2 : Co-polymer information. Chemical and structural characteristics of SMA variants as per manufacturer. Ratio, styrene to maleic acid/maleimide; Mw, weight average molecular weight

Name	Manufacturer	Apolar Subunit	Polar Subunit	Chemical Modifications	Ratio (S:M)	Mw (kDa)
SMA-EA	Anatrace	Styrene	Maleic acid	Ethanolamine	1.3 : 1	7.8
SMA-ED	Anatrace	Styrene	Maleic acid	Ethylenediamine	1.3 : 1	7.8
SMAd-A	Anatrace	Styrene	Maleimide	Dehydrated ethylenediamine	1.3 : 1	7.8
SMA-QA	Anatrace	Styrene	Maleimide	Aminoethyltrimethylammonium	1 : 1	9

3.1.9 BmrA Solubilisation Efficiency

The efficiency of SMA variants SMA-EA and SMA-ED to extract BmrA from *E. coli* was first tested. Supernatant and pellet samples were investigated by western blot (Figure 3.9 A and B) and analysed by densitometry of western blots (Figure 3.9 C).

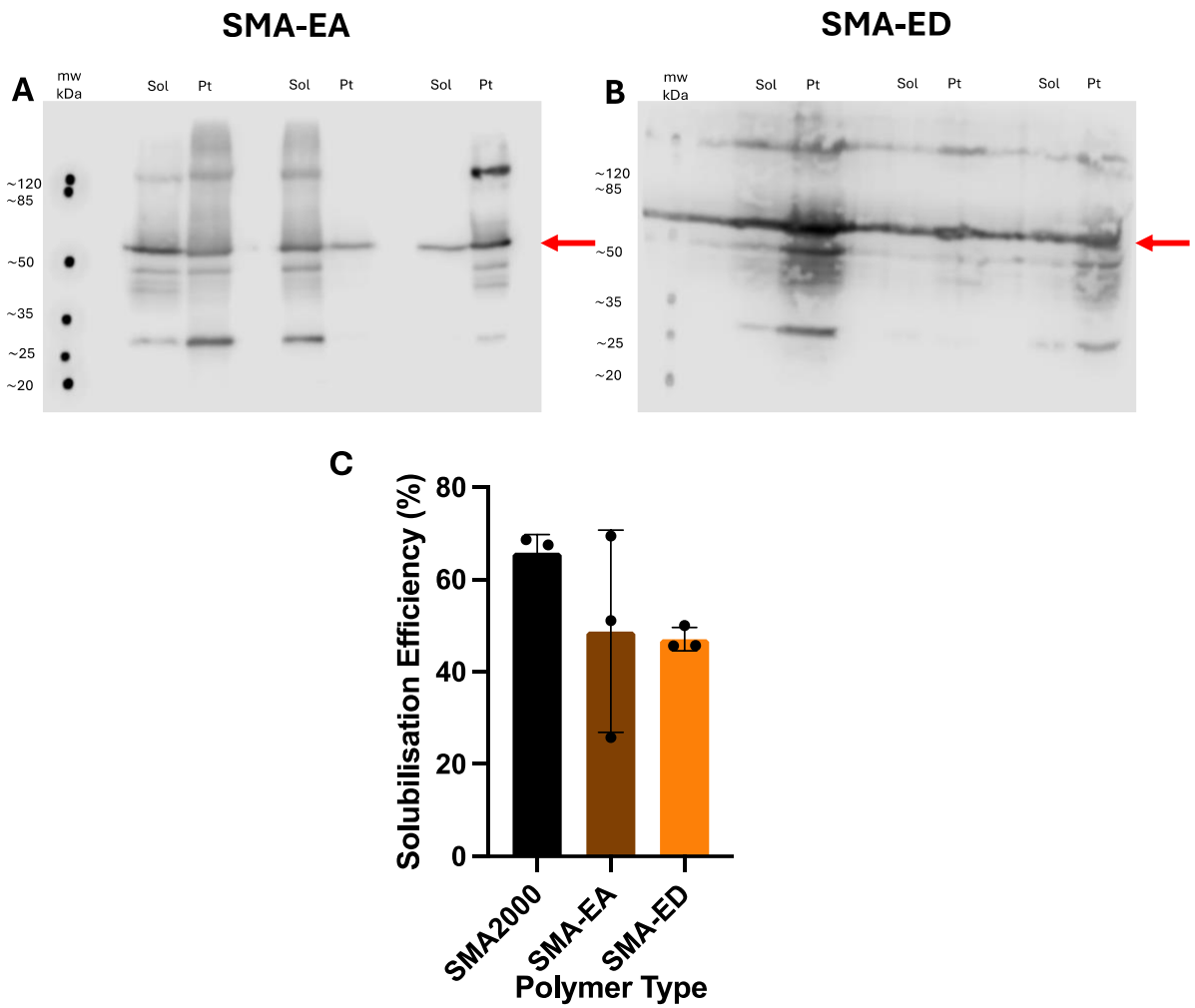

Figure 3.9 : SMA variants SMA-EA and SMA-ED are able to solubilise BmrA. BmrA and *E. coli* membranes (60mg/ml) were mixed with equal volume of 5% (w/v) SMA-EA (A) and SMA-ED (B) for 1 hour at room temperature. Samples were then centrifuged (100,000 x g, 20 min, 4°C) with supernatant (Sol) and pellet (Pt) samples collected. 10µl samples of biological repeats were analysed by western blot, probed with 1:4000 mouse α-his Ab and 1:10000 α-mouse-HRP Ab. Membrane visualised using West Pico Plus and LI-COR imaging system. Solubilisation efficiency calculated by densitometry (C) with data shown as mean ± SD, n ≥3. Data analysed by one-way ANOVA with no significance found. SMA data reproduced from Figure 3.2.

SMA-EA and SMA-ED were both able to solubilise BmrA with bands corresponding to BmrA highlighted on western blots in figure 3.9 A and B. Analysis of efficiency in figure 3.9 C shows SMA-EA and SMA-ED are comparable to SMA2000 in the solubilisation of BmrA. SMA2000 maintains an efficiency of 66±3.9% while SMA-EA and SMA-ED exhibit efficiencies of 49±22% and 47±2.5% respectively. However, SMA-EA also appeared to exhibit a higher degree of variability when compared to SMA2000 and SMA-ED.

3.1.10 BmrA Purity

The ability to use the modified SMA polymers for BmrA purification was also investigated using Ni-affinity chromatography (Figure 3.10 A - D) and analysed by densitometry (Figure 3.10 E).

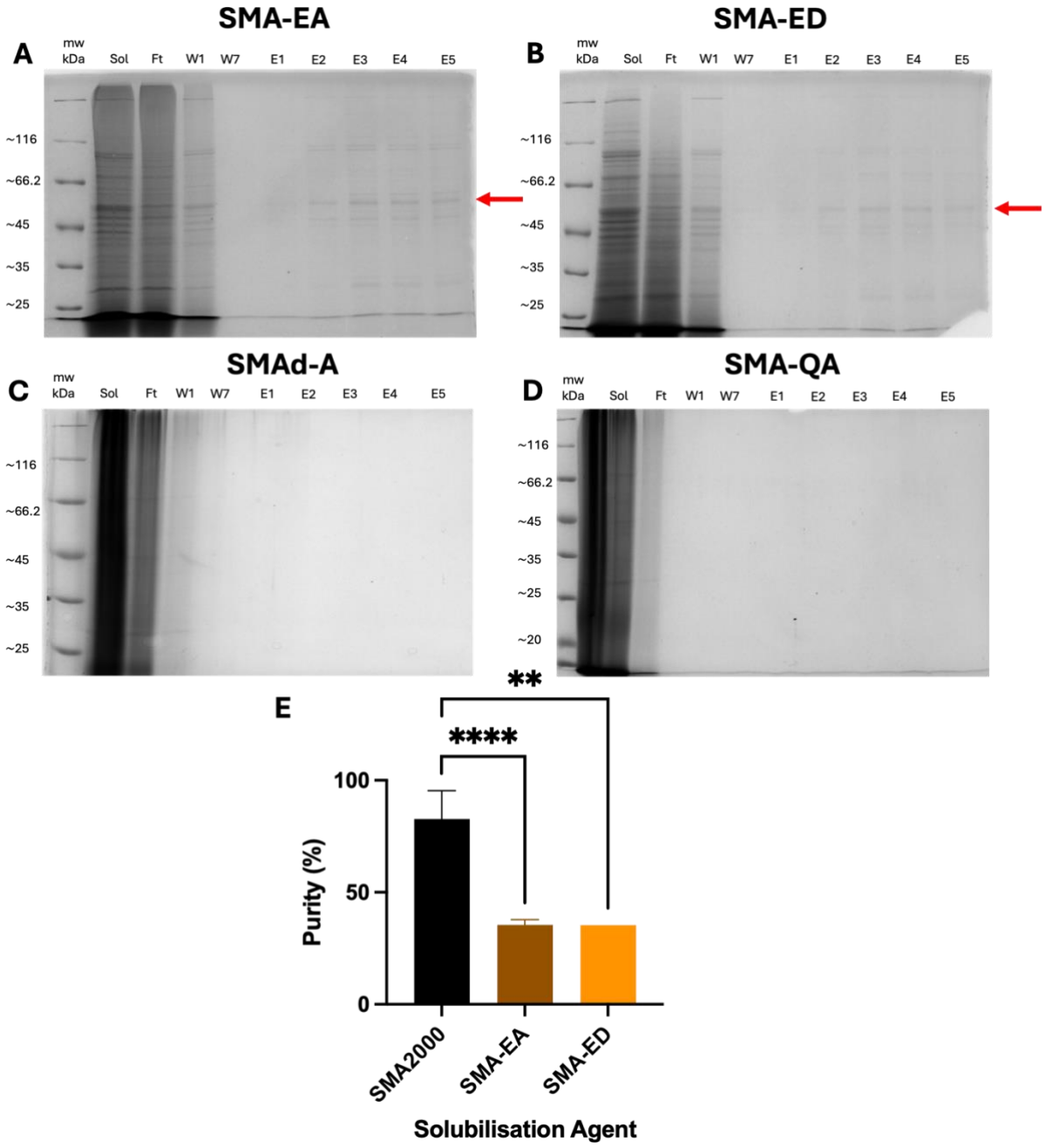

Figure 3.10 : SMA variants SMA-EA and SMA-ED exhibit a significantly lower level of purity when compared to SMA2000. Purification SDS-PAGE gels of SMA-EA (A), SMA-ED (B), SMAd-A (C) and SMA-QA (D) solubilised $BmrA^{+}$ *E. coli* membranes (60mg/ml). 20µl samples of solubilised (Sol), pellet (Pt), washes one and seven (W1 and W7) and elutions one to five (E1-5) loaded and stained with Instantblue. E) BmrA purity calculated by densitometry and presented as mean ± SD, n ≥1. Data analysed by one-way ANOVA with ****p ≤ 0.0001 and ** p ≤ 0.01. SMA data reproduced from Figure 3.3.

SMA-EA and SMA-ED are both able to produce purified BmrA as shown in figure 3.10 A and B, with bands corresponding to BmrA found in E1 to E5. However, they are not very intense and present with multiple contaminating bands. In contrast, SMAd-A and SMA-QA do not seem to produce any purified BmrA with no protein observed in any of the elution fractions as seen in figure 3.10 C and D. Due to this, SMAd-A and SMA-QA were not further tested. Upon analysis SMA variants SMA-EA and SMA-ED were found to provide significantly lower levels of BmrA purity when compared to SMA2000 in figure 3.10 E. SMA2000 maintains a mean purity of 83±12.6%, while SMA-EA and SMA-ED produce only 35±2.4% and 35% purity respectively.

3.1.11 BmrA Yield

The yield of purified BmrA was then investigated by running samples on SDS-PAGE alongside BSA controls (Figure 3.11 A and B) and analysed by densitometry (Figure 3.11 C).

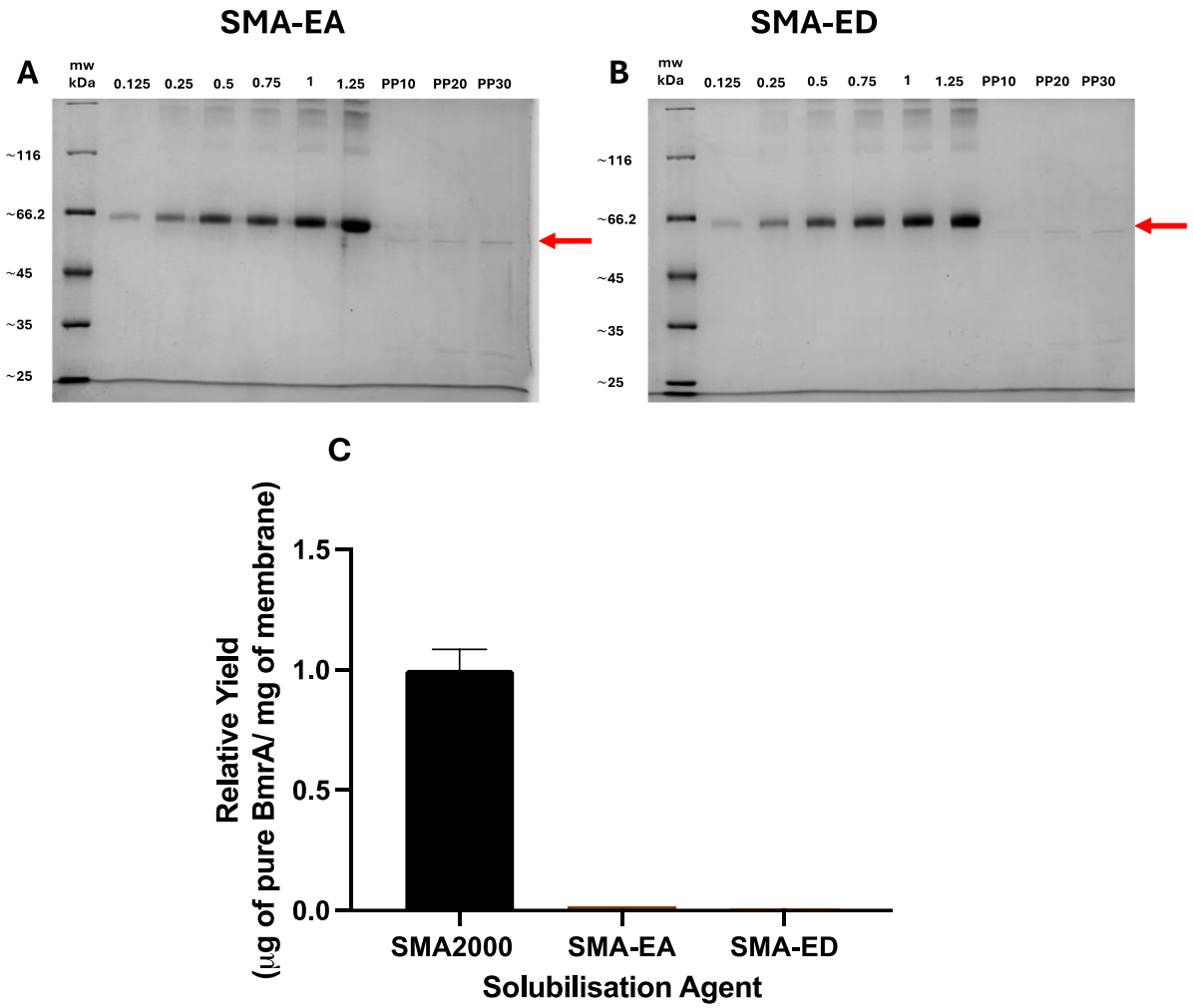

Figure 3.11 : SMA variants SMA-EA and SMA-ED produce a lower level of BmrA yield when compared to SMA2000. Quantification SDS-PAGE gel of SMA-EA (A) and SMA-ED (B) solubilised and purified BmrA. 20µl samples of a standard range of BSA (0.125-1.25µg/ml) loaded alongside 10µl , 20µl and 30µl of pooled purified protein (PP10, PP20 and PP30). C) BmrA relative yield was calculated by densitometry and presented as mean ± SEM, n ≥1. SMA data reproduced from Figure 3.6.

There is a low presence of BmrA in SDS-PAGE when utilising SMA-EA and SMA-ED in figure 3.11 A and B. The relative yield was analysed in figure 3.11 C with SMA-EA and SMA-ED presenting with yields of 0.015µg/mg and 0.007µg/mg. While they appear to produce a much lower yield when compared to SMA2000, no statistical significance was found. SMA variants were not taken forward for further testing attributing to the low efficiency and BmrA purity and yield.

3.1.12 DIBMA and Glyco-DIBMA

The next polymers to be tested were DIBMA and Glyco-DIBMA. This group were developed in response to the magnesium sensitivity reported with SMA2000 (Gulamhussein, *et al.,* 2020) and the difficulty in spectroscopy study reported with SMA2000 and SMA variants due to absorption around 260 nm (Oluwole, *et al.,* 2017).

In place of the aromatic styrene, DIBMA contains an aliphatic diisobutylene group in a 1:1 ratio with maleic acid (Figure 3.12). This reduces overall polymer hydrophobicity and results in a polymer that does not absorb UV in the region of 260nm. DIBMA has been shown to exhibit a lower sensitivity to magnesium and a larger disc size but can produce lower efficiencies when compared to SMA2000 (Oluwole, *et al.,* 2017). To investigate the reported magnesium tolerance, DIBMA was selected for study.

Glyco-DIBMA is a functionalised variant of DIBMA (Figure 3.12) that is partially amidated with the sugar residue meglumine (Table 3.3) created in response to lower solubilisation efficiencies reported for DIBMA. This modification reduces polymer charge, increases hydrophobicity and maintains solubilisation efficiency. Glyco-DIBMA has been shown to successfully solubilise BmrA (Gulamhussein, *et al.,* 2020) and produce discs of similar size to SMA2000 (Danielczak, *et al.,* 2022) and was therefore also selected for study.

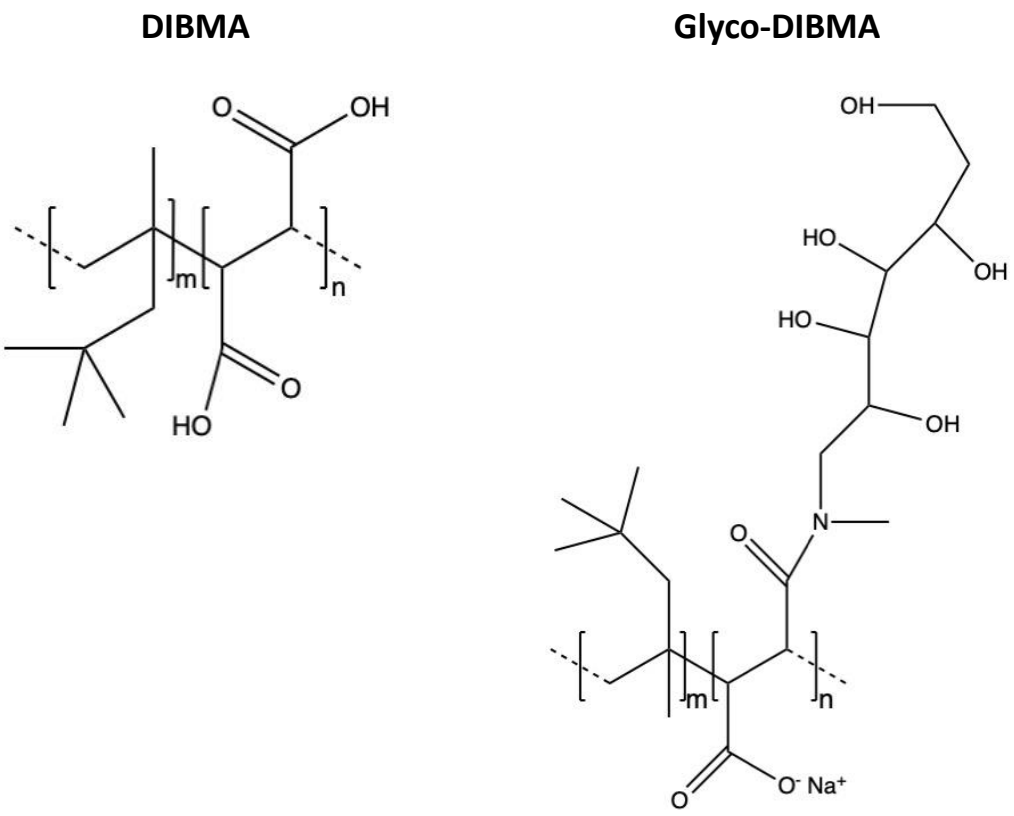

Figure 3.12 : Representation of the chemical structure of DIBMA and Glyco-DIBMA. 'm' represents the number of repeating apolar diisobutylene moiety while 'n' represents number of repeating the polar maleic acid moiety. Created using ChemDraw v21.0.0.

Table 3.3 : Co-polymer information. Table of chemical and structural characteristics of DIBMA and Glyco-DIBMA as per manufacturer. Ratio, diisobutylene to maleic acid; Mw, weight average molecular weight; Mn, number average molecular weight.

Name	Manufacturer	Apolar Subunit	Polar Subunit	Chemical Modifications	Ratio (D:M)	Mw (kDa)	Mn (kDa)
DIBMA Monosodium Salt	Glycon Biochemicals	Diisobutylene	Maleic acid	N/A	1 to 1	12	8.4
Glyco-DIBMA	Glycon Biochemicals	Diisobutylene	Maleic acid	Partial amidation with N-methyl-D-glucamine	1 to 1	15.7	-

3.1.13 BmrA Solubilisation Efficiency

The efficiency of DIBMA and Glyco-DIBMA to solubilise BmrA from *E. coli* was investigated. Supernatant and pellet samples were probed in western blots (Figure 3.13 A and B) and analysed by densitometry of western blots (Figure 3.13 C).

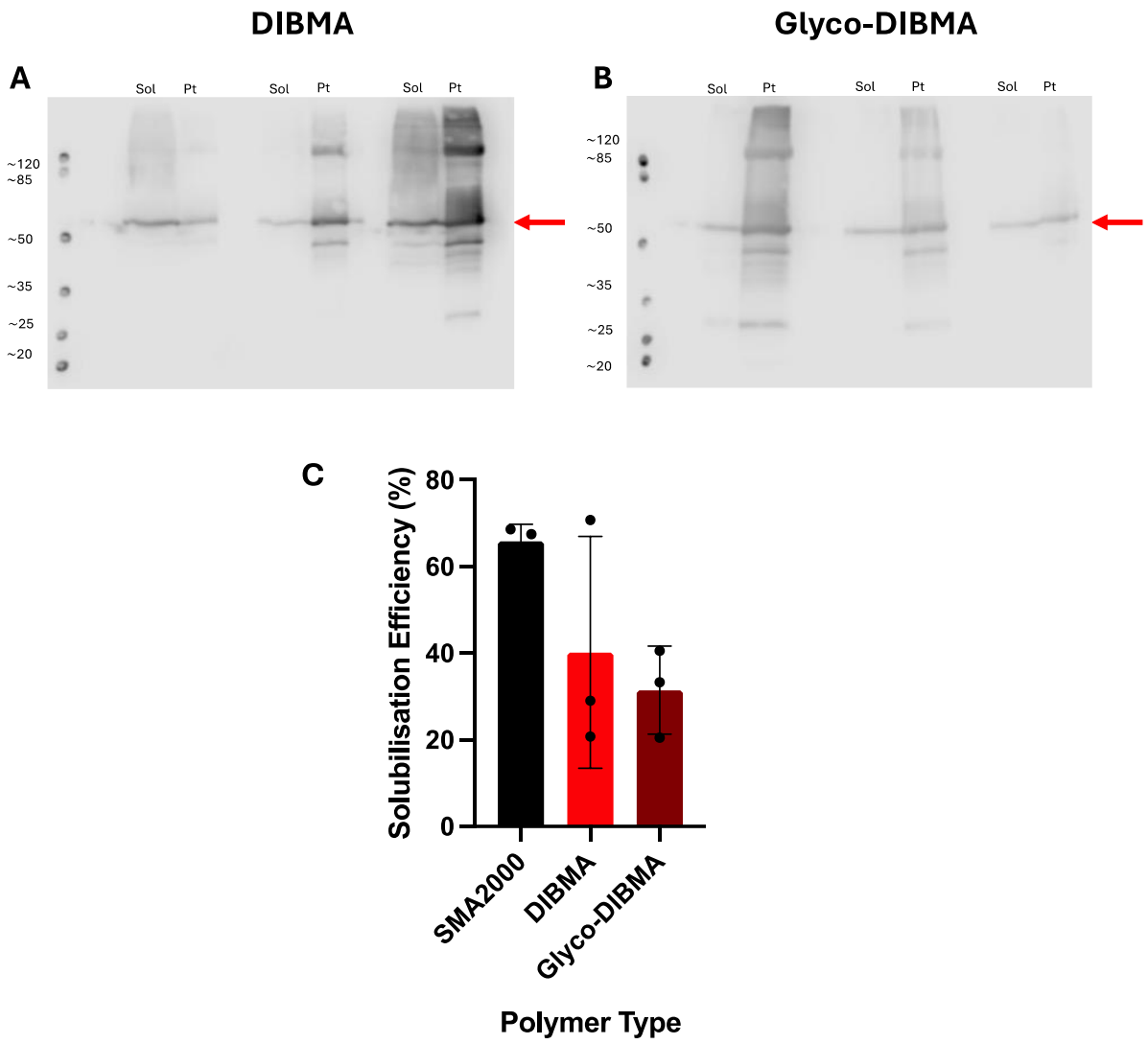

Figure 3.13 : DIBMA and Glyco-DIBMA exhibit a lower solubilisation efficiency when compared to SMA2000. BmrA$^+$ *E. coli* membranes (60mg/ml) were mixed with equal volume of 5% (w/v) DIBMA (A) and Glyco-DIBMA (B) for 1 hour at room temperature. Samples were then centrifuged (100,000 x g, 20 min, 4°C) with supernatant (Sol) and pellet (Pt) samples collected. 10µl samples were analysed by western blot, probed with 1:4000 mouse α-his and 1:10000 Ab α-mouse-HRP. Membrane visualised using West Pico Plus and LI-COR imaging system. Solubilisation efficiency calculated by densitometry (C) with data shown as mean ± SD, n ≥3. Data analysed by one-way ANOVA with no significance found. SMA data reproduced from Figure 3.2.

DIBMA and Glyco-DIBMA are both able to solubilise BmrA as shown in figure 3.13 A and B, with bands corresponding to BmrA highlighted. Although the solubilisation efficiency appears lower for DIBMA and Glyco-DIBMA (40±27% and 31±10% respectively) when compared to SMA2000 (66±4%), this was not statistically significant.

3.1.14 BmrA Purity

The affinity purification of DIBMA and Glyco-DIBMA solubilised BmrA was then tested (Figure 3.14 A and B) and purity analysed by densitometry (Figure 3.14 C).

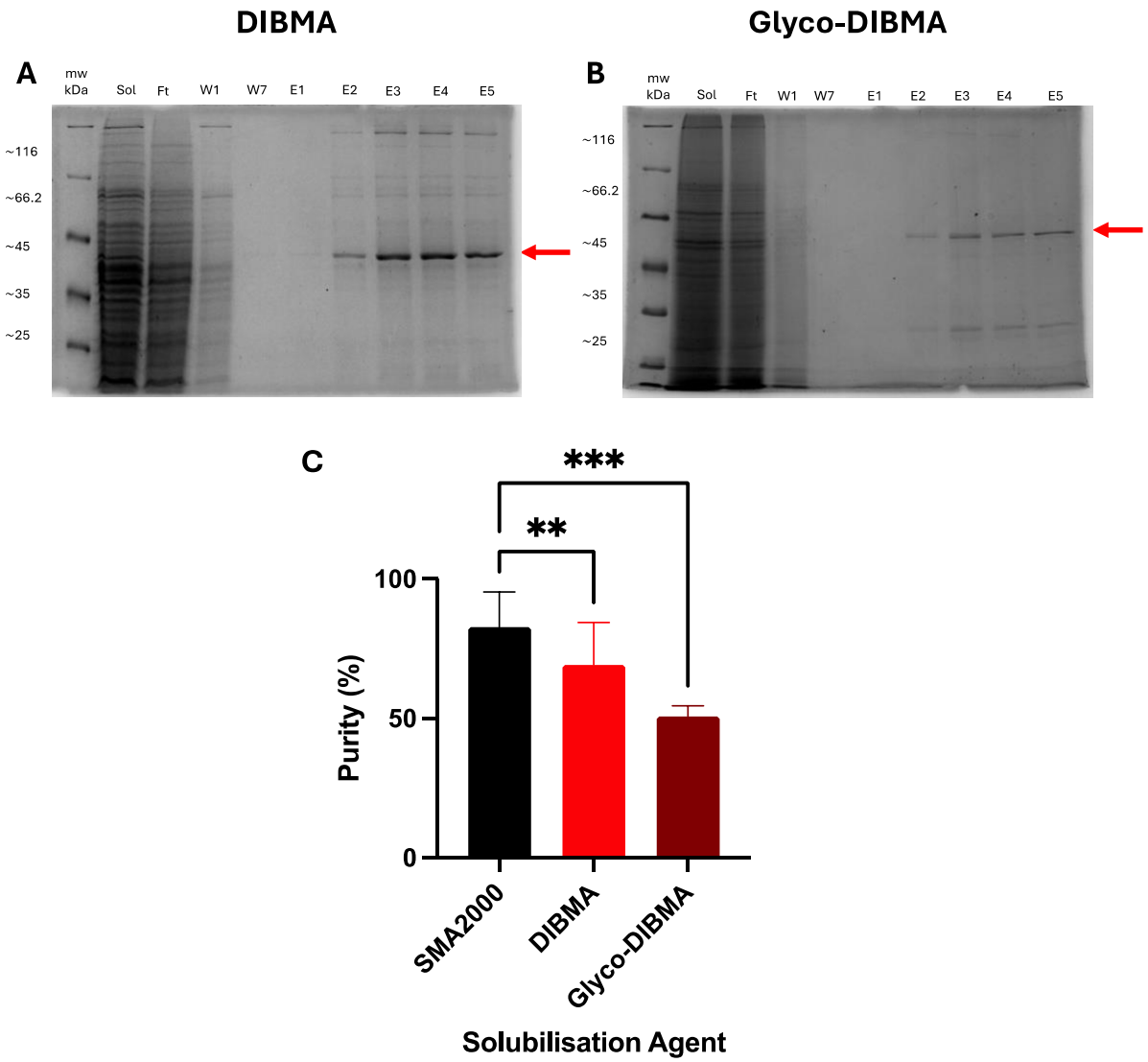

Figure 3.14 : DIBMA and Glyco-DIBMA produce a significantly lower level of purity when compared to SMA2000. Purification SDS-PAGE gel of DIBMA (A) and Glyco-DIBMA (B) solubilised BmrA^{+} *E. coli* membranes (60mg/ml). 20µl samples of solubilised (Sol), pellet (Pt), washes one and seven (W1 and W7) and elutions one to five (E1-5) loaded and stained with Instantblue. C) BmrA purity calculated by densitometry and presented as mean ± SD, n ≥3. Data analysed by one-way ANOVA with ***p ≤ 0.001 and ** p ≤ 0.01. SMA data reproduced from Figure 3.3.

DIBMA and Glyco-DIBMA are both able to produce purified BmrA as shown in figure 3.14 A and B, with bands corresponding to BmrA found in E1 to E5. However, DIBMA appears to have higher intensity BmrA bands when compared to Glyco-DIBMA. Both show contaminating bands, but with distinctly different profiles. Analysis of BmrA purity in figure 3.14 C found that both DIBMA and Glyco-DIBMA produce a significantly lower level of BmrA purity (69±15% and 51±4% respectively) when compared to SMA2000 (83±13%).

3.1.15 BmrA Yield

The yield of purified BmrA was then investigated by running samples on SDS-PAGE alongside BSA controls (Figure 3.15 A and B) and analysed by densitometry (Figure 3.15 C).

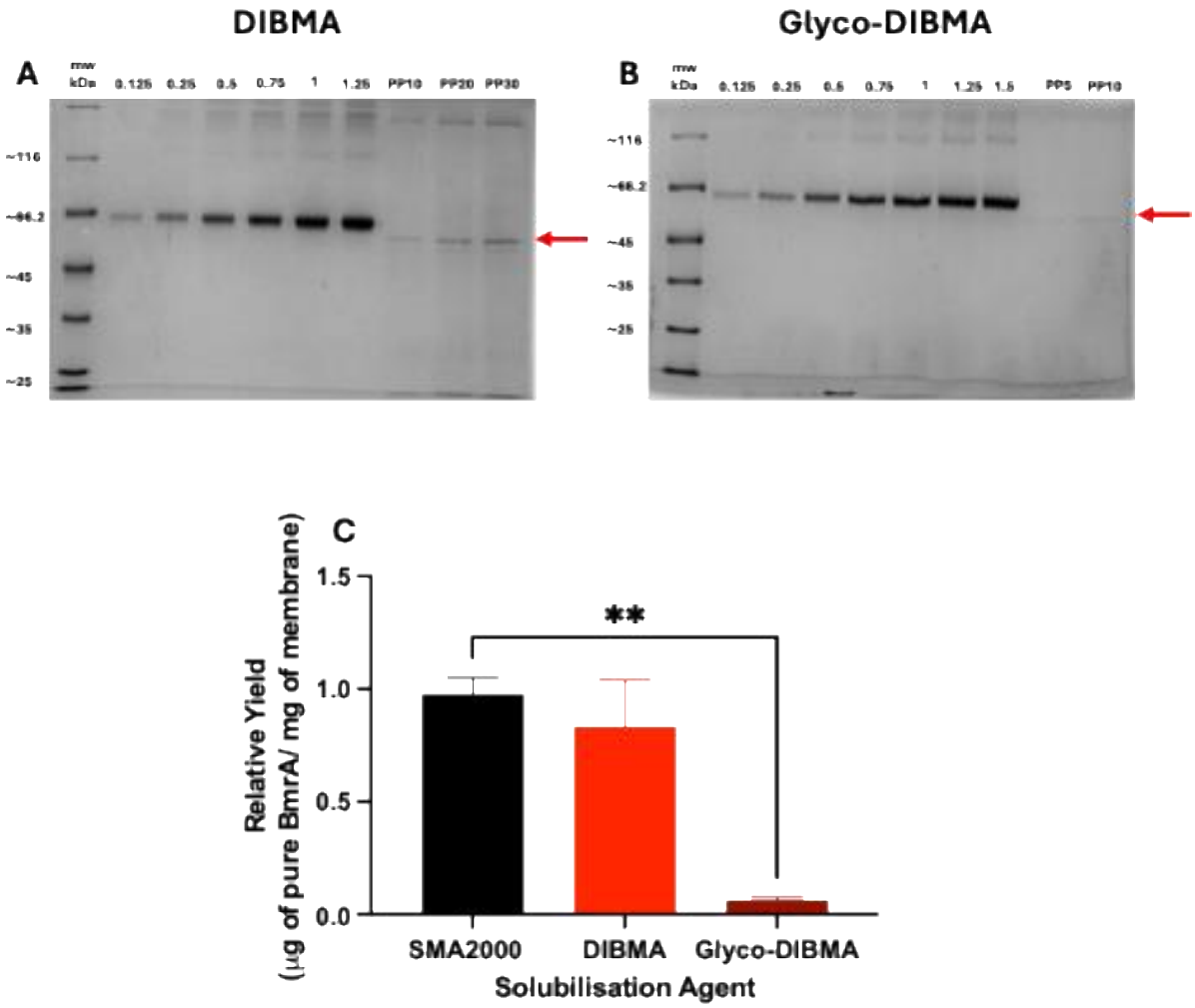

Figure 3.15 : Glyco-DIBMA exhibits a lower level of protein yield when compared to SMA2000. Quantification SDS-PAGE gel of DIBMA (A) and Glyco-DIBMA (B) solubilised BmrA. 20µl samples of a standard range of BSA (0.125-1.25µg/ml) loaded alongside 10µl , 20µl and 30µl of pooled purified (PP10, PP20 and PP30) or 5µl and 10µl (PP5 and PP10). C) BmrA relative yield was calculated by densitometry and presented as mean ± SEM, n ≥3. Analysed with one-way ANOVA showing significance **p ≤0.01. SMA data reproduced from Figure 3.6.

Highlighted bands corresponding to BmrA can be seen in figure 3.15 A and B. The presence is low with both polymers, however BmrA appears more intense in DIBMA when compared to Glyco-DIBMA. A low yield is confirmed in figure 3.15 C where the average data shows Glyco-DIBMA produces a significantly lower yield of BmrA with 0.06±0.02µg/mg when compared to SMA2000 with 0.975±0.4µg/mg. However, DIBMA provides a comparable yield of BmrA with 0.8±0.7µg/mg.

3.1.16 Sensitivity

One of the previously reported advantages of using DIBMA is a higher tolerance to magnesium (Oluwole, *et al.,* 2017). To confirm this tolerance, DIBMA solubilised protein-lipid and lipid-only discs were tested in sensitivity assays using a centrifugation and SDS-PAGE based assay (Figure 3.16 A and B) and a light scattering assay (Figure 3.16 C).

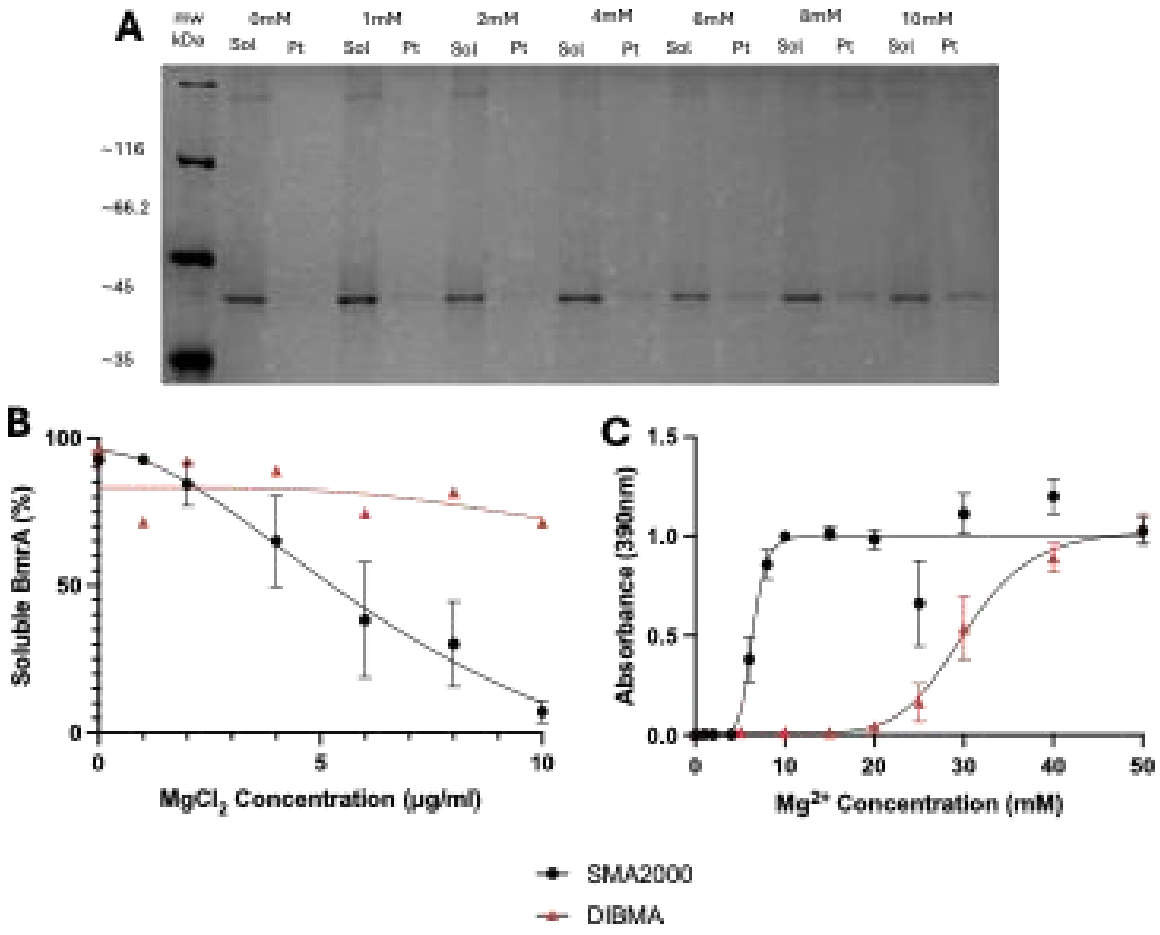

Figure 3.16: DIBMA solubilised protein-lipid and lipid-only discs exhibit a lower sensitivity to magnesium when compared to SMA2000. A) SDS-PAGE gel of DIBMA solubilised and purified BmrA mixed with different concentrations of magnesium (0-10mM) and centrifuged (100,000 x g, 20 min, 4°C) with supernatant (Sol) and pellet (Pt) samples taken and loaded onto SDS-PAGE and stained with Instantblue. B) Graph showing loss of soluble BmrA as magnesium concentration increases. Percentage of soluble BmrA (%) calculated by densitometry and presented as mean ± SEM, n ≥3. C) A graph showing an increase in scattering of lipid-only nanodiscs as magnesium concentration increases. Purified lipid-only nanodiscs are mixed with different concentrations of magnesium (0-50mM) in a 96 well plate format and scanned at 390nm. Data presented as mean ± SEM, n ≥3. SMA data reproduced from Figure 3.7.

As the concentration of magnesium increases from 0mM to 10mM, there is a partial shift of protein from the soluble (sol) to the insoluble (pt) fractions following centrifugation in SDS-PAGE as seen in figure 3.16 A. However, the majority of BmrA remains in the soluble fraction. This is evidenced in figure 3.16 B with DIBMA exhibiting a higher tolerance to magnesium with limited BmrA loss up to 10mM magnesium when compared to SMA2000. This is further supported in figure 3.16 C, with DIBMA lipid-only samples beginning to precipitate around 20mM magnesium with an EC_{50} of 30mM, unlike SMA2000 with maximal scattering around 10mM magnesium and an EC50 of 6mM. The sensitivity of Glyco-DIBMA purified BmrA and lipid-only samples was not tested due to low purity and yield.

3.1.17 AASTY

The final category of polymers explored in this project are the AASTYs. Produced using RAFT rather than free-radical polymerisation, this set of 6 commercially available polymers consist of acrylic acid and styrene in a 1:1 ratio (Figure 3.17 and Table 3.4). These polymers display a highly alternating polymeric structure and have been shown to solubilise membrane proteins in discs ~ 18 nm (Smith, *et al.,* 2020). This is similar to SMA2000, however AASTY also exhibits an increased tolerance to magnesium (Timcenko, *et al.,* 2022).

AASTY

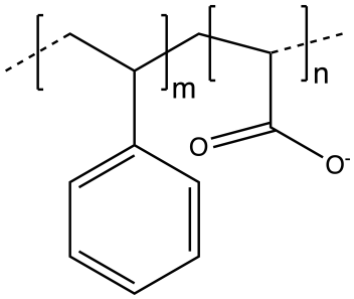

Figure 3.17 : Representation of the chemical structure of AASTY. 'm' represents the number of repeating apolar styrene moiety while 'n' represents the number of repeating polar acrylic acid moiety. Created using ChemDraw v21.0.0.

Table 3.4 : Co-polymer information. Table of chemical and structural characteristics of AASTY polymers as per manufacturer. Ratio, percentage of acrylic acid to styrene; Mw, weight average molecular weight.

Name	Manufacturer	Apolar Subunit	Polar Subunit	Ratio (AA%:S%)	Mw (kDa)
AASTY 6-45	Cube Biotech	Styrene	Acrylic acid	45 : 55	5.5
AASTY 6-50	Cube Biotech	Styrene	Acrylic acid	50 : 50	5.5
AASTY 6-55	Cube Biotech	Styrene	Acrylic acid	55 : 45	5.5
AASTY 11-45	Cube Biotech	Styrene	Acrylic acid	45 : 55	11
AASTY 11-50	Cube Biotech	Styrene	Acrylic acid	50 : 50	11
AASTY 11-55	Cube Biotech	Styrene	Acrylic acid	55 : 45	11

3.1.18 Concentration Trial

The manufacturer of AASTY co-polymers recommends use at a final concentration of 0.5% w/v, which is in contrast to the standard protocol of 2.5% w/v polymer. To confirm this lower concentration was sufficient, a small-scale solubilisation trial was undertaken. Supernatant (Sol) and Pellet (Pt) samples were investigated by western blot (Figure 3.18 A - F) and analysed by densitometry (Figure 3.18 G and H).

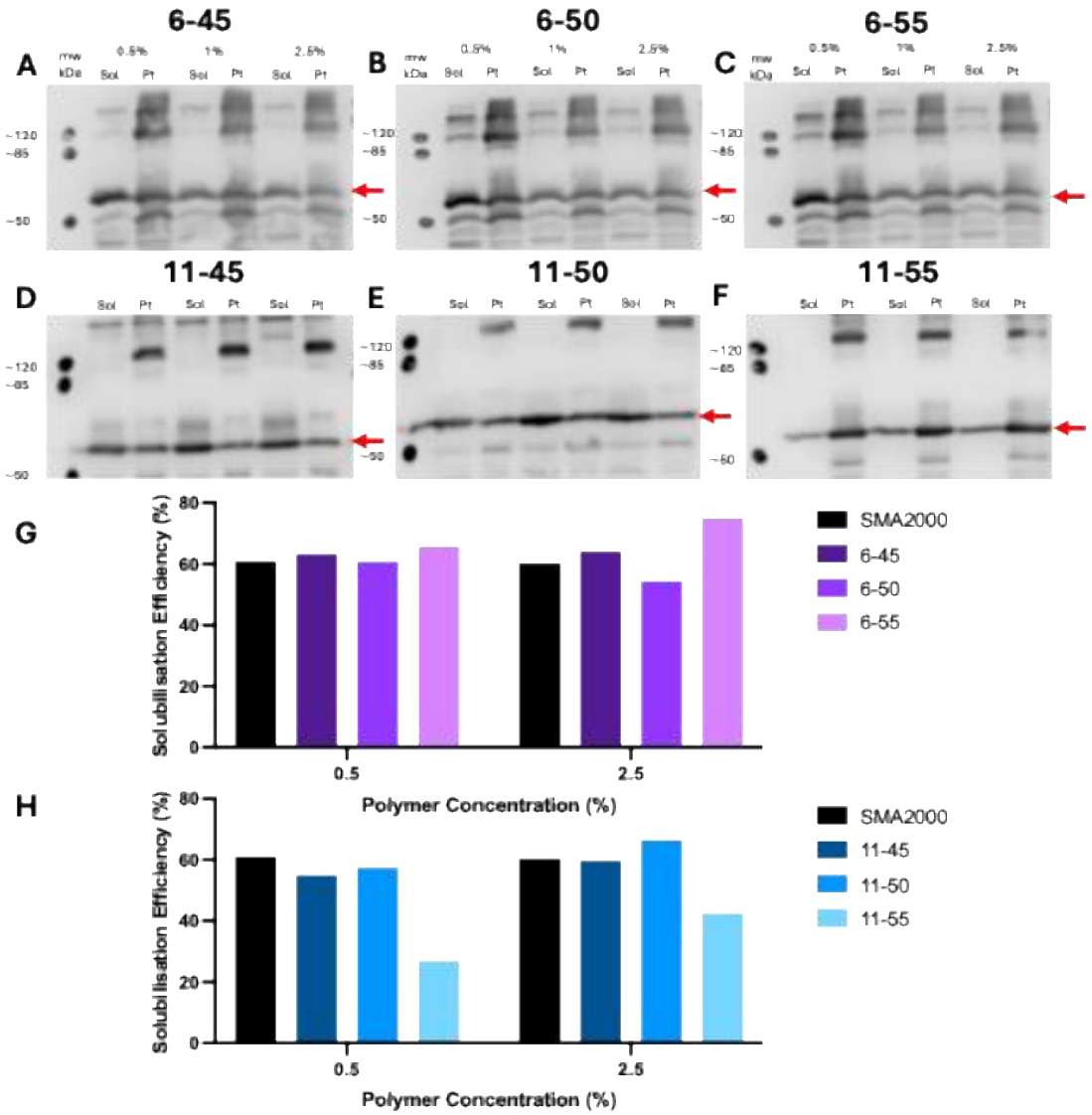

Figure 3.18 : Limited differences in solubilisation efficiency when utilising AASTY co-polymers at 0.5% and 2.5%. BmrA and *E. coli* membranes (60mg/ml) were mixed with 6-45 (A), 6-50 (B), 6-55 (C), 11-45 (D), 11-50 (E) and 11-55 (F) at a final concentration of 0.5, 1 and 2.5% (w/v) for 1 hour at room temperature. Samples centrifuged (100,000 x g, 20 min, 4°C) with supernatant (Sol) and pellet (Pt) samples collected. 10µl samples were analysed by western blot, probed with 1:4000 mouse α-his Ab and 1:10000 α-mouse-HRP Ab. Membrane visualised using West Pico Plus and LI-COR imaging system. Solubilisation efficiency calculated by densitometry with data for 6kDa (G) and 11kDa (H) shown as mean, n = 1.

All AASTY polymers were capable solubilising BmrA at all tested concentrations with bands corresponding to BmrA highlighted in figure 3.18 A - F. Analysis of efficiency in figure 3.18 G and H found limited differences in the solubilisation efficiency of BmrA when using AASTY polymers at 0.5% or 2.5% concentration. Due to this, AASTY polymers were utilised at 0.5% for all further experimentation as suggested by the supplier unless otherwise stated.

3.1.19 6kDa – BmrA Solubilisation Efficiency

The group of 6kDa AASTY co-polymers were investigated in more detail for their ability to solubilise BmrA. Supernatant and pellet samples were probed in western blots (Figure 3.19 A - C) and analysed by densitometry of western blots (Figure 3.19 D).

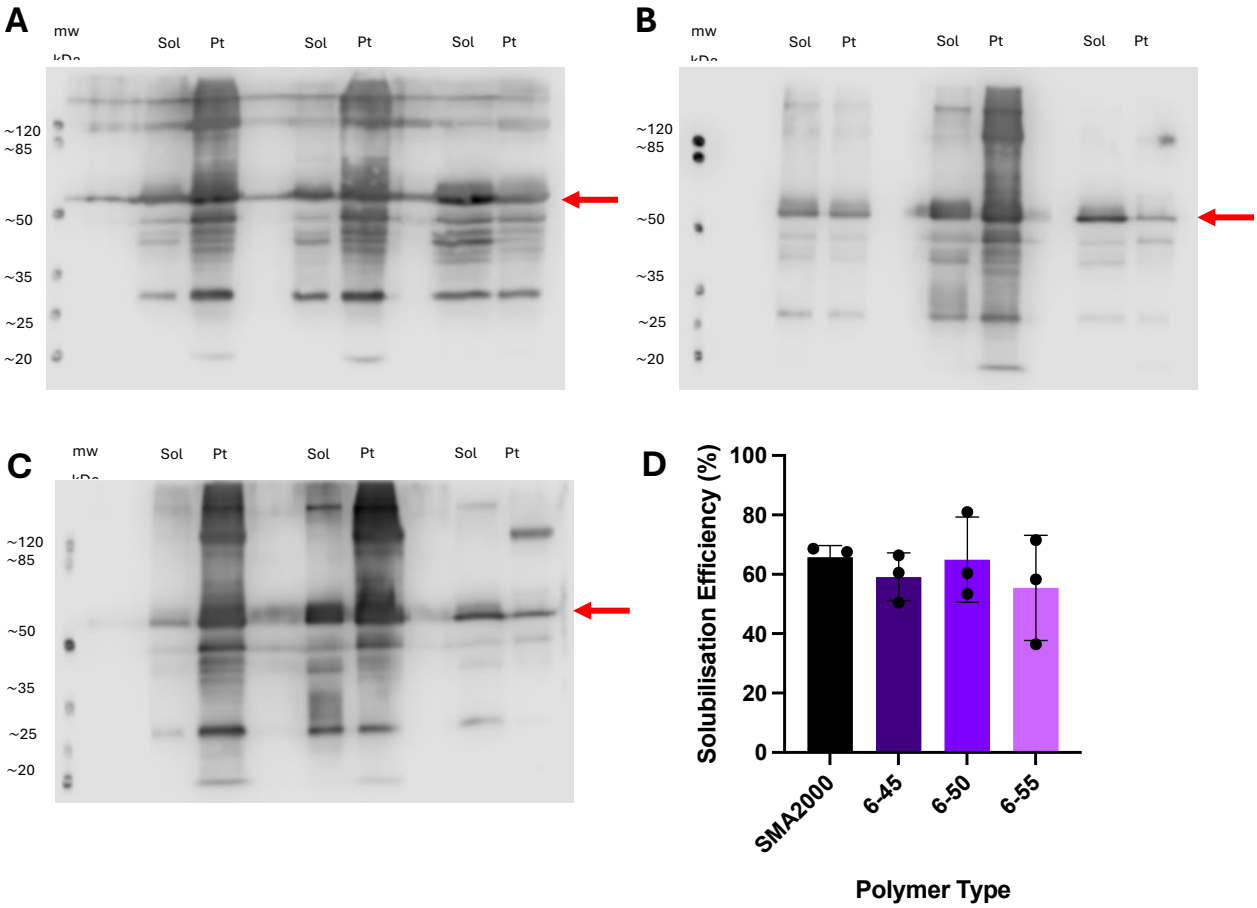

Figure 3.19 : AASTY (6kDa) exhibit a similar solubilisation efficiency when compared to SMA2000. BmrA and *E. coli* membranes (60mg/ml) were mixed with equal volume of 1% (w/v) 6-45 (A), 6-50 (B) and 6-55 (C) for 1 hour at room temperature. Samples were then centrifuged (100,000 x g, 20 min, 4°C) with supernatant (Sol) and pellet (Pt) samples collected. 10µl samples were analysed by western blot, probed with 1:4000 mouse α-his Ab and 1:10000 α-mouse-HRP Ab. Membrane visualised using West Pico Plus and LI-COR imaging system. Solubilisation efficiency calculated by densitometry (D) with data shown as mean ± SD, n ≥3. Data analysed by one-way ANOVA with no significance found. SMA data reproduced from Figure 3.2.

Similarly to previous western blot results, all three 6kDa AASTY co-polymers are able to solubilise BmrA with bands corresponding to BmrA highlighted in western blots shown in figure 3.19 A, B and C. Densitometric analysis shows that all 6kDa AASTY polymers exhibited a similar solubilisation efficiency when compared to SMA2000 in Figure 3.19 D. 6-50 exhibits

the highest mean efficiency at 71±17%, closely followed by SMA2000 at 66±4%, then 6-45 at 59±8% with the lowest efficiency being 6-55 with 55±18%.

3.1.20 6kDa – BmrA Purity

The purification of 6kDa AASTY co-polymer solubilised BmrA was then investigated using Ni-affinity chromatography (Figure 3.20 A - C) and analysed by densitometry (Figure 3.20 D).

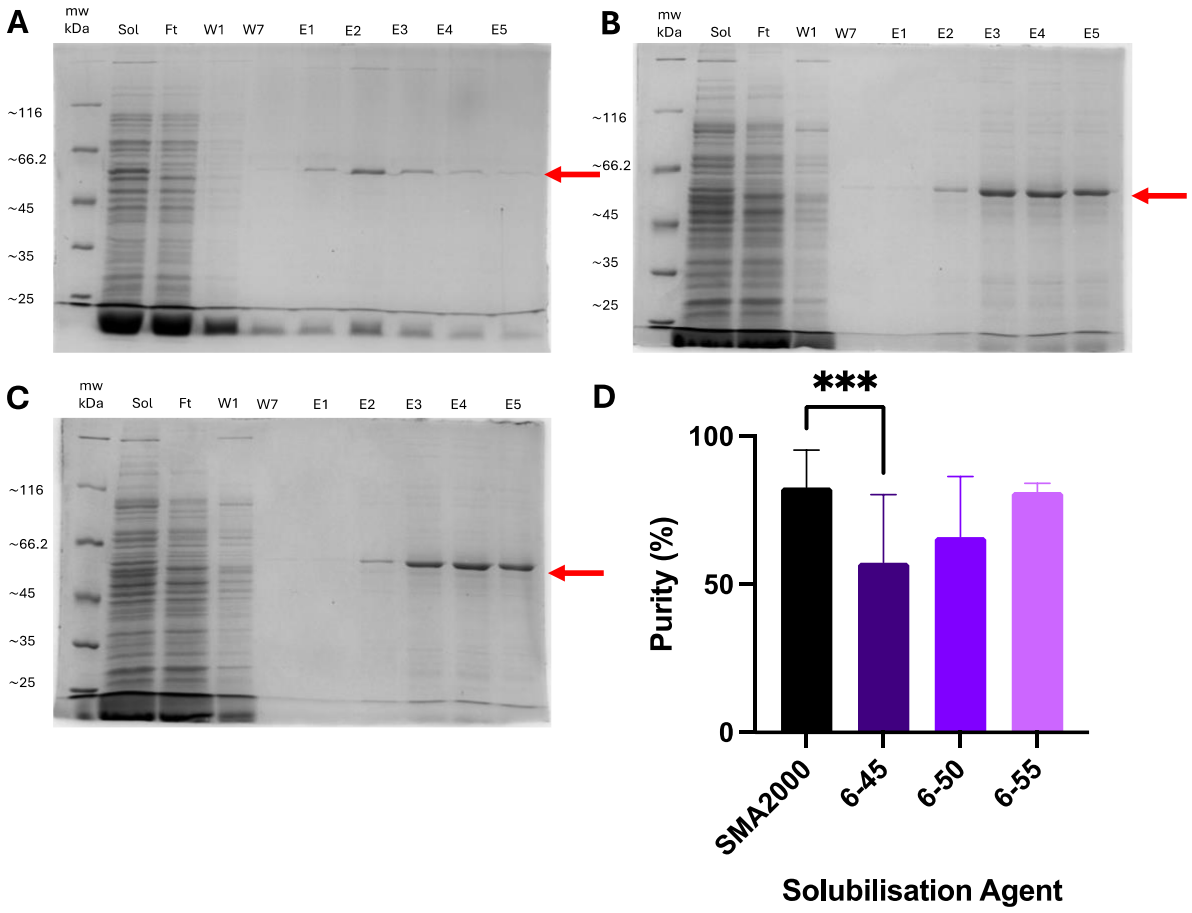

Figure 3.20 : AASTY 6-45 produces significantly lower protein purity when compared to SMA2000. Purification SDS-PAGE gel of 6-45 (A), 6-50 (B) and 6-55 (C) solubilised BmrA^{+} *E. coli* membranes (60mg/ml). 20µl samples of solubilised (Sol), pellet (Pt), washes one and seven (W1 and W7) and elutions one to five (E1-5) loaded and stained with Instantblue. D) BmrA purity calculated by densitometry and presented as mean ± SD, n ≥3. Data analysed by one-way ANOVA with ***p ≤ 0.001. SMA data reproduced from Figure 3.3.

All 6kDa AASTY co-polymers were able to produce purified BmrA as shown by highlighted bands at the correct weight (~65kDa) in figure 3.20 A – C. There are limited contaminating bands in E1 – E5 in all cases, but BmrA solubilised with 6-45 appears less intense and elutes from the column earlier than 6-50 and 6-55. Analysis of the average purity achieved with each

polymer shows that 6-45 produces a significantly lower level of BmrA purity (57±23%) when compared to SMA2000 (83±13%) in figure 3.20 D. However, 6-50 and 6-55 produce comparable levels to SMA2000 with 66±20% and 81±3% purity respectively.

3.1.21 6kDa - BmrA Yield

The yield of BmrA following solubilisation and purification with 6kDa AASTY co-polymers was determined by running samples on SDS-PAGE alongside BSA controls (Figure 3.21 A - C) and analysed by densitometry (Figure 3.21 D).

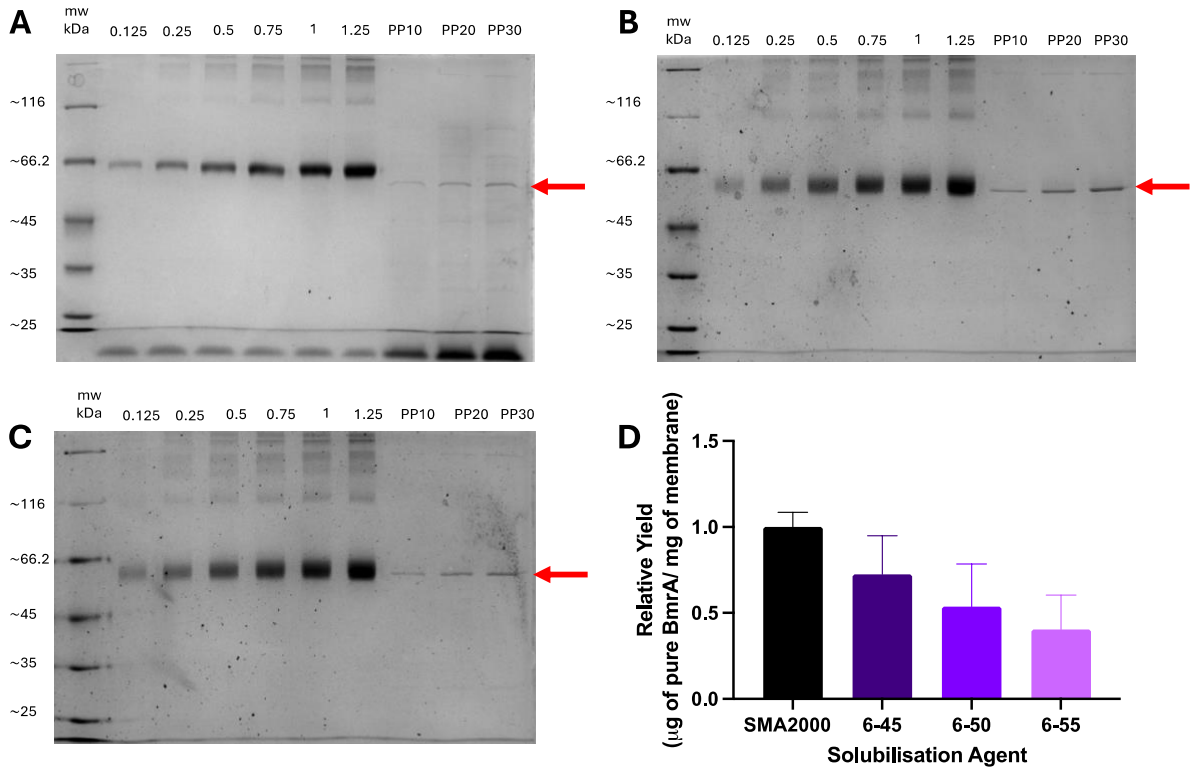

Figure 3.21 : 6kDa AASTY and SMA2000 co-polymers produce comparable levels of protein yield. Quantification SDS-PAGE gel of 6-45 (A), 6-50 (B) and 6-55 (C) solubilised BmrA. 20µl samples of a standard range of BSA (0.125-1.25µg/ml) loaded alongside 10µl , 20µl and 30µl of pooled purified protein (PP10, PP20 and PP30). D) BmrA relative yield was calculated by densitometry and presented as mean ± SEM, n ≥3. Analysed with one-way ANOVA with no significance found. SMA data reproduced from Figure 3.6.

Pooled purified BmrA can be seen in quantification SDS-PAGE gels for all 6kDa AASTY co-polymers in figure 3.21 A, B and C. Analysis of relative yield in figure 3.21 D shows that using any of the 6kDa AASTY polymers produces a comparable yield of BmrA to SMA2000

(0.975±0.4µg/mg). 6-45 has the highest mean with 0.7±0.5µg/mg, followed by 6-50 with 0.5±0.6µg/mg with the lowest yield being 6-55 with 0.4±0.35µg/mg.

3.1.22 6kDa - Sensitivity

To investigate the magnesium sensitivity of the 6kDa AASTY group, protein-lipid and lipid-only discs were tested and analysed by centrifugation and SDS-PAGE based assay (Figure 3.22 A - D) and a light scattering assay (Figure 3.22 E).

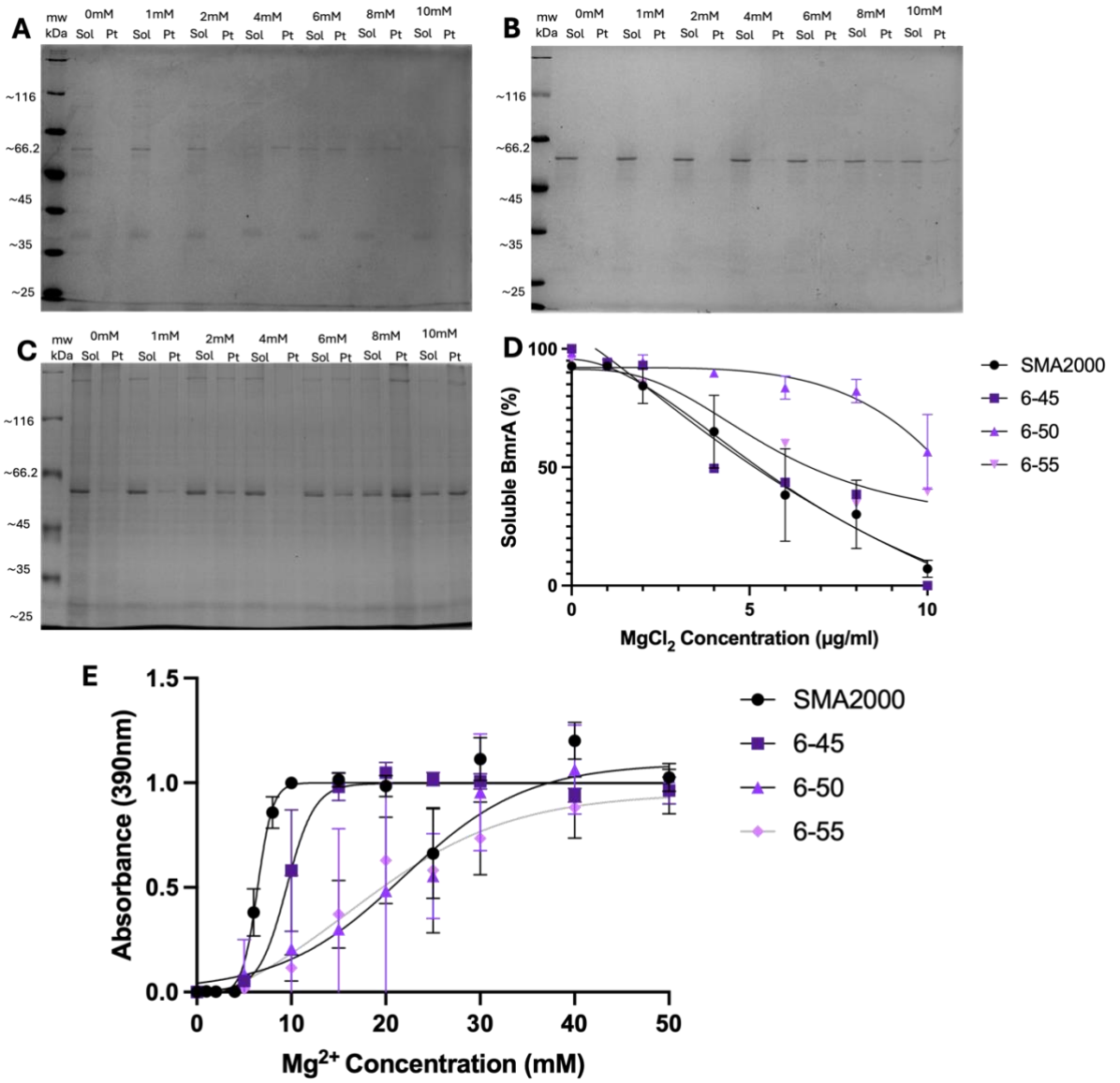

Figure 3.22: 6-50 and 6-55 exhibit a tolerance to magnesium when compared to SMA2000. SDS-PAGE gel of 6-45 (A), 6-50 (B) and 6-55 (C) solubilised and purified BmrA mixed with different concentrations of magnesium (0-10mM) and centrifuged (100,000 x g, 20 min, 4°C) with supernatant (Sol) and pellet (Pt) samples taken and loaded onto SDS-PAGE and stained with Instantblue. D) Graph showing loss of soluble BmrA as magnesium concentration increases with the percentage of soluble BmrA (%) calculated by densitometry. E) Graph showing the increase in scattering as magnesium concentration increases. Data presented as mean ± SEM, n ≥3 with error bars otherwise n = 1. SMA data reproduced from Figure 3.7.

As the concentration of magnesium increases from 0mM to 10mM, there is a partial shift of protein from the soluble (sol) to the insoluble (pt) fractions for all 6kDa AASTY polymers, as seen in figure 3.22 A - C. However, 6-45 stands outs due to a lack of soluble BmrA at 10mM magnesium when compared to 6-50 and 6-55. This is supported in figure 3.22 D, with 6-45 protein-lipid discs presenting with a sensitivity profile very similar to SMA2000. Both exhibit total loss of soluble BmrA at 10mM magnesium, unlike 6-50 and 6-55 which appears to retain some level of soluble BmrA at the same concentration. This relationship is similar in lipid-only

discs in figure 3.22 E, with 6-45 exhibiting sensitivity most like SMA2000 with maximal scattering achieved at ~15mM magnesium and an EC50 of 9.7mM. This is in comparison to 6-50 and 6-55 which display a greater tolerance with maximal scattering observed between 40mM – 50mM magnesium and EC50 values of 23.4mM and 19.4mM respectively.

3.1.23 11kDa – BmrA Solubilisation Efficiency

The efficiency of the 11kDa group of AASTY co-polymers to solubilise BmrA was also investigated. Supernatant and pellet samples were probed in western blots (Figure 3.23 A - C) and analysed by densitometry of western blots (Figure 3.23 D).

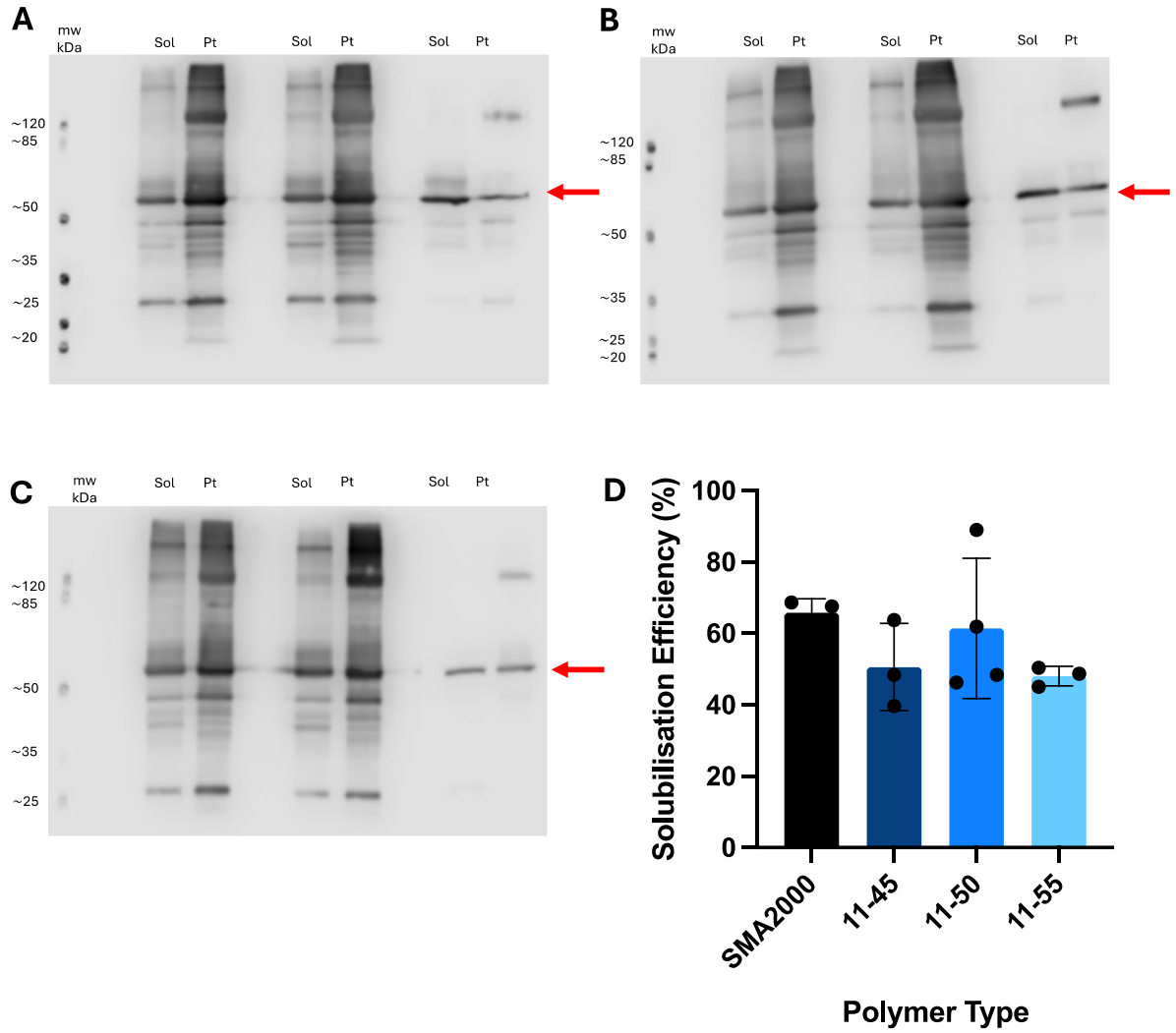

Figure 3.23 : AASTY (11kDa) exhibit a similar solubilisation efficiency when compared to SMA2000. BmrA and *E. coli* membranes (60mg/ml) were mixed with equal volume of 1% (w/v) 11-45 (A), 11-50 (B) and 11-55 (C) for 1 hour at room temperature. Samples were then centrifuged (100,000 x g, 20 min, 4°C) with supernatant (Sol) and pellet (Pt) samples collected. 10µl samples were analysed by western blot, probed with 1:4000 mouse α-his Ab and 1:10000 α-mouse-HRP Ab. Membrane visualised using West Pico Plus and LI-COR imaging system. Solubilisation efficiency calculated by densitometry (D) with data shown as mean ± SD, n ≥3. Data analysed by one-way ANOVA with no significance found. SMA data reproduced from Figure 3.2.

All three of the 11kDa AASTY co-polymers are able to solubilise BmrA as shown in figure 3.23 A - C with highlighted bands corresponding to BmrA present. Following analysis of solubilisation efficiencies in figure 3.23 D, the 11kDa AASTY co-polymers are comparable to SMA2000. While SMA2000 achieves the highest mean efficiency with 66±4%, this is closely followed by 11-50 with 61±20% efficiency, before dropping to 51±12% with 11-45 and 48±3% with 11-55.

3.1.24 11kDa – BmrA Purity

The purification of 11kDa AASTY solubilised BmrA was then tested using Ni-affinity chromatography (Figure 3.24 A - C) with purity analysed by densitometry (Figure 3.24 D).

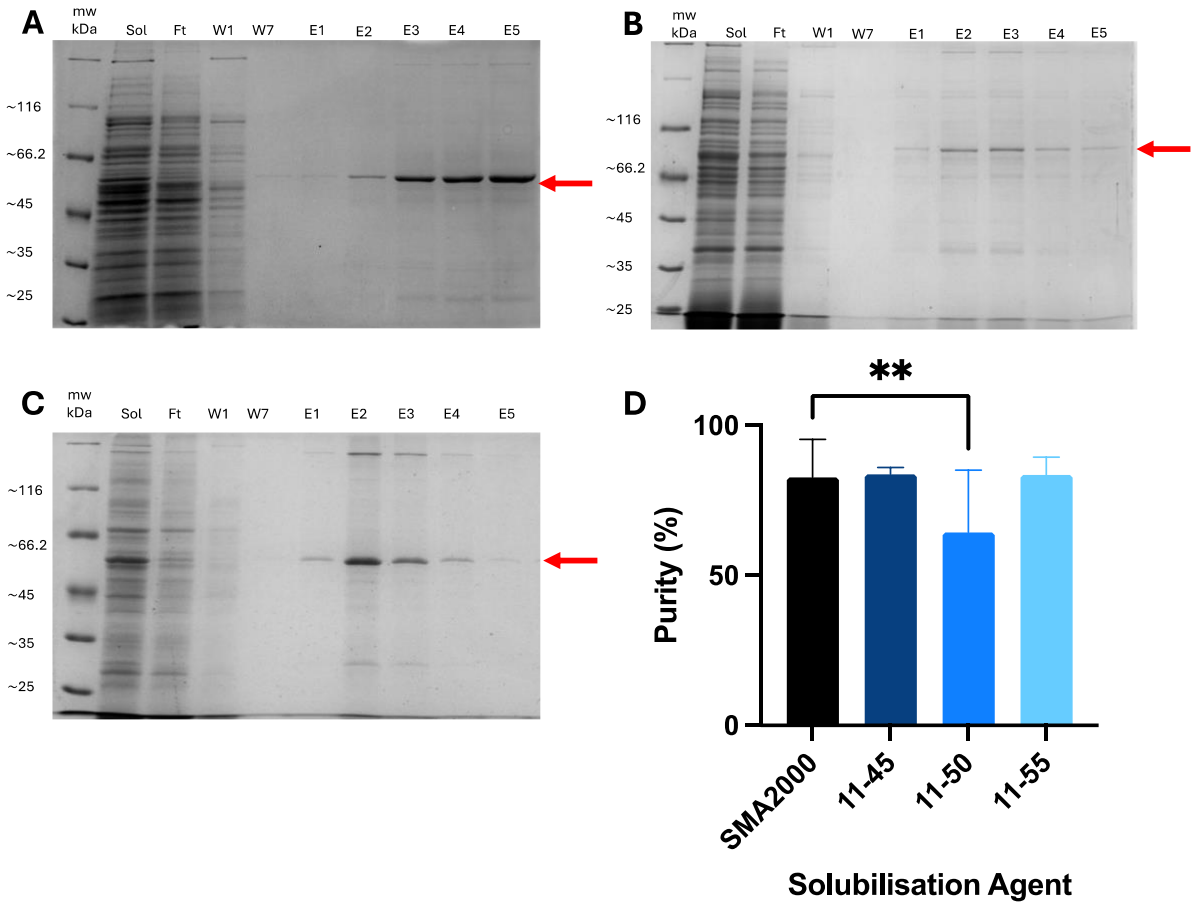

Figure 3.24: AASTY 11-50 produces significantly lower levels of purity when compared to SMA2000. Purification SDS-PAGE gel of 11-45 (A), 11-50 (B) and 11-55 (C) solubilised BmrA^{+} *E. coli* membranes (60mg/ml). 20µl samples of solubilised (Sol), pellet (Pt), washes one and seven (W1 and W7) and elutions one to five (E1-5) loaded and stained with Instantblue. D) BmrA purity calculated by densitometry and presented as mean ± SD, n ≥3. Data analysed by one-way ANOVA with **p ≤ 0.01. SMA data reproduced from Figure 3.3.

All 11kDa AASTY co-polymers are able to produce purified BmrA as shown by BmrA bands in elution fractions on SDS-PAGE gels in figure 3.24 A, B and C. However, 11-50 appears to show a lower presence of BmrA and a higher number of contaminating bands when compared to 11-45 and 11-55. 11-45 solubilised BmrA also appears to elute later than 11-50 or 11-55 solubilised BmrA. Following analysis of average purity in figure 3.24 D, 11-50 was found to produce significantly lower levels of BmrA purity with 64±21% when compared to SMA2000

with 83±13%. However, 11-45 and 11-55 produce comparable purity levels with 84±2% and 84±6 respectively.

3.1.25 11kDa – BmrA Yield

The yield of BmrA following solubilisation and purification with the 11kDa AASTY co-polymers was also determined running samples on SDS-PAGE alongside BSA controls (Figure 3.25 A - C) and analysed by densitometry (Figure 3.25 D).

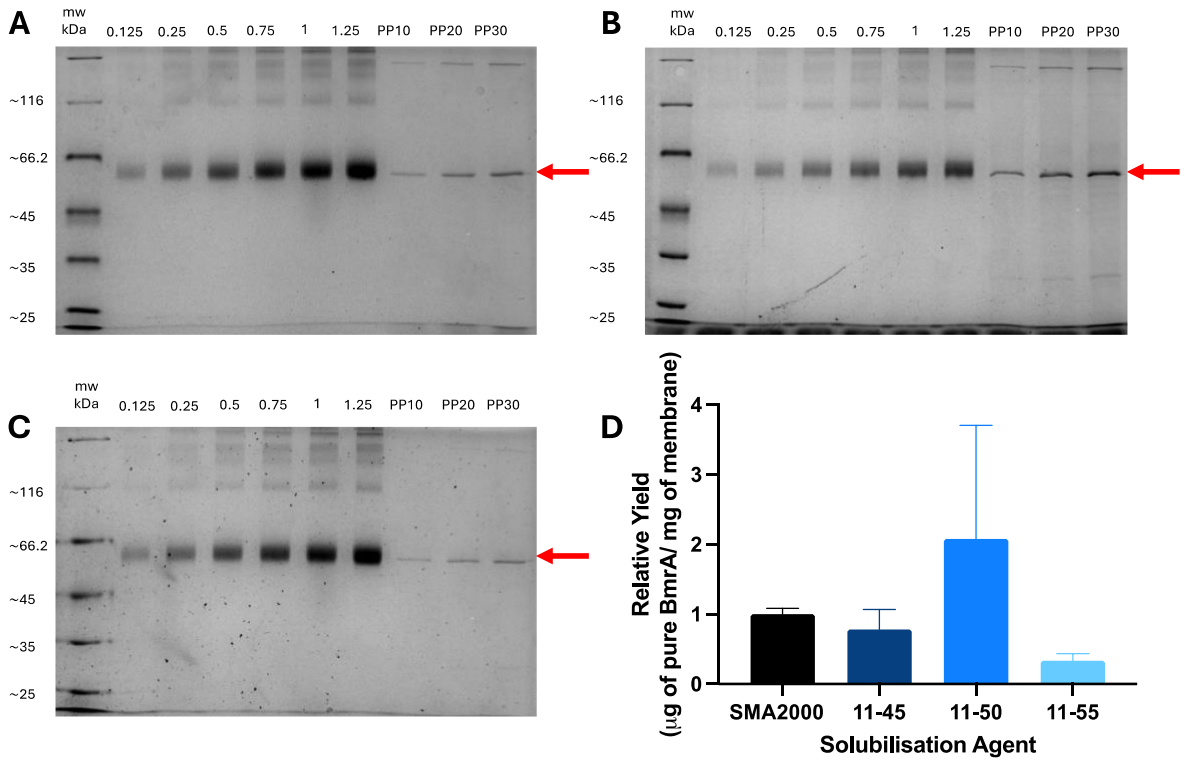

Figure 3.25: 11kDa AASTY and SMA2000 co-polymers produce comparable levels of protein yield. Quantification SDS-PAGE gel of 11-45 (A), 11-50 (B) and 11-55 (C) solubilised BmrA. 20µl samples of a standard range of BSA (0.125-1.25µg/ml) loaded alongside 10µl , 20µl and 30µl of pooled purified (PP10, PP20 and PP30). D) BmrA relative yield was calculated by densitometry and presented as mean ± SEM, n ≥3. Analysed with one-way ANOVA with no significance found. SMA data reproduced from Figure 3.6.

Pooled purified BmrA can be seen in quantification SDS-PAGE gels for all 11kDa AASTY co-polymers in figure 3.25 A - C. Following analysis of relative yield, all 11kDa AASTY polymers produced comparable levels of protein yield in figure 3.25 D, with 11-50 exhibiting the highest yield of 2±4µg/mg. This is followed by SMA2000 with 0.975±0.4µg/mg and 11-45 with 0.78±0.6µg/mg. 11-55 produces the lowest yield of BmrA with 0.3±0.2µg/mg.

3.1.26 11kDa – Sensitivity

The 11kDa AASTY group sensitivity to magnesium was also tested in sensitivity assays with purified protein-lipid and lipid-only discs by centrifugation and SDS-PAGE based assay (Figure 3.26 A - D) and a light scattering assay (Figure 3.26 E).

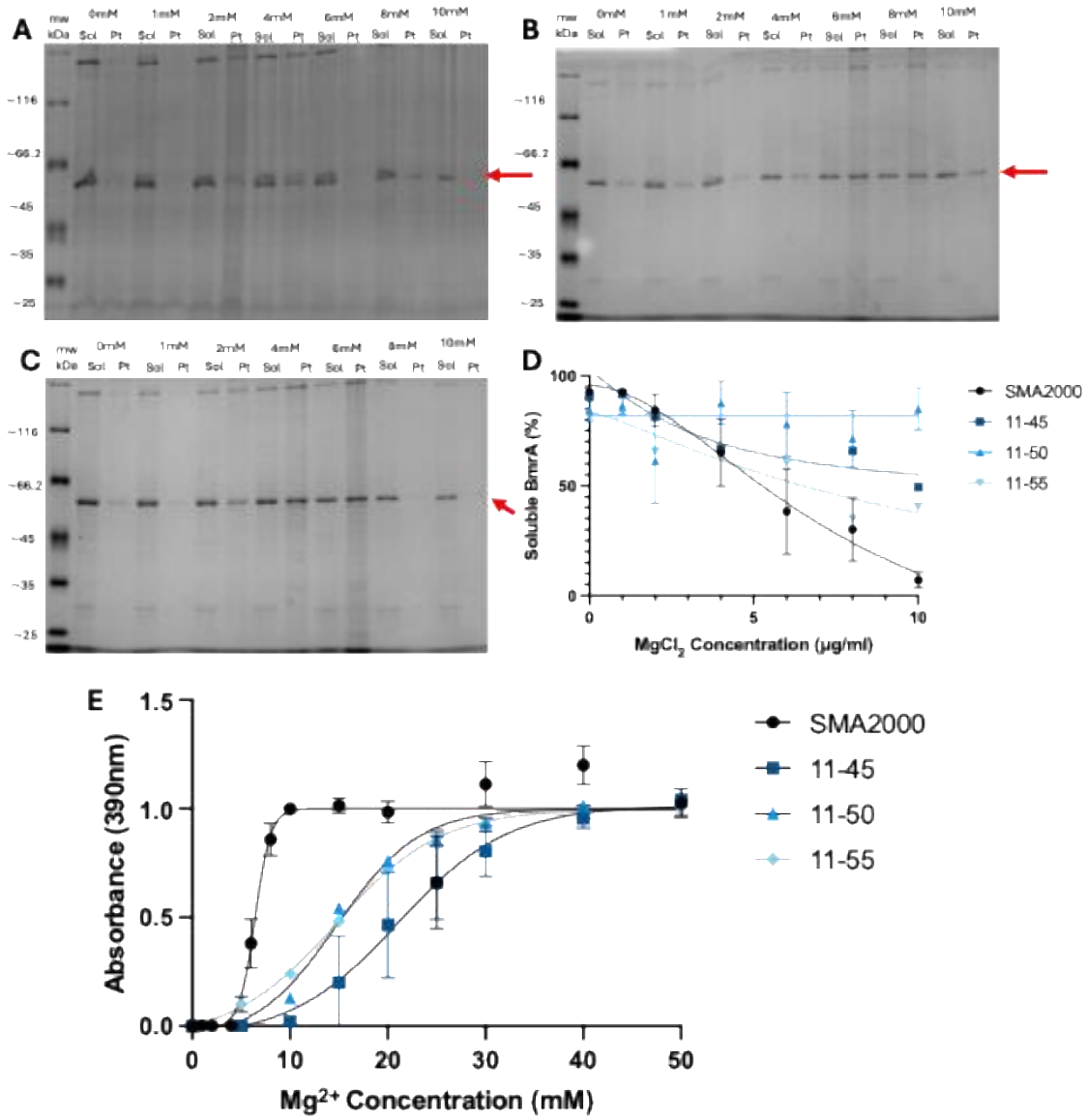

Figure 3.26 : 11kDa AASTY co-polymers display an increased tolerance to magnesium when compared to SMA2000. SDS-PAGE gel of 11-45 (A), 11-50 (B) and 11-55 (C) solubilised and purified BmrA mixed with different concentrations of magnesium (0-10mM) and centrifuged (100,000 x g, 20 min, 4°C) with supernatant (Sol) and pellet (Pt) samples taken and loaded onto SDS-PAGE with LSB. D) Graph showing loss of soluble BmrA as magnesium concentration increases with the percentage of soluble BmrA (%) calculated by densitometry. E) Graph showing the increase in scattering as magnesium concentration increases. Data presented as mean ± SEM, n ≥3 with error bars otherwise n = 1. SMA data reproduced from Figure 3.7.

As the concentration of magnesium increases from 0mM to 10mM, there is a partial shift of protein from the soluble (sol) to the insoluble (pt) fractions following centrifugation in SDS-PAGE as seen in figure 3.26 A - C. However, all 11kDa polymers appear to retain soluble BmrA in the supernatant fraction at 10mM magnesium unlike SMA2000. This is evidenced in figure 3.26 D with densitometric analysis suggesting all three 11kDa AASTY exhibit some degree of magnesium tolerance, with ~50% of BmrA remaining soluble up to 10mM magnesium in 11-45 and 11-55 discs. 11-50 protein-lipid discs also appear to remain stable up to 10mM magnesium. A similar relationship is seen in figure 3.26 E, with 11kDa AASTY lipid-only discs exhibiting half maximal scattering around 15mM – 20mM magnesium. 11-45 had the highest EC50 with 21.9mM, followed by 11-55 with 15.7mM and 11-50 with 15.2mM.

3.1.27 Comparison of Sensitivity

Data from both protein-lipid and lipid-only sensitivity assays were further analysed to compare co-polymer sensitivity at a defined concentration (Figure 3.27).

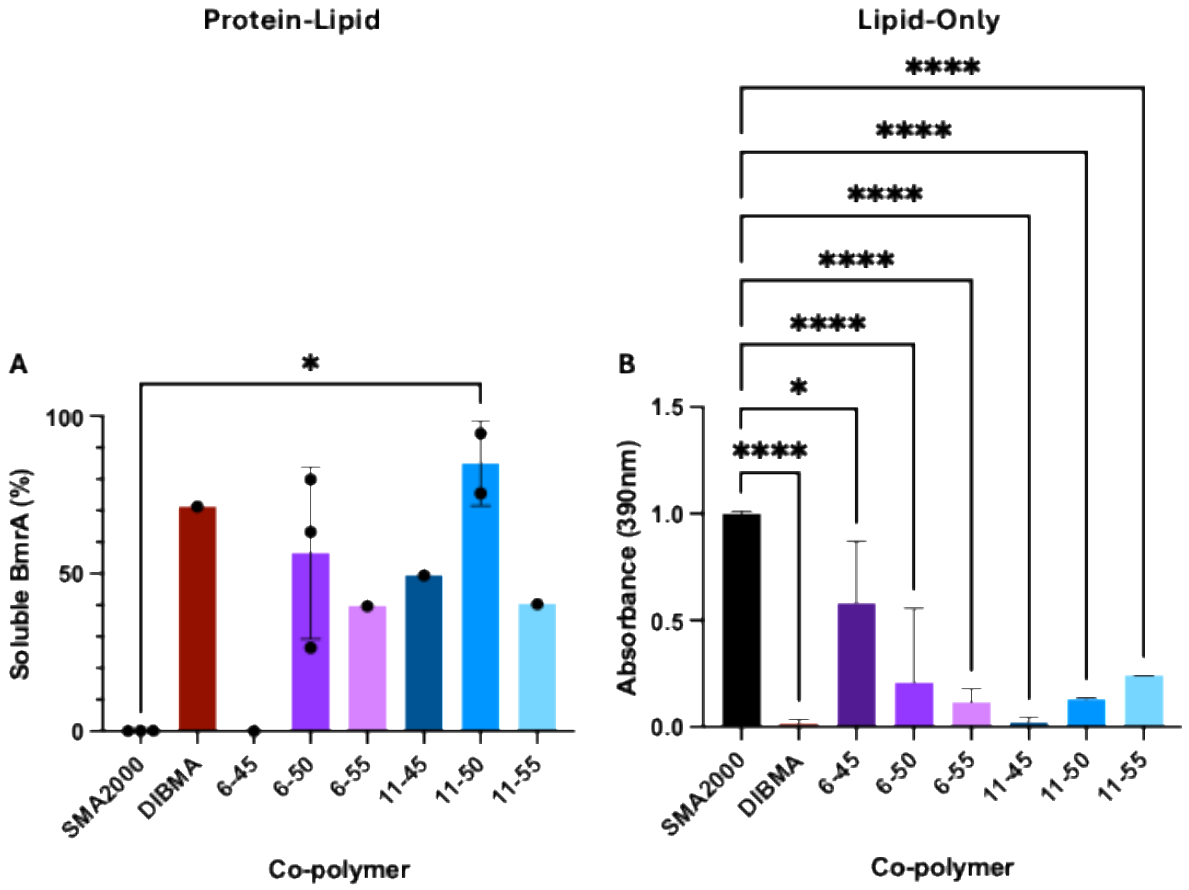

Figure 3.27 : SMA displays a significantly higher sensitivity to magnesium when compared to alternative co-polymers. Graphs comparing the percentage of soluble BmrA remaining in protein-lipid nanodiscs (A) and the level of scattering from lipid-only nanodiscs (B) at 10mM magnesium. A) Percentage of soluble BmrA (%) calculated by densitometry, with error bars where shown presented as mean ± SEM, n ≥3 otherwise n = 1. B) Scattering at 390nm measured and plotted as mean ± SEM n ≥3. Data analysed by one-way ANOVA with *p ≤ 0.05 and ****p ≤ 0.0001.

At 10mM magnesium, SMA2000 nanodiscs are significantly more sensitive when compared to alternative co-polymers as shown in figure 3.27. In figure 3.27 A, 11-50 solubilised protein-lipid nanodiscs were found to be significantly less sensitive to magnesium when compared to SMA2000. However, for lipid-only nanodiscs in figure 3.27 B SMA2000 is significantly more sensitive than all other tested co-polymers.

Section Two : Solubilisation of an ABC transporter from Insect Cells

In order to probe the utility of the tested polymers for proteins in other expressions systems, and the possible influence of different lipid environments, an alternative expression host was utilised. In this section, Sf9 insect cells overexpressing the ABC transporter MRP4 were used.

3.2.1 Insect membrane solubilisation kinetics

To initially investigate overall ability to solubilise membranes a simple light scattering assay was used. Sf9 membrane preparations, which are cloudy and scatter light due to their insolubility in aqueous solution, were mixed with 2.5% final w/v of polymer, and light scattering monitored over time. As SMALPs are formed the solution clarifies and the light scattering decreases. This provided a quick assay to study solubilisation kinetics with the various co-polymers.

3.2.2 DIBMA and Glyco-DIBMA

DIBMA and Glyco-DIBMA were tested in the scattering assay (Figure 3.28).

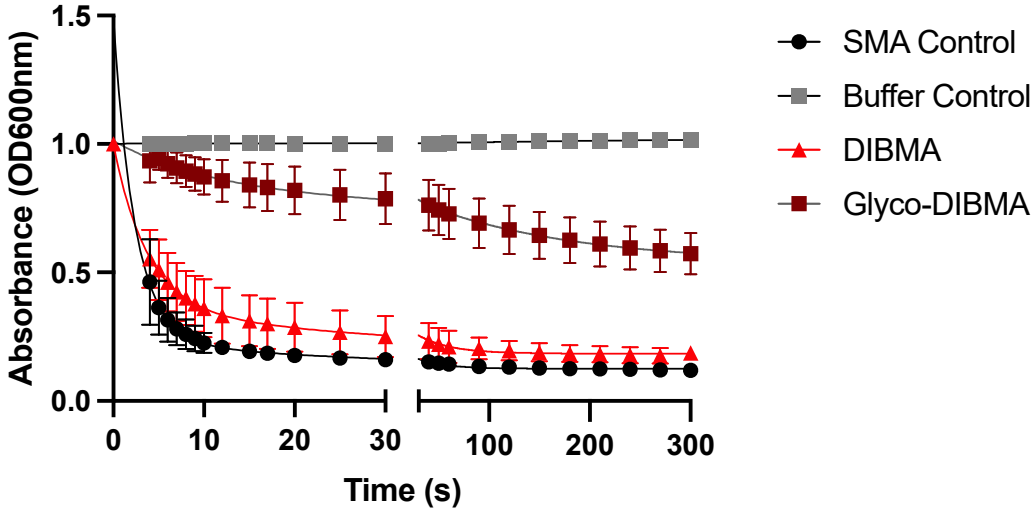

Figure 3.28 : Glyco-DIBMA is less able to solubilise Sf9 membranes when compared to DIBMA and SMA2000. Samples of Sf9 membranes (60mg/ml) were mixed with an equal volume of 5% w/v DIBMA and Glyco-DIBMA with the scattering (600 nm) profile tracked over five minutes. Produced using GraphPad v. 10.0.3 (217) with data presented mean ± SEM, n ≥3 with two-phase decay line plotted.

SMA2000, DIBMA and Glyco-DIBMA are all able to solubilise Sf9 membranes as shown by the decrease in light scattering observed in figure 3.28. With SMA2000, a very fast decrease in light scattering is seen - decreasing to 0.23 in just 10 seconds. DIBMA acts slightly slower but generally similar to SMA2000, decreasing to 0.36 in 10 seconds. However, Glyco-DIBMA exhibits a much slower solubilisation profile reaching only 0.87 in 10 seconds. Unlike SMA2000 and DIBMA, it also does not reach plateau within five minutes.

3.2.3 AASTY 6kDa

The 6kDa AASTY group were also tested in the light scattering assay (Figure 3.29).

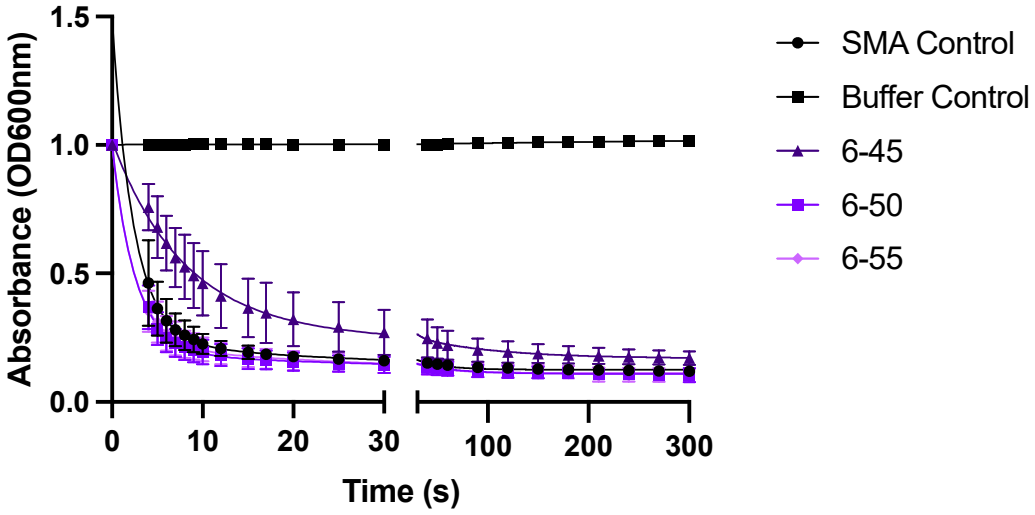

Figure 3.29 : All 6kDa AASTY co-polymers were able to solubilise Sf9 membranes. Samples of Sf9 membranes (60mg/ml) were mixed with an equal volume of 5% w/v AASTY 6-45, 6-50 and 6-55 with the scattering (600 nm) profile tracked over five minutes. Produced using GraphPad v. 10.0.3 (217) with data presented mean ± SEM, n ≥3 with two-phase decay line plotted.

All three 6kDa AASTY co-polymers were able to solubilise Sf9 membranes in figure 3.29, with 6-50 and 6-55 working at rates similar to that of SMA2000. Within 10 seconds, 6-50 reaches 0.19 while 6-55 reaches 0.2, both values lower than that of SMA2000 with 0.23. However, 6-45 stands out as having slightly slower solubilisation kinetics compared to the rest of the set, reaching only 0.46 at 10 seconds.

3.2.4 AASTY 11kDa

The 11kDa AASTY group were also tested in the light scattering assay (Figure 3.30).

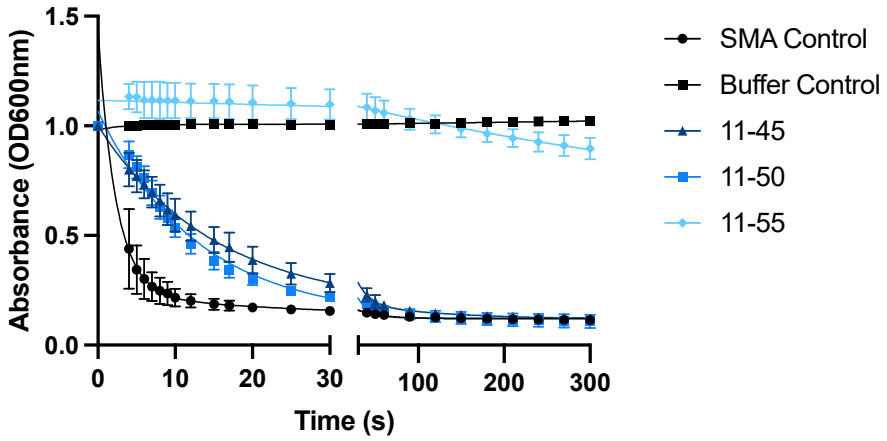

Figure 3.30 : 11-55 exhibits an increase in scattering unlike 11-50 and 11-45. Samples of Sf9 membranes (60mg/ml) were mixed with an equal volume of 5% w/v AASTY 11-45, 11-50 and 11-55 with the scattering (600 nm) profile tracked over five minutes. Produced using GraphPad v. 10.0.3 (217) with data presented mean ± SEM, n ≥3 with two-phase decay line plotted.

Results between the 11kDa AASTY group in figure 3.30 vary more than other co-polymers previously explored in the same assay. 11-45 and 11-50 both reduce the scattering profile in a similar manner to SMA2000 but with a slower decrease before plateauing to the same level as SMA2000. 11-45 and 11-50 reached 0.6 and 0.53 in 10 seconds compared to SMA2000 that reached 0.23 in the same time period. In contrast, 11-55 exhibits an initial increase in the scattering profile with a very slow decrease to just below the buffer control after five minutes.

3.2.5 MRP4 Solubilisation efficiency

To complement the light scattering assays which measured overall membrane solubilisation, the protein specific solubilisation of ABC transporter MRP4 was investigated with selected polymers utilised (Figure 3.31). SMA2000 remains as a positive control with good purity and yield in previous trials. DIBMA was selected due to its tolerance to magnesium, alongside a different apolar subunit to SMA2000 with a reportedly larger nanodisc size. AASTY 6-50 and 11-50 were also selected as they display a tolerance to magnesium and contain a different polar subunit to both SMA2000 and DIBMA.

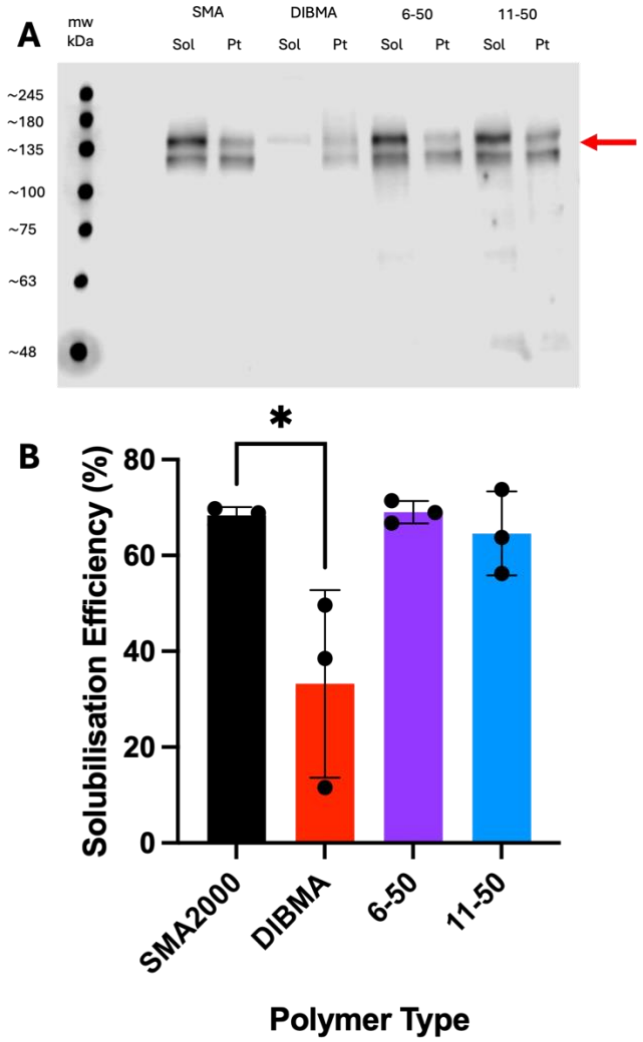

Figure 3.31 : DIBMA is significantly less efficient at solubilising MRP4 from Sf9 membranes when compared to SMA2000. MRP4⁺ Sf9 membranes (60mg/ml) were mixed with equal volume of 5% (w/v) SMA2000 and DIBMA, or 1% 6-50 and 11-50 for 1 hour at room temperature. Samples were then centrifuged (100,000 x g, 20 min, 4°C) with supernatant (Sol) and pellet (Pt) samples collected. A) 10µl samples were analysed by western blot, probed with 1:100 rat α-MRP4 Ab and 1:3000 α-rat-HRP Ab. Membrane visualised using West Pico Plus and LI-COR imaging system. B) Solubilisation efficiency calculated by densitometry (C) with data shown as mean ± SD, n ≥3. Data analysed by one-way ANOVA with *p ≤ 0.05.

All four of the selected polymers were able to solubilise MRP4 from Sf9 membranes as shown in figure 3.31 A with double bands associated with MRP4 found in the sol lanes for all polymers. Upon analysis of polymer efficiency in figure 3.31 B, DIBMA was significantly less efficient with only 33±20% of MRP4 solubilised when compared to SMA2000 with 68±2%. 6-50 achieves slightly higher efficiency than SMA2000 with 69±2% while 11-50 maintains 65±9% efficiency. This is similar to results shown for BmrA solubilisation efficiency in figures 3.2, 3.13, 3.19 and 3.23.

Section Three : BmrA Functional Analysis

The ability to extract and purify a target protein is not the only important feature of co-polymer solubilisation. It is arguably more important that the purified protein is correctly folded and retains function and so functional studies were next undertaken.

3.3.1 Binding Assay

The four selected polymers were therefore taken forward for functional analysis of purified BmrA. These studies began with a binding assay to confirm BmrA is folded correctly and able to undergo conformational changes upon binding to a known substrate (Hoechst 33342) in a tryptophan quenching assay (Figure 3.32).

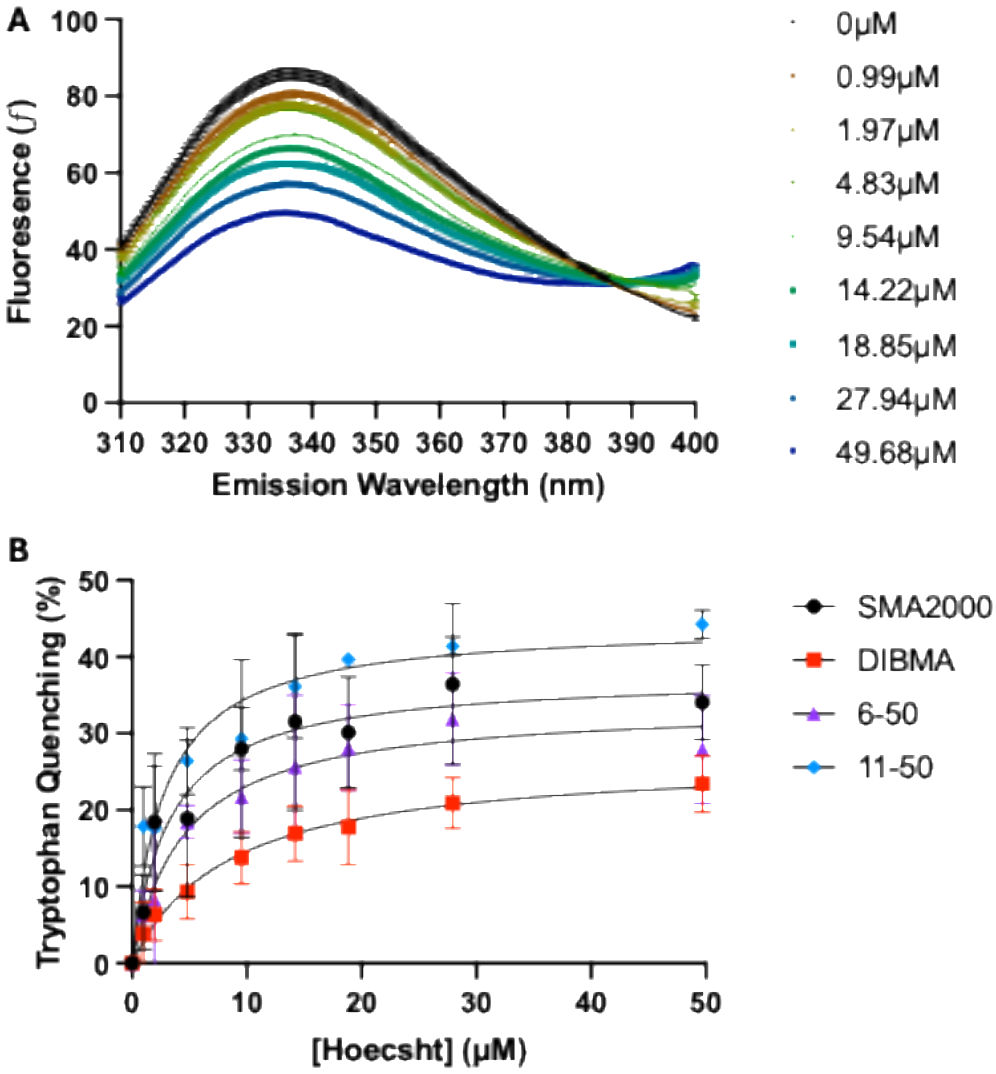

Figure 3.32 : BmrA nanodiscs produced with selected polymers are able to bind Hoechst 33342. A) Fluorescent trace of tryptophan quenching assay with SMA2000 solubilised and purified BmrA showing the decrease in fluorescence as Hoechst 33342 is successively added (0μM-50μM). Data shown as mean ± SEM, n ≥5. B) Tryptophan quenching of BmrA solubilised and purified with each of the selected polymers at 335 nm was measured upon successive addition of Hoechst 33342. Quenching dilution and inner filter corrected using NATA with data shown as mean ± SD, n ≥3. Produced using GraphPad v.10.0.3 (217) with non-linear regression one site binding curve fit.

Table 3.5 : Binding assay parameters for BmrA-Hoechst 33342. Tryptophan quenching of BmrA solubilised and purified with each of the selected polymers was measured upon binding of Hoechst 33342. Data shown as mean ± SEM, n ≥3. *p ≤ 0.05 significantly different to SMA2000.

Polymer	**K_d (μM)**	**Maximal Quenching (%)**
SMA2000	6.4 ± 3.9	41 ± 1.5
DIBMA	9.3 ± 2.6	27 ± 1 *
6-50	4.4 ± 1.5	34 ± 5.3
11-50	3.3 ± 1	45 ± 0.9

SMA2000 solubilised and purified BmrA displays a decrease in fluorescence upon successive addition Hoechst 33342 as shown in figure 3.32 A. Fluorescence intensity dropped from ~85a.u. at 0µM Hoechst to ~50a.u. at 49.68µM Hoechst in a dose-responsive manner. Upon dilution and inner filter correction using NATA, tryptophan quenching of BmrA solubilised and purified with each of the selected polymers was measured at 335 nm and displayed in figure 3.32 B. In each case, BmrA was able to bind Hoechst 33342 with quenching increasing as Hoechst concentration increases. Parameters of the assay displayed in table 3.5 reveal that SMA2000, DIBMA, 6-50 and 11-50 all display similar K_d values between 3.3±1µM and 9.3 ± 2.6µM, but DIBMA presented with a significantly lower maximal quenching with 27 ± 1% when compared to SMA2000 with 41 ± 1.5% and 11-50 with 45±0.9%. These values align with previous data for BmrA in Morrison *et al.,*2016 and for other membrane proteins with SMA2000 (Akram, *et al.,* 2022).

3.3.2 ATPase Assay

A better measure of overall function of ABC transporters would be to measure transport activity, but this isn't possible with polymer lipid discs as it requires a confined space on one side of the membrane. An alternative measure of overall activity that is frequently used is an ATPase assay. This has proved challenging with SMA2000 due to its sensitivity to magnesium, a required co-factor. However, DIBMA, 6-50 and 11-50 all display some degree of magnesium tolerance. Therefore, an ATPase assay was next utilised, which involves a colorimetric assay to measure phosphate produced during ATP turnover (Figure 3.33, Table 3.6).

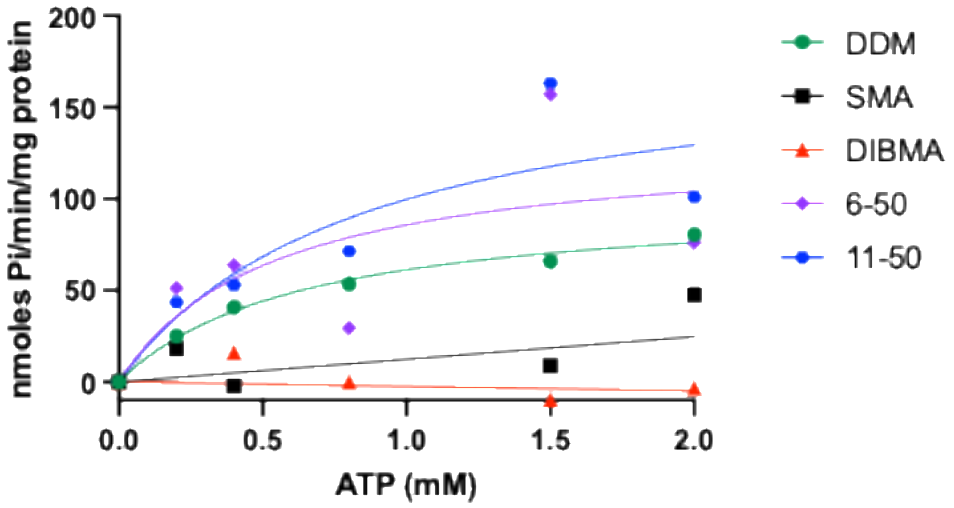

Figure 3.33 : DDM, 6-50 and 11-50 solubilised BmrA exhibit ATPase activity unlike SMA2000 and DIBMA solubilised BmrA. Graph showing ATPase activity of BmrA solubilised using selected polymers at different ATP concentrations. Produced using GraphPad v.10.0.3 (217), n = 1 with Michaelis-Menten non-linear curve fit.

Table 3.6 : Parameters of Michaelis-Menten curve fit for selected solubilisation agents. Km, concentration at which half maximal velocity is achieved. Vmax, maximal reaction velocity when substrate saturated.

Solubilisation Agent	**Km (mM)**	**Vmax (mol/s)**
DDM	0.6	100
6-50	0.5	132
11-50	0.8	184

DDM, 6-50 and 11-50 solubilised BmrA exhibit ATPase activity in figure 3.33, with phosphate production increasing as ATP concentration was increased. This is in contrast to SMA2000 and DIBMA solubilised BmrA – which do not display ATPase activity. At 2mM ATP, 11-50 solubilised BmrA displayed the highest phosphate turnover at 101 nmoles Pi/min/mg protein, followed by DDM solubilised BmrA with 81 nmoles Pi/min/mg protein. 6-50 solubilised BmrA displayed the lowest turnover at 76 nmoles Pi/min/mg protein. However, these values are considerably lower than the µmoles Pi/min/mg protein reported in existing literature (Ravaud, *et al.*, 2006). Parameters of curve fitting shown in Figure 3.33 are highlighted in table 3.6, with DDM, 6-50 and 11-50 solubilised BmrA displaying comparable Km and Vmax values. 6-50 solubilised BmrA exhibits the lowest Km at 0.5mM suggesting a higher affinity, while 11-50 solubilised BmrA displays the highest Vmax at 184 mol/s suggesting a higher efficiency.

Summary

Many of the co-polymers tested in the solubilisation of BmrA exhibited a good degree of efficiency, with the exception of SMA variants SMAd-A and SMA-QA. While SMA-EA and SMA-ED were able to solubilise BmrA, they were unable to produce a good purity and yield and so all four SMA variants were not further tested. This may suggest an incompatibility for SMA variants in the study of ABC transporters such as BmrA.

Glyco-DIBMA was another co-polymer that produced low purity and yield of BmrA and so was not tested for sensitivity. Comparative study of insect membrane solubilisation kinetics exhibited similar results with Glyco-DIBMA displaying a lower efficiency when compared to both DIBMA and SMA2000, and as such Glyco-DIBMA was not further tested. DIBMA on the other hand, produced a viable yield of BmrA and was tested for sensitivity despite low purity levels. Results show DIBMA displays a tolerance to magnesium when compared to SMA2000 but remains as one of least efficient co-polymers for the solubilisation of BmrA and MRP4.

The AASTY co-polymer group exhibited interesting results in this study and appears to produce a good purity and yield of BmrA when compared to SMA2000 - even at lower solubilisation concentrations of 0.5% instead of 2.5% used for all other polymers. This promoted the AASTY group for further investigation including sensitivity trials where they displayed varying levels of tolerance to magnesium. Interestingly, 11-55 also exhibited a distinct solubilisation kinetic profile when compared to all other co-polymers tested – suggesting differences in the mode of solubilisation across co-polymers.

Functional study of the selected polymers – SMA2000, DIBMA, 6-50 and 11-50 – showed that in all cases, co-polymer solubilised BmrA was able to bind substrate suggesting binding site accessibility and an ability to undergo conformational change when embedded in the nanodisc. However, SMA2000 and DIBMA solubilised BmrA did not display ATPase activity unlike 6-50 and 11-50 solubilised BmrA along with BmrA detergent micelles.

Overall, co-polymer solubilisation produces a comparable yield but significantly higher purity of BmrA when compared to detergent solubilisation in most cases. Results from this study

along with the ease and low cost of co-polymer implementation in the laboratory supports the application of co-polymers in membrane protein study.

These solubilisation trials have successfully highlighted a selected group of polymers – SMA2000, DIBMA, 6-50 and 11-50 – for further study. This is due to their chemical and structural characteristics alongside promising results in this chapter including protein purity and yield, sensitivity and functional activity as shown in table 3.7.

Table 3.7: Ranking co-polymers based on results from solubilisation trials and functional study. Qualitative colour-code ranking of co-polymers. In columns displaying all three colours, Green represents the highest values; Amber, average values; Red, lowest values. In columns display only green and red, Green represents positive functionality while Red represents negative functionality. N/A is non-applicable.

Co-polymer	Solubilisation Efficiency	Purity	Yield	Sensitivity	Binding	ATPase
SMA2000						
SMA-EA				N/A	N/A	N/A
SMA-ED				N/A	N/A	N/A
DIBMA						
Glyco-DIBMA				N/A	N/A	N/A
6-45					N/A	N/A
6-50						
6-55					N/A	N/A
11-45					N/A	N/A
11-50						
11-55					N/A	N/A

To further probe co-polymer compatibility for functional study of ABC transporters, we now turn to the other major component of plasma membranes – phospholipids. Protein-lipid, protein-protein and lipid-lipid interactions have been shown to play a role in the maintenance of protein structure and therefore function. Utilising co-polymer solubilisation methods, we benefit from retaining the native phospholipid environments and therefore interactions, and so next series of methods including TLC, laurdan and mass photometry were used to probe lipid and nanodisc characteristics.

4. Results Chapter Two – Nanodisc Characterisation

4.1 Introduction

The development of co-polymer solubilisation and introduction of novel co-polymers has been greatly beneficial for many areas of biological research. They have been shown to solubilise a diverse range of membrane proteins and provide the opportunity to probe protein-lipid interactions, as the native phospholipid environment is retained. However, co-polymer nanodiscs can exhibit a high level of variance in regard to size, composition and binding affinity, and have been theorised to hold ABC transporters too tightly for substrate transport (Pollock, *et al.,* 2018).

To probe these characteristics, SMA2000, DIBMA, AASTY 6-50 and AASTY 11-50 (Figure 4.1 and Table 4.1) were selected for further study based on their performance in solubilisation trials, reported data in existing literature and their structural information. SMA2000 is the industry standard and utilised in this study as it provides a high level of efficiency, purity and yield in BmrA solubilisation trials.

While DIBMA exhibited a low efficiency and protein purity in BmrA solubilisation trials, it was selected for further study due to its decreased magnesium sensitivity when compared to SMA2000. It also displays an aliphatic diisobutylene in a 1:1 ratio and is reportedly ~20nm in diameter which differs to the aromatic styrene in a 2:1 ratio and ~10 nm diameter of SMA2000, presenting an interesting study of chemical and structural differences.

Two AASTY co-polymers (6-50 and 11-50) were also selected for further study based on existing literature and performance in BmrA solubilisation trials. Both provide a high solubilisation efficiency with good levels of protein purity and yield. They also appear to be less sensitive to magnesium when compared to SMA2000 and support the solubilisation of functional BmrA as studied in binding and ATPase assays. Structurally, 6-50 and 11-50 provide an interesting study as they both contain 50% acrylic acid in place of maleic acid and display a larger nanodisc size of ~18 nm when compared to SMA2000 but differ by molecular weight at 6kDa and 11kDa.

4.2 Selected Co-polymer Structural Information

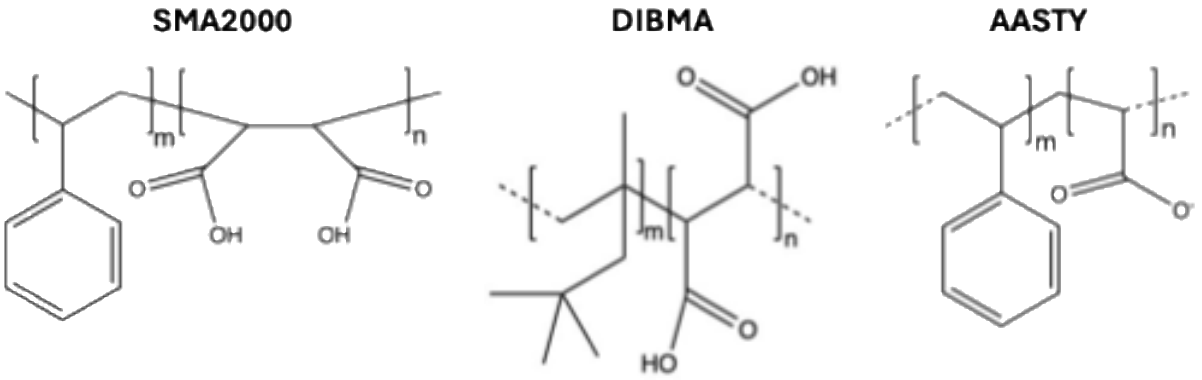

Figure 4.1 : Representation of the chemical structure of SMA2000, DIBMA and AASTY co-polymers. 'm' represents the apolar styrene or diisobutylene moiety while 'n' represents the polar maleic acid or acrylic acid moiety. Created using ChemDraw v21.0.0.

Table 4.1 : Co-polymer information. Table of chemical and structural characteristics of co-polymers as per manufacturer. Ratio, percentage of apolar to polar subunits; Mw, weight average molecular weight.

Name	Manufacturer	Apolar Subunit	Polar Subunit	Ratio (A:P)	Mw (kDa)
SMA	Cray Valley	Styrene	Maleic acid	2:1	7.5
DIBMA	Glycon Biochemicals	Diisobutylene	Maleic acid	1:1	12
6-50	Cube Biotech	Styrene	Acrylic acid	1:1	5.5
11-50	Cube Biotech	Styrene	Acrylic acid	1:1	11

The first nanodisc characteristic explored was size, distinguished in this study by mass photometry. Utilising this technique, single particles in an aqueous solution are added to a glass slide. As they absorb to the surface, the refractive index changes and is measured by a laser microscope and related to mass calibration curves. This provides details such as sample homogeneity, oligomeric state and single particle mass and has been proven in the membrane protein study (Olerinyova, *et al.,* 2021).

4.3 Protein-Lipid Mass Photometry

To begin, BmrA nanodiscs solubilised with SMA2000, DIBMA, 6-50 or 11-50 and purified by Ni-affinity chromatography were tested by mass photometry (Figure 4.2).

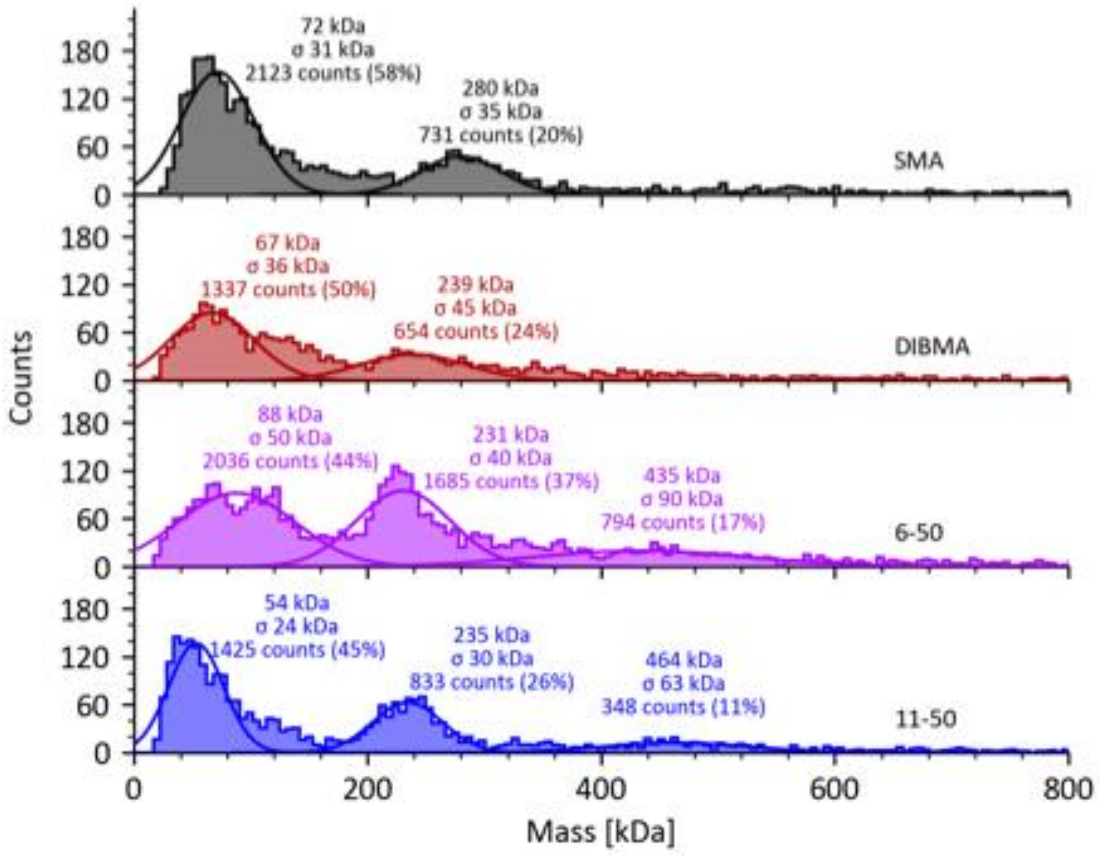

Figure 4.2: SMA2000, DIBMA, 6-50 and 11-50 co-polymers produce protein-lipid nanodiscs of a similar mass. Samples of purified BmrA solubilised with 2.5% (w/v) SMA2000 and DIBMA, and 0.5% (w/v) 6-50 and 11-50 were analysed by mass photometry. Counts plotted against mass (kDa) on a stacked graph, with masses of identified peaks labelled. n = 1 per condition.

As shown in figure 4.2, all of the selected polymers produced protein-lipid nanodiscs with similar sample profiles when analysed by mass photometry. All contain an initial low mass peak between 54 and 88 kDa – attributed to a contaminating presence such as excess polymer or empty nanodiscs. The second peak between 231 and 280 kDa likely represents a population of protein-lipid nanodiscs containing functional BmrA, which functions as a homodimer of ~130 kDa (Dalmas, *et al.,* 2005) with ~100 kDa of mass contributed by lipids and co-polymer belt as shown in mass photometry studies of empty SMALPs (Olerinyova, *et al.,* 2021). Alternatively, the low mass peak may represent a population of monomeric BmrA with

subsequent peaks representing higher order oligomeric states of BmrA, or an association of multiple nanodiscs.

Conversely to existing literature, SMA2000 protein-lipid nanodiscs appear to have the highest mass of ~280kDa when compared to the other three co-polymers with an average mass of ~235kDa. The AASTY co-polymers 6-50 and 11-50 also appear to produce a third population of higher mass particles at ~445kDa, suggesting AASTY co-polymers produce a more heterogeneous nanodisc population when compared to SMA and DIBMA.

4.4 Lipid-Only SEC

To further probe nanodisc size, lipid-only discs solubilised with SMA2000, DIBMA, 6-50 and 11-50 were analysed by SEC (Figure 4.3). SEC is a purification technique that separates molecules based on size by filtration through a matrix. Lipid-only nanodiscs are produced using DMPC as a simplified membrane model and utilised in further study to highlight differences in nanodisc mass based on co-polymer utilised for solubilisation, while reducing the variance exhibited when conducting the same experiments with protein containing nanodiscs.

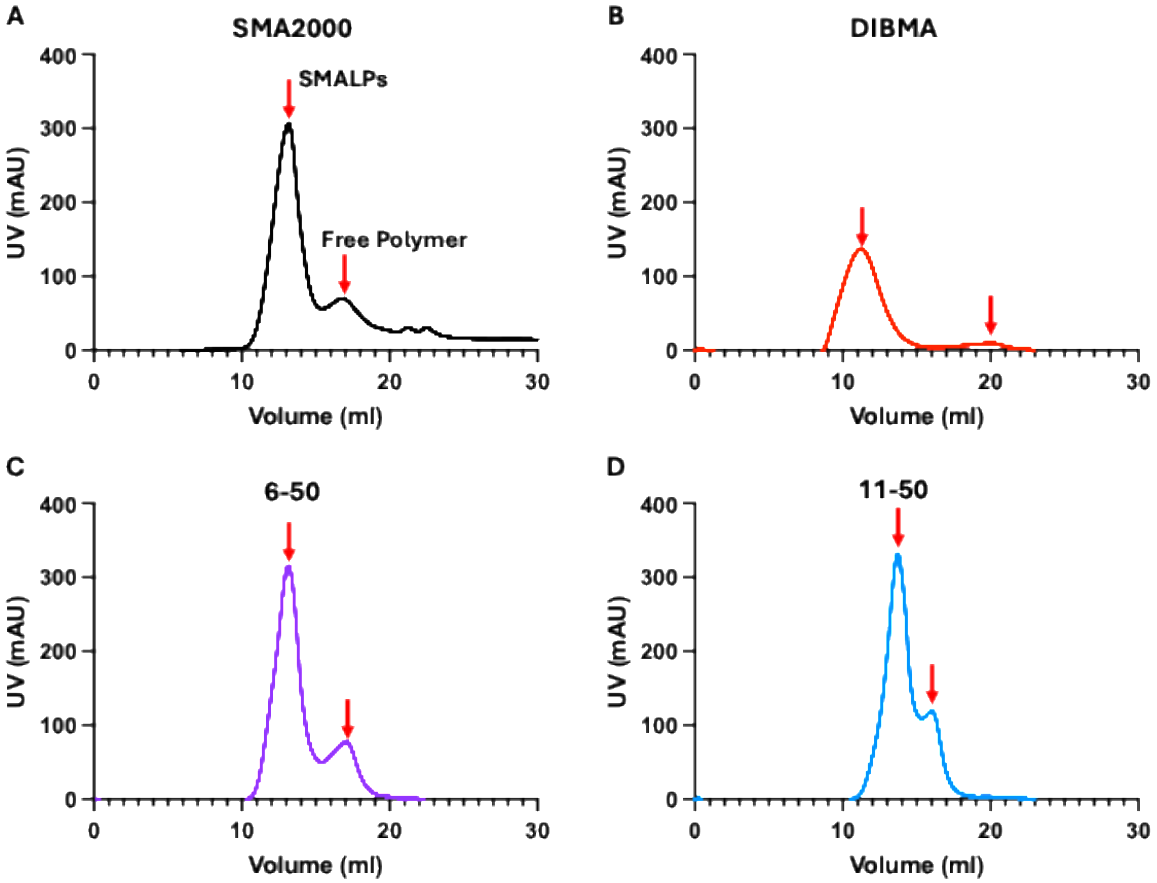

Figure 4.3: SMA2000, DIBMA, 6-50 and 11-50 solubilised lipid-only nanodiscs exhibit similar SEC traces. SEC profiles of 500µl lipid-only nanodiscs solubilised with 2.5% (w/v) SMA2000 (A) and DIBMA (B), and 0.5% (w/v) 6-50 (C) and 11-50 (D), eluted in 0.5ml fractions from superdex 200 increase 10/300 column. UV absorbance (mAU) plotted against volume (ml). Peaks associated to SMALPs and free polymer highlighted.

All four co-polymers presented with strikingly similar SEC profiles in figure 4.3 with lipid only nanodiscs eluting between 10 – 20ml – which is supported in existing literature (Hesketh, *et al.,* 2020). The first peak in all four cases represents a population of lipid-only nanodiscs and the second peak being excess polymer.

DIBMA solubilised lipid-only nanodiscs appear to produce a lower concentration when compared to SMA2000, 6-50 and 11-50, however this is deceptive because DIBMA does not contain the styrene group, and thus the absorbance at 280nm is lower. DIBMA lipid-only nanodiscs also elute at ~11ml, which is earlier when compared to SMA2000 and 6-50 lipid-only nanodiscs which elute at ~13ml, and 11-50 lipid-only nanodiscs that elute slightly later at ~14ml.

While SEC does not provide definitive and reproducible measurements of particle size and is complicated by the fact that the nanodiscs are not spherical, the speed of elution gives a good indication as larger particles are unable to enter pores with the column packing material and as such are washed through the column quicker with the inverse for smaller particles. Results in figure 4.3 suggest that DIBMA lipid-only nanodiscs are the largest followed by SMA2000 and 6-50 lipid-only nanodiscs, with the smallest particles being 11-50 lipid-only nanodiscs.

4.5 Lipid-Only Mass Photometry

Lipid-only nanodiscs produced using SMA2000, DIBMA, 6-50 and 11-50 and purified by SEC were then analysed by mass photometry to probe particle size of an 'empty' nanodisc (Figure 4.4).

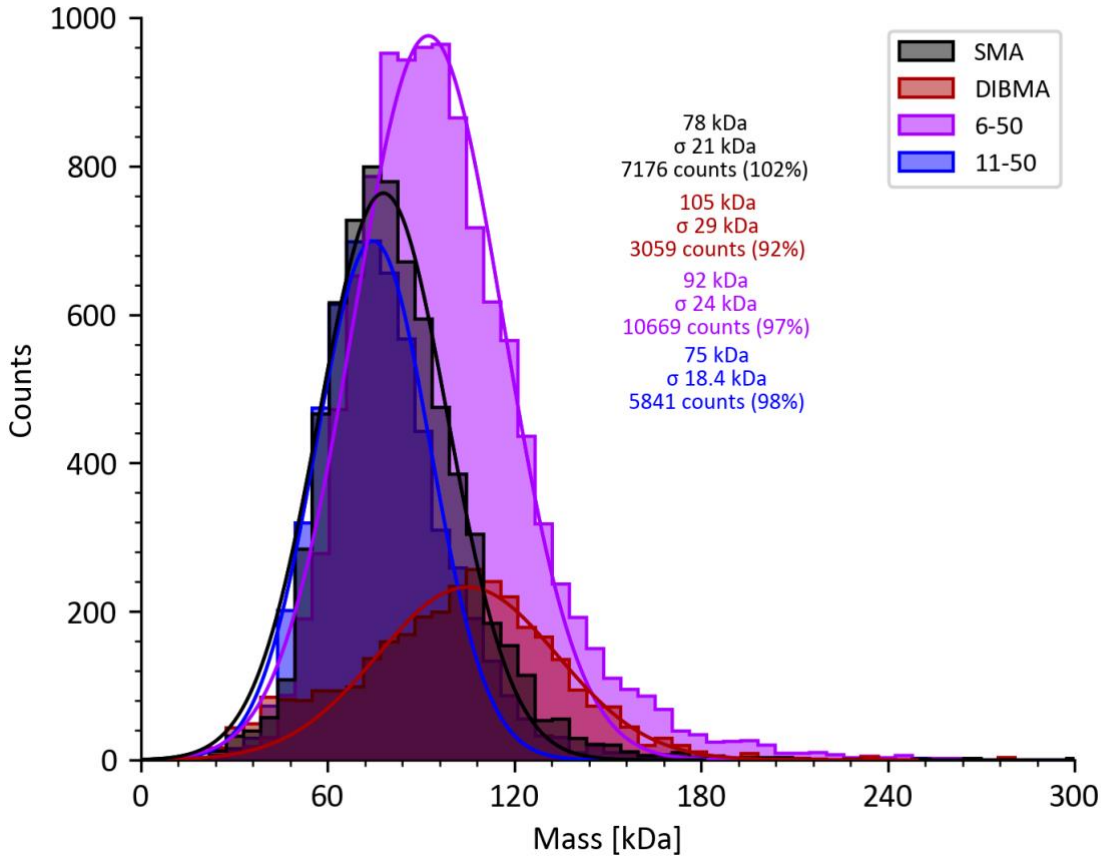

Figure 4.4 : SMA2000, DIBMA, 6-50 and 11-50 co-polymers produce lipid-only nanodiscs of a similar mass. Samples of SEC purified lipid-only nanodiscs solubilised with 2.5% (w/v) SMA2000 and DIBMA, and 0.5% (w/v) 6-50 and 11-50 were analysed by mass photometry. Counts plotted against mass (kDa), with masses of identified peaks labelled. n = 1 per condition.

As shown in figure 4.4, lipid-only nanodiscs produced using SMA2000, DIBMA, 6-50 and 11-50 all display a distinct single peak between 75kDa and 105kDa. These values align with existing literature (Olerinyova, *et al.,* 2021) and further supports the populations found in SEC profiles of protein-lipid samples in figure 4.2.

In contrast to results in figure 4.2, DIBMA lipid-only nanodiscs display the largest mass of 105kDa, which better supports existing literature in which DIBMA nanodiscs are generally larger than SMA nanodiscs (Oluwole, *et al.,*2017). SMA2000 and 11-50 lipid-only nanodiscs exhibit similar masses of 75kDa and 78kDa, with 6-50 lipid-only nanodiscs displaying a slightly larger mass of 92kDa.

The curve distribution of each population is similar, but DIBMA and 6 -50 lipid-only nanodiscs appear to display the widest distribution – suggesting a higher degree of heterogeneity.

4.6 Binding Activity

Mass photometry can also be utilised to investigate binding and unbinding based on particle interaction with the glass slide, with positive values representing binding activity and negative values representing unbinding activity. Lipid-only nanodiscs produced with SMA2000, DIBMA, 6-50 and 11-50 and purified by SEC were tested (Figure 4.5).

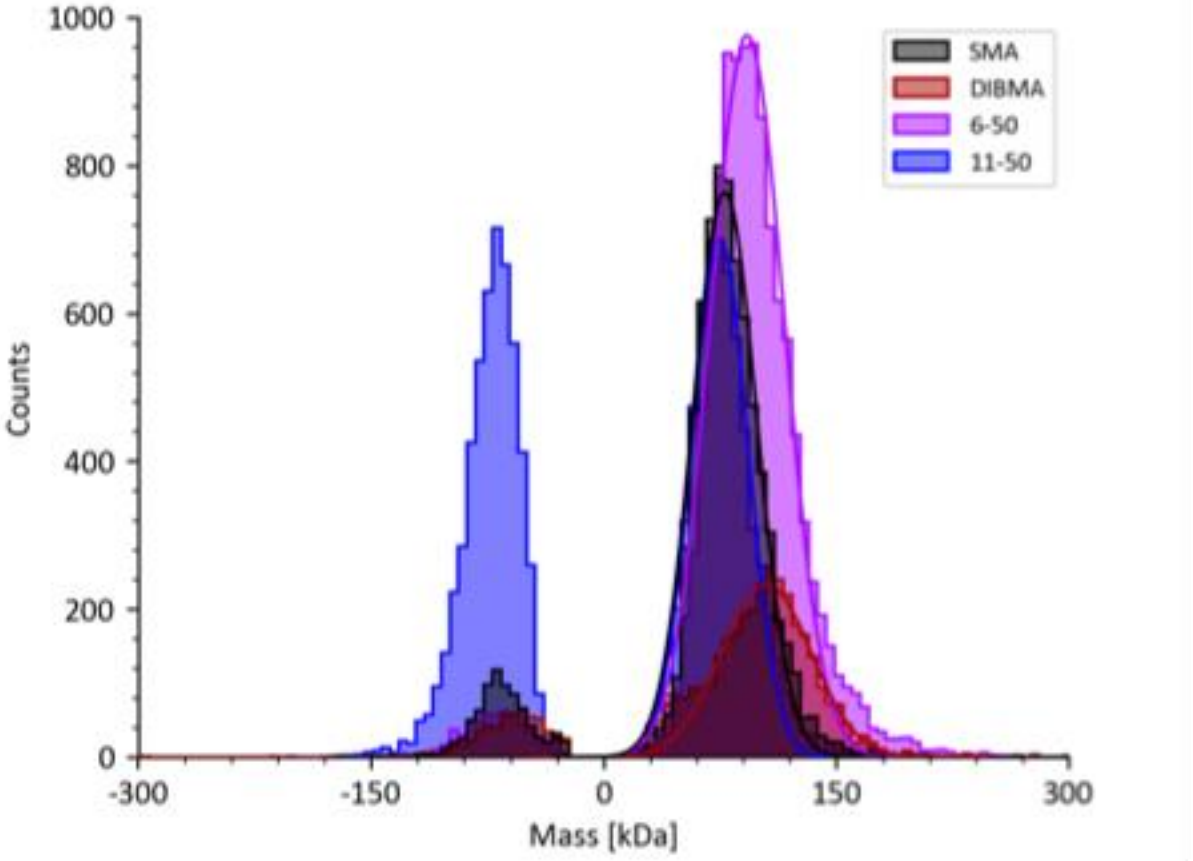

Figure 4.5 : 11-50 displays a contrasting binding/unbinding profile when compared to SMA2000, DIBMA and 6-50. Samples of SEC purified lipid-only nanodiscs solubilised with 2.5% (w/v) SMA2000 and DIBMA, and 0.5% (w/v) 6-50 and 11-50 were analysed by mass photometry. Counts plotted against mass (kDa), with negative values representing unbinding events and positive representing binding events. n = 1 per condition. Data reproduced from Figure 4.4 with extended negative axis.

Lipid-only nanodiscs produced using SMA2000, DIBMA, 6-50 and 11-50 were able to bind and unbind to the glass slide in varying degrees as shown in figure 4.5. However, 11-50 lipid-only nanodiscs stand out due to the increased level of unbinding activity, exhibiting an equal distribution of binding to unbinding. This is in contrast to the other three co-polymers which exhibit much lower levels of unbinding activity.

4.7 Sample Homogeneity

Co-polymer nanodiscs are known to be rather heterogenous and exhibit multiple populations in regard to nanodisc size. To probe this, two separate samples of SMA2000 lipid-only nanodiscs were tested by mass photometry (Figure 4.6). One sample represents a single SEC

elution fraction taken from the centre of the peak attributed to lipid-only nanodiscs, while the other sample contains pooled SEC elution fractions across the range of the peak attributed to lipid-only nanodiscs.

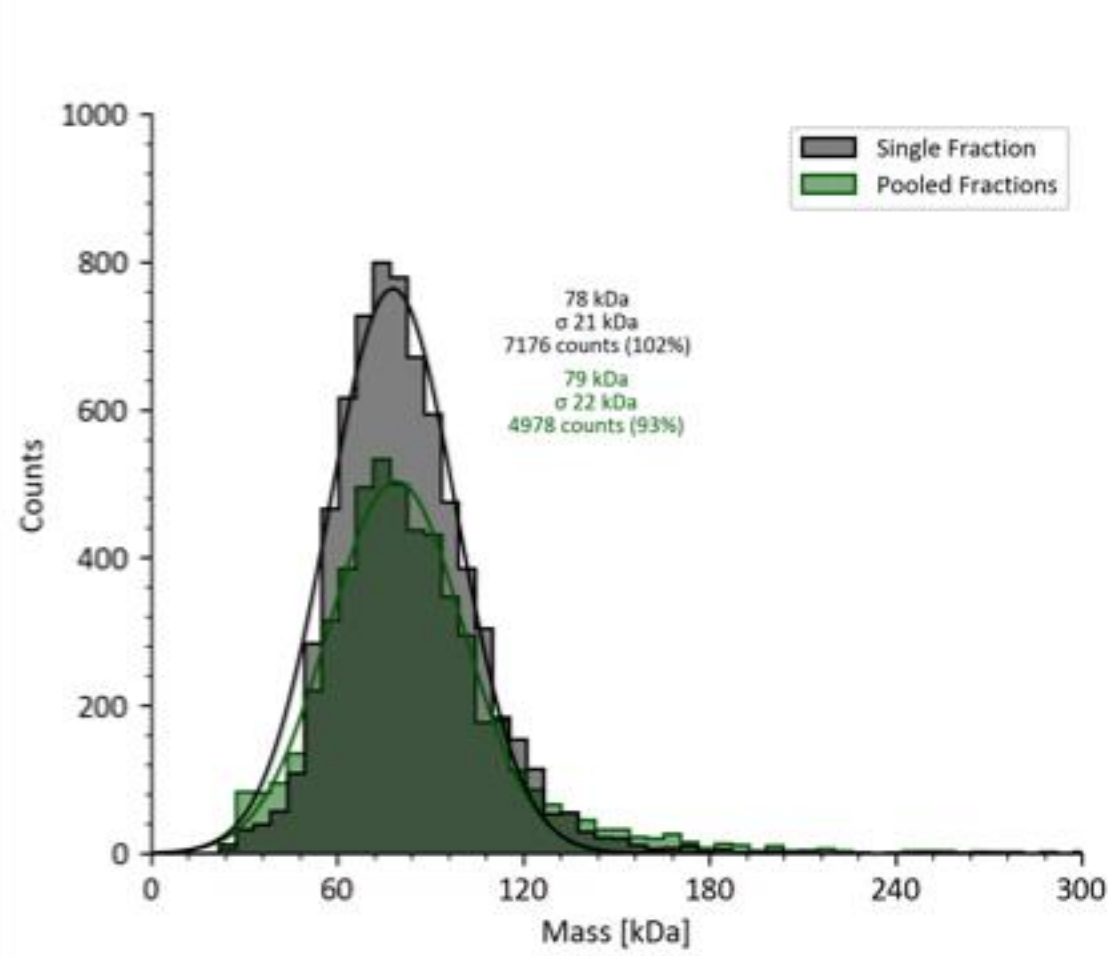

Figure 4.6 : Limited differences in the mass distribution of SMA2000 lipid-only nanodiscs when using pooled or single SEC fractions. Samples of SEC purified lipid-only nanodiscs solubilised with 2.5% (w/v) SMA2000 were analysed by mass photometry, with one sample containing the innermost peak fraction and the other sample containing pooled peak fractions. Normalised counts plotted against mass (kDa), with masses of identified peaks labelled. n = 1 per condition.

As shown in figure 4.6, there are limited differences in the mass reported for lipid-only nanodiscs captured in single or pooled SEC elution fractions with 78kDa and 79kDa. While the count number is slightly higher in single fraction lipid-only nanodiscs, this can be attributed to sample dilution carried out during optimisation. However, the distribution of pooled lipid-only nanodiscs appears to be slightly wider, suggesting that pooled samples present a less homogenous population.

4.8 Lipid Composition

Another variable reported for co-polymer nanodiscs is lipid composition. The ability to retain native phospholipids is a major advantage of co-polymer solubilisation and previous studies have found enhancements of different lipid classes co-purifying with specific proteins in nanodiscs when compared to crude membranes (Teo, *et al.,* 2019). However, it remains a little controversial in the literature as to whether the polymers exhibit preferences for certain lipids (Teo, *et al.,* 2019, Ayub, *et al.,* 2020 and Dominguez Pardio, *et al.,* 2017).

To investigate lipid composition of co-polymers nanodiscs, MTBE lipid extraction was performed on crude membrane and co-polymer solubilised membrane samples. Dried down lipid extracts were rehydrated and analysed by TLC (Figure 4.7) – a technique to separate lipids based on polarity. This provided information regarding lipid class preferences for tested co-polymers in both bacterial and insect expression systems.

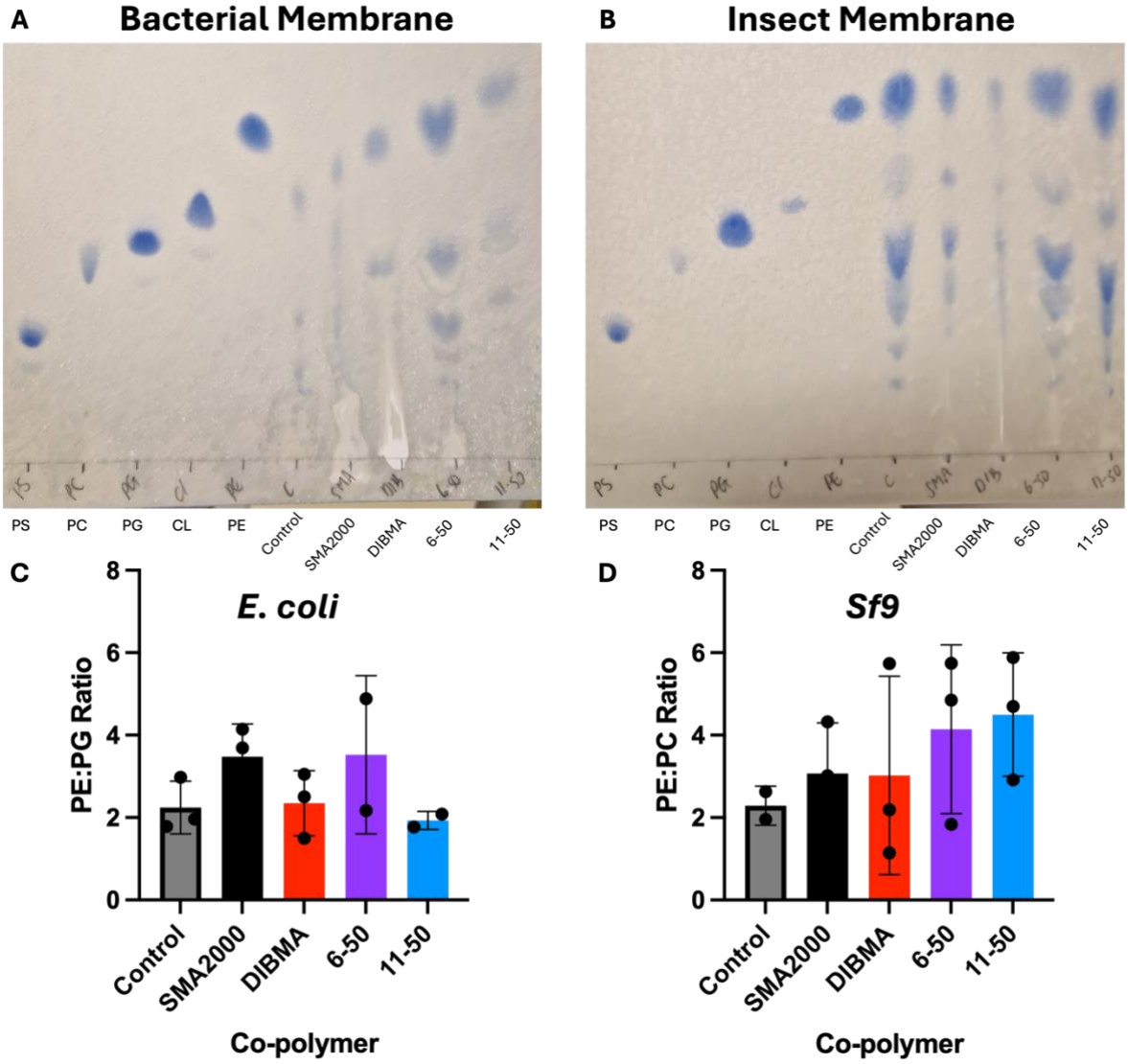

Figure 4.7 : MTBE extraction and TLC of co-solubilised lipids found in co-polymer nanodiscs was successful, with an enrichment of PE in co-solubilised when compared to crude membranes. TLC of MTBE extracted lipids from *E. coli* (A) and Sf9 (B) co-polymer nanodiscs following solubilisation at 2.5% (w/v) with SMA2000 and DIBMA, and 0.5% (w/v) 6-50 and 11-50, compared to the lipids extracted from the crude membrane preparation (control). 50µg of pure lipid standards were loaded alongside. Densitometric analysis of distinct lipid bands seen in TLC sample lanes representing PE, PG and PC was conducted with the ratio of PE:PG in *E. coli* membranes (C) and PE:PC in Sf9 membranes (D) plotted on GraphPad v.10.0.3 (217) with mean ± SD, n ≥3. Data analysed by one-way ANOVA with no significance found.

MTBE lipid extraction and TLC was successfully conducted in this study as shown in figure 4.7 A and B, with a good separation of lipids using this solvent system. However significant contaminating bands and lane smearing can be seen, especially in the case of DIBMA samples in both figure 4.7 A and B. This made analysis of Rf values difficult and therefore not reported in this analysis.

There also appears to be interference close to the sample line in figure 4.7 A, with blebbing seen towards the base of the TLC plate. This is more present in SMA2000 and DIBMA when compared to 6-50 and 11-50 sample lanes, suggesting this relationship may be related to polymer interference based on the increased concentration of co-polymer used for SMA2000 and DIBMA solubilisation when compared to the AASTYs. However, this relationship is not as prevalent in figure 4.7 B with insect membranes.

PE and PG are the major phospholipid classes in bacterial membranes and were selected for analysis of *E. coli* TLC. While DIBMA and 11-50 nanodiscs displayed a similar ratio of PE:PG to crude membrane samples, SMA and 6-50 nanodiscs appear to be enriched in PE with ~3.5:1 PE:PG. Insect membranes are primarily composed of PE and PC with these classes selected for comparison of Sf9 TLC. All nanodiscs displayed an enrichment in PE when compared to crude membranes with PE:PC ratios of ~3:1 for SMA2000 and DIBMA, ~4:1 for 6-50 and ~4.5 for 11-50.

4.9 Membrane Fluidity

It is well reported that functional study of ABC transporters in SMALPs is difficult – with ATPase assays unapplicable in most cases. It is hypothesised that this difficulty may be due to the requirement of magnesium as a co-factor for ATPase activity, with the use of magnesium resulting in the precipitation of SMALPs (Gulamhussein, *et al.,* 2020). But this does not seem the case for DIBMA, which displays a decreased sensitivity to magnesium but does not appear to produce functionally active BmrA in ATPase assays as shown in previous results. Another hypothesis is that the co-polymer outer ring of nanodiscs is too rigid to allow full conformational change of membrane proteins (Pollock, *et al.,* 2018). It has previously been shown that certain polymer nanodiscs do not allow full function of the GPCR rhodopsin, whereas others do, and it is suggested this is due to the lipid packing within the discs (Grime, *et al.,* 2021).

To investigate this issue, a laurdan assay was employed to probe phospholipid packing and membrane fluidity of nanodiscs produced using SMA2000, DIBMA, 6-50 and 11-50 (Figure 4.8). Laurdan is a fluorescent dye that integrates into the hydrophobic core of bilayers, where

changes in temperature and membrane polarity causes spectral shifts with fluorescence measured.

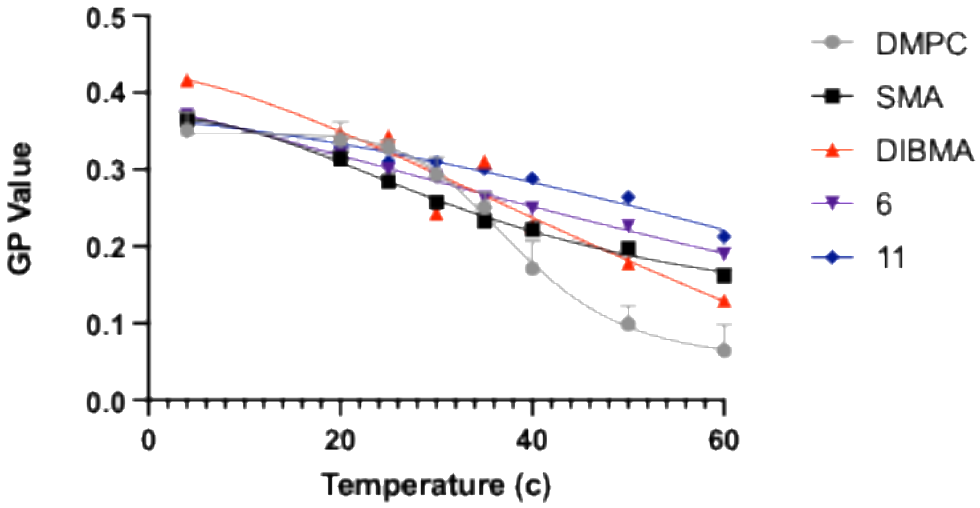

Figure 4.8 : All lipid-only nanodiscs display reduced membrane fluidity when compared to DMPC liposomes. Samples of DMPC liposomes and DMPC lipid-only nanodiscs solubilised with SMA2000, DIBMA, 6-50 and 11-50 were mixed with 5µl 1mM laurdan at room temperature. Samples were then incubated at temperatures between 5°C and 60°C for 5 minutes with fluorescence measured in triplicate per temperature condition, with n ≥1. Produced using GraphPad v.10.0.3 (217) with non-linear regression inhibitor vs response curve fit.

Membrane fluidity is greatly affected in co-polymer lipid-only nanodiscs when compared to DMPC liposomes in figure 4.8 – as supported in existing literature (Pardo, *et al.,* 2017). DMPC liposomes display decreased lipid packing as the temperature increased, represented by the decrease in GP values from ~0.35 at 5°C to ~0.05 at 60°C. This is markedly different to all four of the co-polymer lipid-only nanodiscs with high levels of lipid packing across the same temperature range, as represented by the limited decrease in GP values from ~0.4 at 5°C to ~0.15 at 60°C with little evidence of laurdan spectral shifts observed. While DMPC liposomes display a clear sigmoidal shaped curve with a sharp gel-to-fluid transition temperature of ~37°C, this is not witnessed in co-polymer lipid-only samples.

Summary

Co-polymer nanodisc characteristics differ depending on the co-polymer utilised for solubilisation. While SMA2000, 6-50 and 11-50 produce lipid-only nanodiscs of similar sizes with an average mass of ~80kDa, DIBMA lipid-only nanodiscs are larger with a mass of 105kDa – which is supported in existing literature as well as SEC data. However, the opposite

relationship is witnessed in protein-lipid nanodiscs, with SMA2000 appearing to produce the largest nanodisc with a mass of 280kDa when compared to DIBMA, 6-50 and 11-50 with an average mass of 235kDa.

Analysis of the lipid composition of co-polymer nanodiscs produced with Sf9 and *E. coli* membranes by TLC found an enrichment of PE when compared to crude membrane samples. However, this relationship is not as present in bacterial membrane samples and needs further defining due to issues with contamination and polymer interference in TLC.

Utilisation of co-polymer solubilisation results in a decrease membrane fluidity as shown by laurdan assays when compared to DMPC liposomes. This is regardless of co-polymer type, with SMA2000, DIBMA, 6-50 and 11-50 nanodiscs all displaying limited evidence of laurdan spectra shift and gel-to-fluid transition based on temperature. This evidence further supports the theory that nanodiscs are held to tightly to allow for full conformational change to support substrate transport (Pollock, *et al.,* 2019).

Co-polymers are a good alternative to detergents for the solubilisation of diverse range of membrane proteins. Their utilisation is easy to implement with low costs, results in increased protein purity and stability with limited necessity for further sample processing for techniques such as cryo-EM. However, co-polymer solubilisation is still somewhat limited for the functional study of ABC transporters such as BmrA due to the reduced nanodisc membrane fluidity. This is hypothesised to be the reason for why ABC transporters are often non-functional in co-polymer nanodiscs.

In order to take advantage of the benefits from both systems, the ability to swap in and out of nanodiscs, micelles and proteoliposomes would be beneficial. This has been shown in recent studies (Rehan, *et al.,* 2017, Hesketh, *et al.,* 2020) but is probed further in the following chapter.

5. Results Chapter Three – BmrA Reconstitution

5.1 Introduction

All of the explored methods of membrane protein solubilisation including detergents, amphipols, MSPs and co-polymers present with their own advantages and disadvantages. Their utilisation typically involves optimisation on a case-to-case basis depending on the target membrane protein along with many other factors such as pH, time and temperature. In order to reduce the time spent optimising and produce highly stable proteins applicable for downstream analysis, the ability to reconstitute utilising different systems has been explored.

While detergents are highly efficient and provide a good protein yield, they are known to interfere with protein-lipid interactions and may result in decreased protein stability (Sych, Levental and Sezgin, 2022). On the other hand, co-polymers display high efficiencies and good protein purity, producing nanodiscs that retain native protein-lipid interactions resulting in highly stable membrane proteins. However, they display a sensitivity to divalent cations and functional study of ABC transporters can be difficult as shown in previous results and existing literature (Gulamhussein, *et al.,* 2020, Pollock, *et al.,* 2022). The use of proteoliposomes is common in membrane protein research as it provides the opportunity to modify lipid composition to probe lipid-dependent protein structure and function (Sejwal, *et al.,* 2017).

In order to take advantage of the benefits from different systems, investigations into the reconstitution of BmrA from co-polymer nanodiscs (SMA, DIBMA, 6-50 and 11-50) into DMPC proteoliposomes and DDM micelles have been conducted (Figure 5.1).

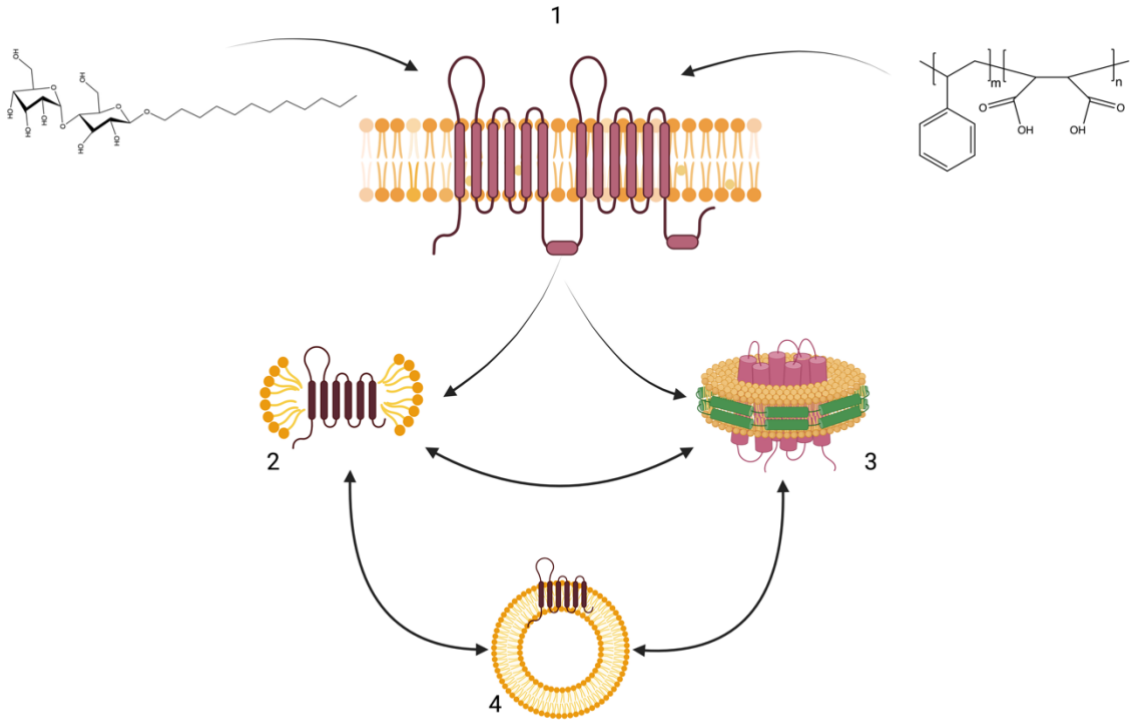

Figure 5.1 : Schematic representation highlighting the pathways of solubilisation and the ability to swap between systems. 1 : Membrane samples are mixed with either detergents or co-polymers for initial stages of solubilisation depending on desired applications. 2 : For structural study, detergent micelles are commonly utilised, but they do not co-solubilise lipids that are not tightly associated with the protein. 3 : For applications requiring lipids, the use of co-polymers is common as they retain the native phospholipid environment and protein-lipid interactions. But functional study is limited for ABC transporters. 4 : Proteoliposomes are useful in functional study of ABC transporters and provide an opportunity to modulate lipid composition to measure effects. Membrane proteins are able to be transferred between 2, 3 and 4 utilising different methods.

5.2 Reconstitution from SMALPs to proteoliposomes

5.2.1 Effect of Magnesium on Reconstitution Efficiency

The reconstitution of membrane proteins from detergent micelles into proteoliposomes is well studied and commonly involves the dilution of a sample to below CMC value in order to disassociate micelles (Goddard, *et al.,* 2015). When mixed with lipids, membrane proteins gravitate towards the protective hydrophobic core of the lipid bilayer resulting in the production of proteoliposomes.

However, reconstitution from co-polymer nanodiscs to proteoliposomes is less defined due to its novelty (Hesketh, *et al.,* 2020) and explored in this research. While co-polymer nanodisc stability is a major advantage for many applications, it presents an issue when attempting reconstitution. Unlike micelles, co-polymer nanodiscs are less likely to disassociate when co-polymer concentration is reduced and as such requires a different approach. To do this, nanodisc sensitivity to divalent cations is utilised with the addition of magnesium along with gentle heat used to stimulate nanodisc disassociation and reconstitution (Figure 5.2).

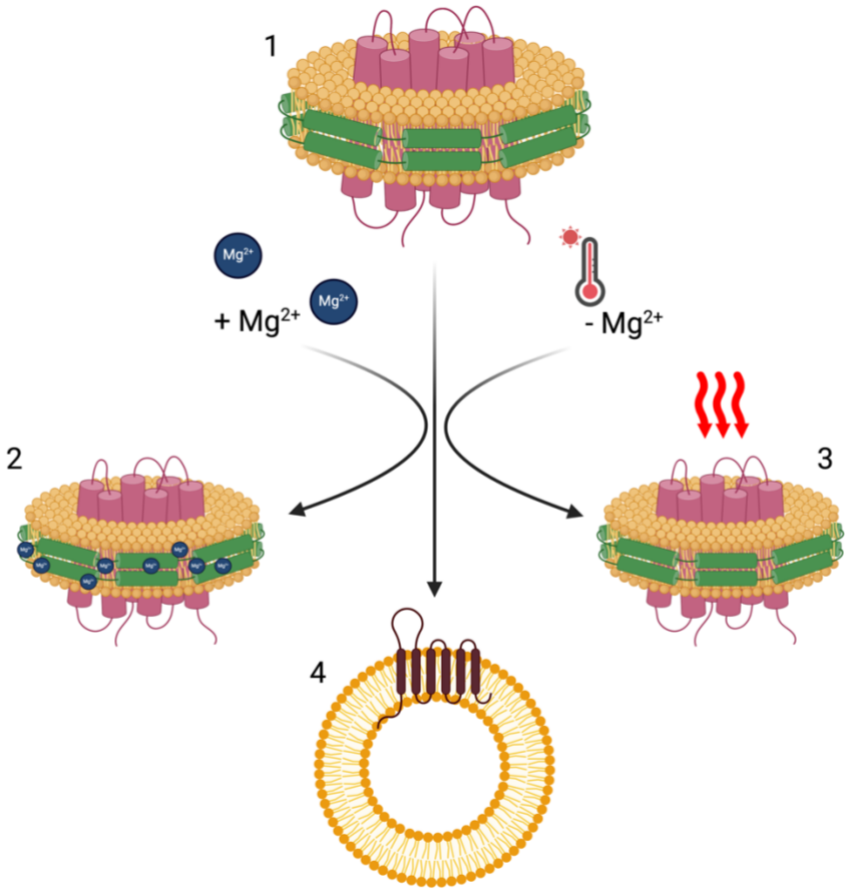

Figure 5.2 : Schematic representation of the pathway of BmrA reconstitution from SMALPs to proteoliposomes. 1 : SMALPs containing BmrA are prepared and purified. 2 : Reconstitution of BmrA from SMALPs to proteoliposomes can be carried out utilising nanodisc sensitivity to divalent cations, with magnesium added to encourage SMALP dissociation. 3 : Reconstitution of BmrA from SMALPs to proteoliposomes may also be carried out without magnesium, applying only gentle heat in order to encourage SMALP disassociation. 4 : Using these methods, BmrA can be transferred from native lipid containing SMALPs to proteoliposomes of defined lipid compositions.

To test both methods of reconstitution from SMA solubilised nanodiscs into DMPC proteoliposomes, purified BmrA nanodiscs were subjected to gentle heat in the absence or presence of magnesium with DMPC liposomes produced by extrusion (Figure 5.3).

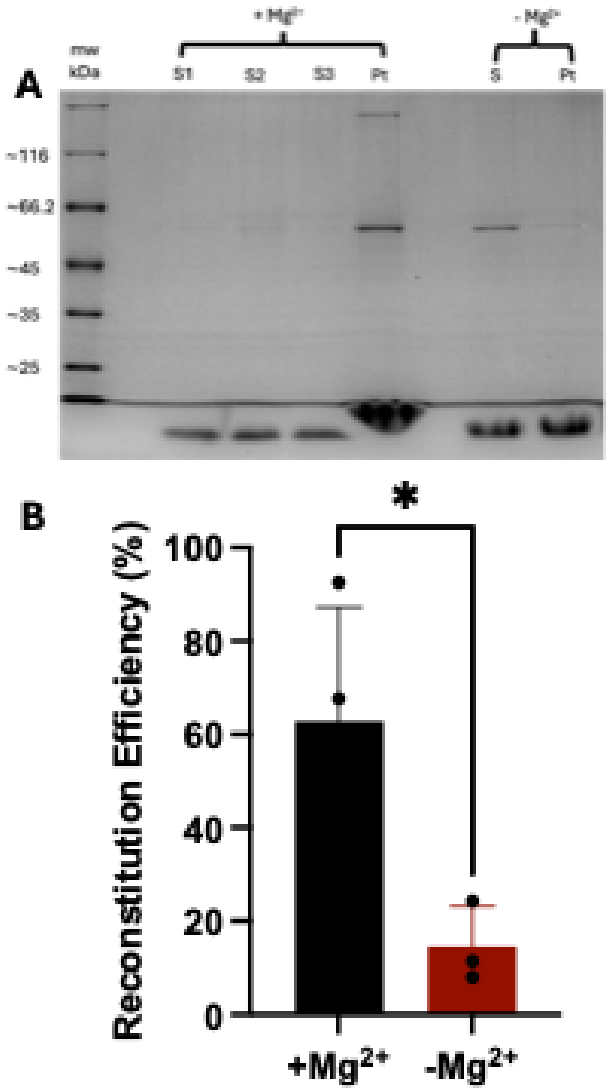

Figure 5.3 : The use of Mg^{2+} significantly increases the reconstitution efficiency of BmrA from SMALPs to proteoliposomes. A) Purified BmrA SMALPs were mixed with DMPC liposomes at a ratio of 1:100 protein: lipid in the presence ($+Mg^{2+}$) or absence ($-Mg^{2+}$) of 10mM magnesium and incubated at 37°c for 30 minutes. Samples were then successively centrifuged (100,000 x g, 20 min, 4°C) with supernatant (S1, S2, S3) and pellet (Pt) samples collected, loaded on SDS-PAGE and stained with Instantblue. B) Reconstitution efficiency calculated by densitometry using ImageJ and presented as mean ± SD, n ≥ 3. Data analysed by unpaired T-test with *p ≤ 0.05. Produced using GraphPad v. 10.0.3 (217).

As shown in figure 5.3 A, there are clear differences in the reconstitution of BmrA when using magnesium or not. Samples prepared using magnesium show a distinct BmrA band in the pellet lane, representing the successful disassociation of nanodiscs. However, further study such as sucrose gradient density centrifugation would be required to confirm the transfer of BmrA into proteoliposomes. While some BmrA banding can be seen in supernatant lanes, these are relatively low level with reconstitution appearing to be highly efficient. However, the inverse is witnessed for samples prepared without the use of magnesium. For these

samples, the majority of BmrA is found in the supernatant lane suggesting the bulk of BmrA remains soluble in SMALPs. However, BmrA can still be detected in the pellet lane, suggesting at least some BmrA was successfully reconstituted.

Following densitometric analysis of proteoliposome SDS-PAGE gels, the reconstitution efficiency was calculated and shown in figure 5.3 B. While both methods successfully resulted in the reconstitution of BmrA into proteoliposomes, the utilisation of magnesium significantly increased the reconstitution efficiency from 15% to 63%.

5.2.2 Effect of Incubation on Reconstitution Efficiency

The length of incubation at 37°c was also tested in this project in an attempt to optimise BmrA reconstitution, with longer incubations expected to encourage higher efficiencies due to increased membrane fluidity. Samples with and without magnesium were exposed to 37°c heat for 5 or 30 minutes, with the reconstitution efficiency analysed (Figure 5.4).

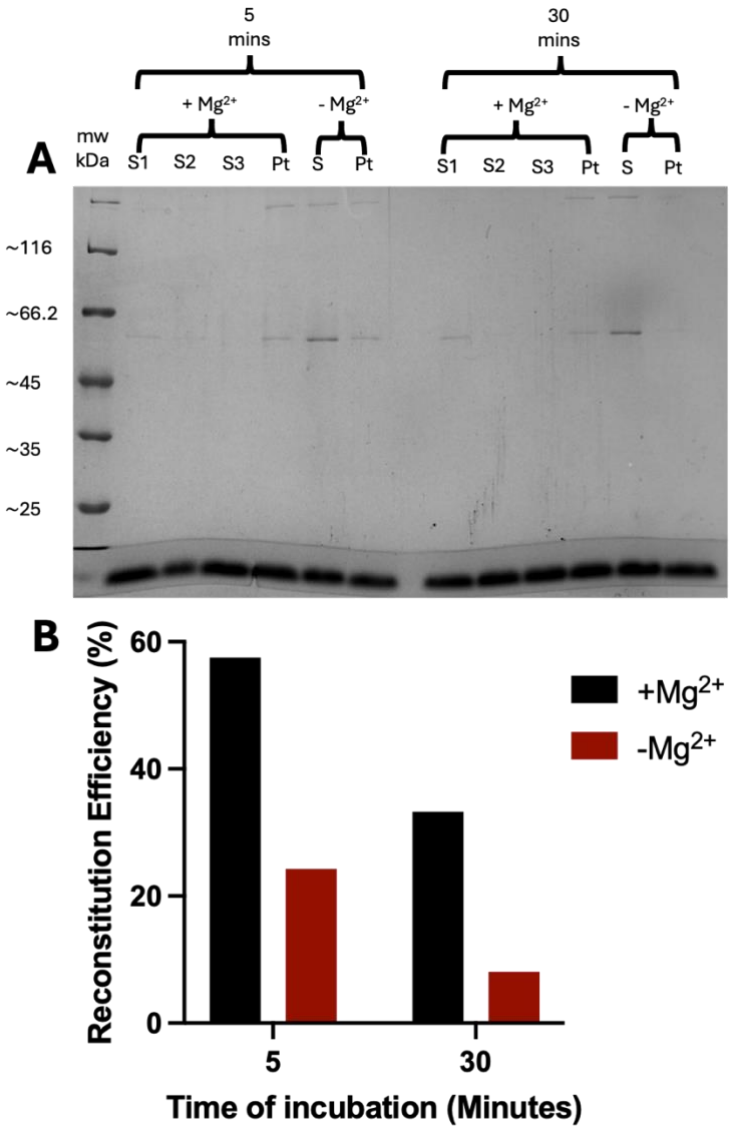

Figure 5.4 : A shorter length of incubation appears to increase the reconstitution efficiency of BmrA from SMALPs to proteoliposomes. A) Purified BmrA SMALPs were mixed with DMPC liposomes at a ratio of 1:100 in the presence (+Mg^{2+}) or absence (-Mg^{2+}) of 10mM magnesium and incubated at 37°c for either 5 or 30 minutes. Samples were then successively centrifuged (100,000 x g, 20 min, 4°C) with supernatant (S1, S2, S3) and pellet (Pt) samples collected, loaded on SDS-PAGE and stained with Instantblue. B) Reconstitution efficiency calculated by densitometry with n = 1. Produced using GraphPad v. 10.0.3 (217).

As shown in figure 5.4 A, the left (5 minutes) and right (30 minutes) sides of the SDS-PAGE gel show near identical banding profiles. Similar to previous results, when magnesium is utilised distinct BmrA bands are seen in the pellet lanes representing successful reconstitution. Some banding can also be seen in the supernatant lanes, but this is limited. On the other hand, when magnesium is not utilised the majority of BmrA is found in the supernatant lane suggesting a higher proportion of BmrA remains in SMALPs. However, less distinct BmrA bands can also be seen in the pellet lane.

Following densitometric analysis shown in figure 5.4 B, there appears to be an increase in reconstitution efficiency from 33% to 58% when decreasing the length of incubation from 30 to 5 minutes when using magnesium. While more repeats would be necessary to confirm this relationship, 5-minute incubations are recommended for BmrA reconstitution from SMALPs to proteoliposomes.

5.3 Co-polymers to DDM

In order to further probe the ability to swap between systems, the transfer of BmrA from co-polymer nanodiscs solubilised with SMA2000, DIBMA, 6-50 and 11-50 to DDM micelles was tested (Figure 5.5).

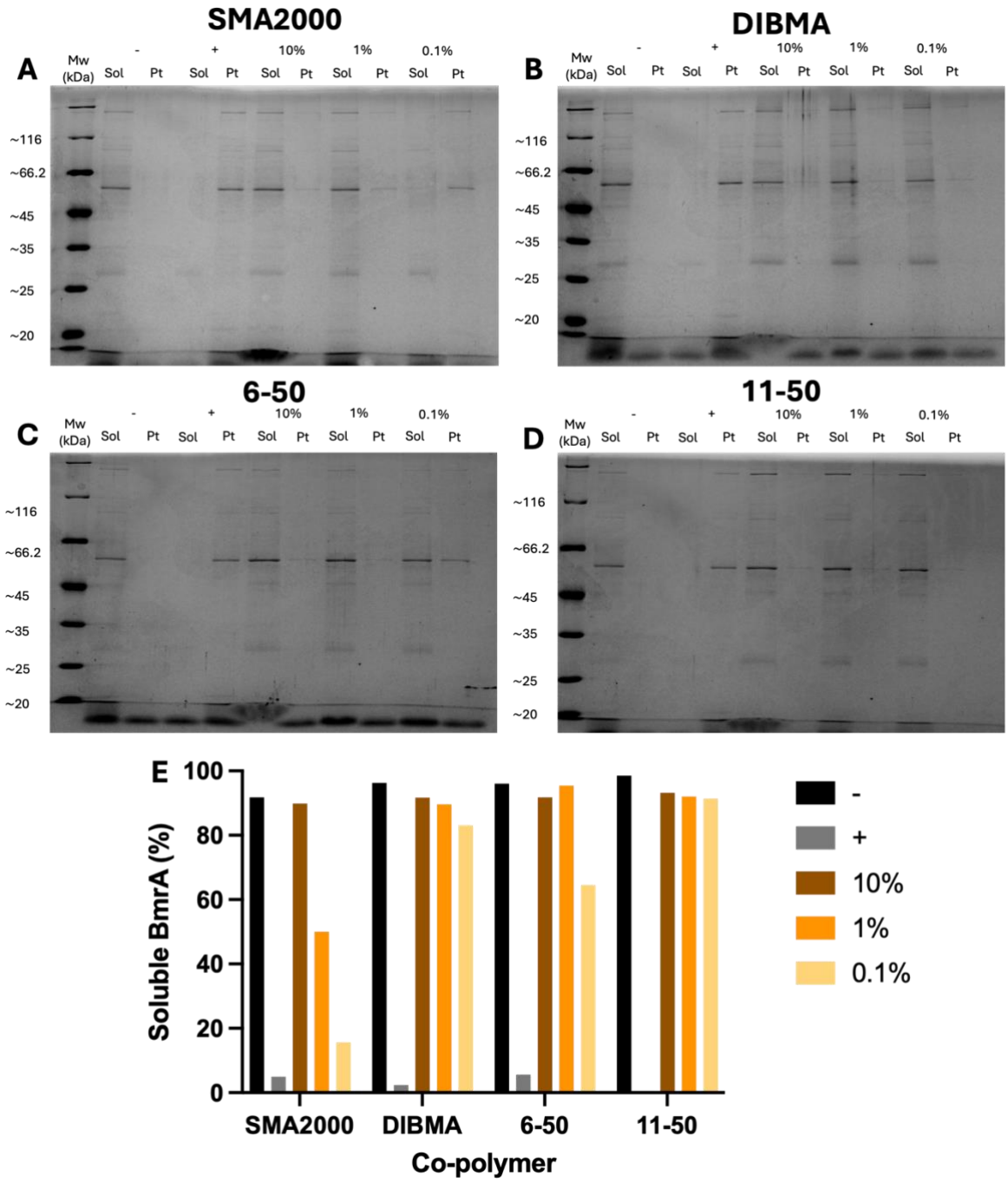

Figure 5.5 : BmrA can successfully be transferred from co-polymer nanodiscs to DDM micelles. Purified BmrA co-polymer nanodiscs solubilised with SMA2000 (A), DIBMA (B), 6-50 (C) and 11-50 (D) are mixed with differing concentrations (10%, 1% and 0.1%) of DDM in the absence (-) or presence (+) of 10mM magnesium. Samples were then centrifuged (100,000 x g, 20 min, 4℃) with supernatant (Sol) and pellet (Pt) samples collected, loaded on SDS-PAGE and stained with Instantblue. E) The percentage of soluble BmrA (%) calculated by densitometry using ImageJ and plotted using GraphPad v. 10.0.3 (217) with n = 1.

All of the co-polymers tested behaved similarly in reconstitution trials from co-polymer nanodiscs to DDM micelles with similar banding profiles in figures 5.5 A, B, C and D. In negative controls (-) where buffer is added to nanodisc samples, the majority of BmrA is found in the supernatant lane representing soluble BmrA nanodiscs. However, when 10mM magnesium is

added to nanodisc samples in positive controls (+) the majority of BmrA is found in the pellet lane, representing the dissociation of nanodiscs and the resulting loss of BmrA solubility. As the concentration of DDM added to solution decreases from 10% to 0.1%, BmrA is witnessed at higher concentrations in the pellet lanes in all cases, but more noticeably in figure 5.5 A and C samples produced with SMA2000 and 6-50.

The relationship between DDM concentration and the percentage of BmrA retained in soluble fractions was analysed by densitometry and shown in figure 5.5 E. The addition of magnesium sharply reduces the percentage of soluble BmrA from 96% to 3%, providing evidence for the disassociation of co-polymer nanodiscs at 10mM magnesium. However, soluble BmrA can be retained by the introduction of DDM with 90% BmrA preserved from SMA nanodiscs, 92% from DIBMA and 6-50 nanodiscs and 93% from 11-50 nanodiscs when 10% DDM is added. This is reduced at lower concentrations of DDM -especially for SMA2000 - with only 16% saved from SMA nanodiscs, 83% from DIBMA nanodiscs, 65% from 6-50 nanodiscs and 91% from 11-50 nanodiscs when 0.1% DDM is added.

Summary

The ability to reconstitute membrane proteins in and out of membrane mimetic systems is useful for a wide range of applications. In this chapter, BmrA has been successfully reconstituted from co-polymer nanodiscs to proteoliposomes and DDM micelles.

The reconstitution of BmrA from co-polymer nanodiscs to DMPC proteoliposomes is useful for probing protein functionality and the effect of differing lipid composition on protein structure and function. This reconstitution pathway appears to be significantly more efficient when 10mM magnesium is utilised along with gentle heat when compared to samples subjected to heat only. The efficiency of reconstitution may also improve when incubating samples for 5 minutes when compared to 30 minutes.

BmrA can also be reconstituted into detergent micelles from co-polymer nanodiscs. Negative and positive controls in these experiments provided further evidence of co-polymer sensitivity, with disassociation of co-polymer nanodiscs at 10mM magnesium causing an almost total loss of soluble BmrA. However, the addition of DDM at concentrations between

10% and 0.1% stimulates the production of detergent micelles, with BmrA remaining soluble even in the presence of 10mM magnesium. However, as the concentration of DDM decreases the efficiency of reconstitution also decreases with less soluble BmrA retained at 0.1% when compared to 10%.

6. Discussion

6.1 Comparison of DDM and SMA2000 Solubilisation Methods

Detergent and co-polymer solubilisation methods provide different advantages and disadvantages for the study of membrane proteins, with their utilisation generally depending on downstream applications. In order to define the differences between these methods and provide a basis of comparison for novel co-polymers, industry standards SMA2000 and DDM were selected for study.

DDM is one of the most commonly utilised detergents for membrane protein solubilisation (Stetsenko, *et al.,* 2017) and has been shown to solubilise a wide range of membrane proteins including ABC transporters with efficiencies generally reported to be above 50% (Infed, *et al.,* 2011). In this study, DDM solubilised BmrA at a mean efficiency of 59±18.4% which aligns with existing literature.

Detergent solubilisation is generally considered to be more efficient when compared to co-polymer solubilisation (Morrison, *et al.,* 2021) but this relationship is not witnessed in this study with SMA2000 presenting a mean efficiency of 66±3.9%. While this difference is not statistically significant, SMA2000 appears to produce a slightly higher efficiency with a lower degree of variability when compared to DDM. The increased variability witnessed in DDM trials is likely linked to the requirement of a tightly controlled ratio of detergent to lipids during solubilisation. Detergent micelles also display decreased thermostability so while co-polymer solubilisation is carried out at room temperature, all solubilisations using DDM are conducted at 4°c.

DDM has also been reported to produce a lower protein purity but higher yield when compared to SMA2000 in multiple studies (Gulati, *et al.,* 2014, Morrison, *et al.,* 2016). This relationship was confirmed in this project, with DDM providing double the yield of BmrA but at a significantly reduced purity of 66±9.7% when compared to SMA2000.

Both solubilisation agents have presented with their own drawbacks in this study, but co-polymer solubilisation is generally preferred with nanodiscs providing a unique opportunity to study membrane proteins in their native phospholipid environment. However, SMA2000 has been shown in this study to display a sensitivity to divalent cations with functional applications limited. Due to the ease by which novel co-polymers are manufactured, a wealth of alternatives such as SMA variants, DIBMA and Glyco-DIBMA and AASTY co-polymers are now commercially available and tested in this project to identify suitability for BmrA functional study.

6.2 Comparison of SMA2000 and SMA Variants

SMA variants SMA-EA, SMA-ED, SMAd-A and SMA-QA were among the least successful co-polymers tested in this study, exhibiting lower solubilisation efficiencies and BmrA purity and yield. These co-polymers were introduced to the market with reports of lower nanodisc sensitivity and enhanced stability when compared to SMA2000 (Ravula, *et al.,* 2017a and Ravula, *et al.,* 2018). They also exhibit a broad range of nanodisc diameter controlled by modulating the polymer to lipid concentration with (Ravula, *et al.,* 2017b), making them key targets for study to expand understanding of nanodisc formation.

While SMA-EA and SMA-ED were able to solubilise BmrA at a mean efficiency of 49±22% and 47±2.5% which is comparable to SMA2000, they produce significantly lower purity levels of 35±2.4% and 35% and very low yields of BmrA – making them inapplicable for sensitivity studies. While confirmation of the reported sensitivities would have been useful, SMA-EA has been shown to still display pH and cation sensitivity (Scheidelaar, *et al.,* 2016) and SMA-ED displays lower stability under neutral conditions (Ravula, *et al.,* 2017a). The further modified polymers SMAd-A and SMA-QA performed even worse with no solubilised BmrA detected following purification. They were therefore not included in efficiency, purity and yield analyses and unable to be utilised for sensitivity studies. Similarly to SMA-ED, SMAd-A has been reported to be unsuitable for solubilisation at neutral pH (Ravula, *et al.,* 2017a). While SMA-QA appears to produce monodisperse nanodiscs at 7.5 pH (Ravula, *et al.,* 2018), the dark smearing witnessed in soluble and flow-through lanes on purification SDS-PAGE gels may suggest compatibility issues for both SMA-QA and SMAd-A.

6.3 Comparison of SMA2000, DIBMA and Glyco-DIBMA

DIBMA and Glyco-DIBMA are another group of co-polymers tested in this project due to the reported tolerance to magnesium (Oluwole, *et al.,* 2017), larger nanodisc size (Gulamhussein, *et al.,* 2020), and chemical and structural differences when compared to SMA2000. Previous reports have hypothesised that co-polymers hold membranes too tightly to allow for full conformational change of embedded membrane proteins during transport (Pollock, *et al.,* 2018) with this study showing the difficulty in functionally studying BmrA in SMALPs. A nanodisc with lower sensitivity and a larger diameter may perform better in ATPase and membrane fluidity assays. Here, the efficiency of DIBMA and Glyco-DIBMA and the resulting BmrA purity and yield is compared to SMA2000.

While the solubilisation efficiency of DIBMA at 40±27% is not significantly different to SMA2000, there appears to be a higher degree of variability. Similar results have been shown previously (Gulamhussein, *et al.,* 2020), with DIBMA nanodiscs displaying increased particle size heterogeneity in other studies (Voskoboynikova, *et al.,* 2021). DIBMA also provided a comparable level of protein yield to SMA2000 in this work and in other studies (Gulamhussein, *et al.,* 2020). While the yield of BmrA was comparable, DIBMA produces significantly lower BmrA purity at 69±15%. This may be connected to the increased nanodisc diameter, with a higher chance of co-solubilising proteins being present in larger nanodiscs when compared to smaller ones. While BmrA purity was low for DIBMA, the yield was acceptable and therefore was selected for further study.

On the other hand, Glyco-DIBMA did not meet selection criteria as it displayed low solubilisation efficiency, purity and yield. This co-polymer was developed in response to the low solubilisation efficiencies reported for DIBMA, with partial amidation reducing polymer charge and increasing hydrophobicity. It has been shown to solubilise *E. coli* membranes in previous studies and exhibit an increased tolerance to magnesium (Danielczak, *et al.,* 2022) but is yet to be tested for ABC transporters. While Glyco-DIBMA was able to solubilise BmrA in this study, it exhibited a lower solubilisation efficiency of 31±10% and significantly lower BmrA purity of 51±4% when compared to SMA2000. The yield of purified BmrA was also significantly lower with difficulties experienced during quantification. Due to this, Glyco-DIBMA was not taken forward for further testing.

6.4 Comparison of SMA2000 and AASTY

AASTY polymers are a group of six co-polymers that have been most recently introduced (Smith, *et al.,* 2020). Produced by RAFT, AASTY polymers reportedly produce nanodiscs that are more homogeneous and display a lower sensitivity to divalent cations when compared to SMA and DIBMA nanodiscs (Smith, *et al.,* 2020, Timcenko, *et al.,* 2022). AASTY is a highly repeating co-polymer that contains acrylic acid in place of maleic acid found in SMA2000. This chemical difference is hypothesised to be the reason for a reduced sensitivity with the loss of an exposed carboxyl group leading to reduced electrostatic interactions with divalent cations. The six AASTY polymers tested in this project differed by molecular weight, being either 6kDa or 11kDa, and the ratio of styrene: acrylic acid being either 45%, 50% or 55%.

Unlike the standard 2.5% final concentration utilised for all other polymers tested in this study, AASTY co-polymers were utilised at a final concentration of 0.5%. This was initially recommended by the manufacturer but to confirm this a small-scale concentration trial was conducted for the solubilisation of BmrA. While none of the AASTY polymers showed significant differences in solubilisation efficiency at 0.5% and 2.5%, the maintenance of good efficiency at lower polymer concentrations is useful. 2.5% polymer while widely used, is rather excessive in order to ensure maximal solubilisation but the presence of excess polymer can interfere with SDS-PAGE and spectroscopic study (Gulamhussein, *et al.,* 2020). All AASTY polymers were therefore utilised at 0.5% concentration unless otherwise stated. While different polymer concentrations were only tested in this study for the AASTY polymers, due to the manufacturer's recommendations, it would be a good idea in the future to also test lower concentrations of other polymers, as this may help to counteract some of the limitations.

All AASTY polymers provided a solubilisation efficiency comparable to SMA2000, but 6-50 and 11-50 exhibited the highest efficiency at 71±17% and 61±20% respectively. This may suggest that an equal distribution of polar and apolar subunits benefits the integration and solubilisation of membranes in this case. Studies with SMA of different ratios found SMA1000 with a ratio of 1:1 to exhibit a lower efficiency when compared to SMA2000 at a ratio of 2:1 (Morrison, *et al.,* 2016), however within SMA the maleic acid group has two carboxyl groups,

whereas with AASTY the acrylic acid group contains a single carboxyl group. Therefore, the hydrophobic: hydrophilic balance of 1:1 AASTY is similar to that of 2:1 SMA.

While 11-50 excelled in efficiency, it provided a significantly lower level of BmrA purity at 64±21% when compared to SMA2000. 6-45 solubilised nanodiscs were also significantly less pure at 57±23%, but all other AASTY provided comparable BmrA purity. The diameter of AASTY nanodiscs has been reported to be rather heterogenous depending upon the application and this is confirmed in SEC and mass photometry analysis discussed later. Perhaps 11-50 and 6-45 produce larger nanodiscs which results in the increased presence of co-solubilising proteins.

The yield of BmrA produced with all AASTY co-polymers was comparable to SMA2000 but some interesting patterns emerge. For the 6kDa AASTY group, the yield of BmrA deceased as the percentage of acrylic acid increased. This is in opposition to the study of SMA at different ratios as previously discussed (Morrison, *et al.,* 2016). However, the 11kDa AASTYs did not share this relationship with 11-50 exhibiting the highest yield compared to 11-45 and 11-55 with a mean yield higher than SMA2000. Higher molecular weight polymers are known to exhibit reduced solubility (Wolf, 1985) and perform worse than lower molecular weight polymers (Swainsbury, *et al.,* 2017), but in this study AASTY 6-45, 6-50 and 6-55 do not appear to be more efficient than 11-45, 11-50 and 11-55.

While all AASTY polymers displayed good levels of efficiency, purity and yield, 6-50 and 11-50 were selected for further study. 6-50 was determined to be the superior 6kDa AASTY polymer producing consistently good levels of efficiency, BmrA purity and yield. While 11-50 nanodiscs were significantly less pure, they were produced at the highest yield and at a high efficiency. AASTY co-polymers also provide an interesting study for nanodisc characteristics based on molecular weight and have been shown to solubilise membrane proteins in different conformational states suggesting they can be utilised to produce functional protein.

6.5 Insect Membrane Study

Co-polymers can display widely different solubilisation efficiencies depending on multiple factors including the membrane protein of study and expression model. While some polymers

such as partially esterified SMA1440 are more efficient at solubilising thylakoid membranes than SMA2000 (Brady, *et al.,* 2019), they are less efficient at solubilising bacterial membranes (Hawkins, *et al.,* 2021). Differences in membrane composition and structure can result in different solubilisation efficiencies. To investigate this, the solubilisation efficiency of MRP4 expressed in Sf9 cell was tested using selected polymers SMA2000, DIBMA, 6-50 and 11-50.

DIBMA presented with a significantly lower efficiency of 33±20% when compared to SMA2000 with 68±2% in the solubilisation of MRP4. This is unlike the efficiency displayed for BmrA, suggesting that DIBMA is less capable of solubilising insect membranes when compared to bacterial. On the other hand, 6-50 and 11-50 display efficiencies of ~70% with MRP4 solubilised which is comparable to SMA2000. These values are also comparable to data in BmrA study, suggesting SMA2000 and AASTY 6-50 and 11-50 are equally able to solubilise bacterial and insect membranes.

Unfortunately, the efficiency of DDM to solubilise MRP4 in insect membrane models in this study was not investigated but other groups have reported an efficiency of over 70% for Sf9 expressed PCFT (Date, *et al.,* 2017), suggesting DDM is able to solubilise insect membranes to a similar degree as bacterial. In the future, this would be beneficial to determine if detergents solubilise different expression models to the same efficiency.

The solubilisation of Sf9 membranes was also tested in a scattering assay, utilising the proclivity for Sf9 lipids to optically clear upon solubilisation unlike bacterial membranes. With SMA2000, DIBMA, Glyco-DIBMA and all six AASTY polymers tested, 6-50 and 6-55 appeared to solubilise Sf9 membranes the quickest while all of the 11kDa AASTY polymers exhibited slower solubilisation kinetics. This may provide evidence to support the theory that lower molecular weight polymers are more efficient than larger weight polymers (Swainsbury, *et al.,* 2017) but appears to oppose previously discussed efficiency data.

The majority of the tested co-polymers exhibit sharp decreases in the scattering profile (600 nm) within the first 10 seconds of addition to 60mg/ml Sf9 membranes before plateauing at a constant rate. This suggests that solubilisation occurs in a two-phase process whereby initial integration of co-polymers into the membrane triggers rapid reorganisation before homeostasis is maintained with distinct nanodisc particles formed.

The initial stage of nanodisc formation is difficult to elucidate due to the rapid solubilisation ability displayed by most co-polymers, but hypotheses have been introduced that suggest 'lacy membranes' are formed which are highly porous and scatter more light. Evidence of these structures have been shown in previous EM and computational studies (Ball, *et al.,* 2021, Xue, *et al.,* 2018). The atypical kinetic profile witnessed for 11-55 in this study further supports this theory as unlike all other co-polymers, when 11-55 is added to Sf9 membranes the level of scattering increases. This may be the result of polymer recruitment to vesicles with bigger particles scattering more but may also support the theory of 'lacy membranes'.

While scattering appears to reduce over time to below the buffer control, there is significantly more scattering when compared to the other 11kDa polymer at 5 minutes. While the reason for this is undefined, 11-55 appears to show exhibit much slower solubilisation kinetics and may require more time to adequately solubilise membranes. All solubilisations are conducted over a one-hour period, so while 11-55 is comparable to all others in regard to efficiency, purity and yield in BmrA and MRP4 trials – it would be interesting to see if reducing the solubilisation period would reduce the efficiency exhibited by 11-55. This assay also provided further evidence to support the selection of 6-50 and 11-50 for additional study, as they display the quickest solubilisation kinetics within their separate groups.

6.6 Nanodisc Sensitivity

The next area of study was nanodisc sensitivity to divalent cations in order to identify co-polymers more suitable for functional study of BmrA. This was carried out using two different assays with a scattering based assay for lipid-only nanodiscs and an SDS-PAGE and centrifuge-based assay for protein-lipid nanodiscs. This not only provides more information regarding co-polymer sensitivity to build upon existing literature but also allows for the investigation of how sensitivity is modulated. If differences are consistently shown between protein-lipid and lipid-only nanodiscs, perhaps the solubilised membrane protein plays a role in interactions between divalent cations and the disassociation of nanodiscs.

In protein-lipid nanodiscs, SMA2000 displayed a sensitivity consistent with existing literature with an almost total loss of soluble BmrA at 10mM magnesium. However, DIBMA solubilised BmrA appears to retain the majority of soluble BmrA at the same concentration. This has been

seen in previous studies (Gulamhussein, *et al.,* 2020) with a lower sensitivity confirmed in this study. The AASTY polymers provided more variable results but most also exhibit a decreased sensitivity when compared to SMA2000. 6-45 appears to be the only polymer exhibiting a sensitivity level close to SMA2000, with both nanodiscs disassociating at 10mM. Interestingly, 6-50 and 11-50 display the lowest sensitivity with the majority of BmrA remaining soluble up to 10mM.

Lipid-only nanodiscs were also tested to reduce the complexity of the nanodisc model and determine if sensitivity is reduced or increased with the absence of protein. These assays were tested at much higher concentrations (≤50mM) of magnesium due to the tolerances displayed in previous assays. DIBMA nanodiscs appear to begin disassociating around 20mM with total loss of soluble BmrA at 50mM, which is are significantly higher concentrations than witnessed with SMA2000. Similar to protein-lipid studies, 6-45 stands out in the set as it displays a sensitivity level closest to that of SMA2000 with total loss of soluble BmrA at 20mM magnesium. However, 6-50 and 6-55 remain stable up to ~40mM. The 11kDa group are slightly more variable, with 11-45 exhibiting the lowest sensitivity with around half of the total soluble BmrA lost at ~20mM. This value is ~15mM for 11-50 and 11-55.

The reason for co-polymer sensitivity is still somewhat undefined with conflicting reports. While data in this project supports that sensitivity is protein independent, it is unclear why some co-polymers display decreased sensitivity. While DIBMA displays decreased sensitivity even with the presence of two carboxyl groups in the maleic acid moiety, the more hydrophobic polymer SMA3000 is more sensitive to divalent cations. While AASTY polymers contain only one carboxyl group and exhibit reduced polarity, they display a tolerance to magnesium. Perhaps the reduced charge means magnesium is unable to chelate and stimulate nanodisc disassociation or maybe the orientation of co-polymer and Mg^{2+} interactions are more important in the disassociation of nanodiscs.

6.7 Protein Functionality

With DIBMA, 6-50 and 11-50 all displaying an increased tolerance to magnesium, they were selected alongside SMA2000 for functional study of BmrA. The first indication of BmrA function is the ability to bind known substrates and undergo conformational change in

response, studied in a tryptophan quenching assay which utilises the intrinsic fluorescence of BmrA. As BmrA binds Hoechst 33342, conformational change is triggered which shifts the positioning of tryptophan residues found in intracellular and extracellular spaces, modulating the fluorescent spectra which can be measured using a spectrophotometer.

Purified BmrA solubilised with SMA2000, DIBMA, 6-50 and 11-50 all display some degree of binding with quenching increasing in a dose-responsive manner. This confirmed that BmrA was purified in a correctly folded and functional state in co-polymer nanodiscs. However, parameters deduced from one site binding curves such as K_d and V_{max} suggest that BmrA displays different binding affinities and maximal quenching rates depending on the co-polymer utilised for solubilisation. While no statistical significance was found between the binding affinities, DIBMA displayed the highest K_d indicating a lower level of binding efficiency for DIBMA solubilised BmrA. However, K_d measurements can be skewed by protein concentration, and this has been shown to be rather variable between biological repeats. DIBMA also displayed significantly lower maximal quenching at 27% when compared to SMA2000 and 11-50, suggesting a lower binding capacity. This may suggest that BmrA is less accessible or less able to undergo conformational change when solubilised in DIBMALPs. 6-50 and 11-50 presented with K_d and V_{max} values close to that of SMA2000 but appear to exhibit a lower level of variance for binding affinity. However, 6-50 also showed an increased level of variance in regard to maximal quenching.

To further probe BmrA functionality, a colorimetric ATPase assay based on the detection of inorganic phosphate released during ATP hydrolysis was utilised. It is well established that while detergent micelles are applicable for functional study of BmrA (Oepen, *et al.,* 2021) SMALPs do not display ATPase activity (Pollock, *et al.,* 2022). This is confirmed in this study, albeit at lower concentrations than reported for DDM micelles in existing literature.

While DIBMA nanodiscs displayed a lower sensitivity to magnesium and produces BmrA capable of binding, it does not exhibit ATPase activity. Interestingly however, 6-50 and 11-50 solubilised BmrA did display ATPase activity, with V_{max} values even higher than DDM. This suggests AASTY solubilised BmrA has a higher ATP turnover rate and therefore protein functionality in nanodiscs when compared to micelles.

These results complicate hypotheses regarding how protein functionality is restricted in nanodiscs as while AASTY and DIBMA both display lower sensitivities, DIBMA solubilised BmrA function cannot be proved. This may suggest that nanodisc sensitivity is not the only limiting factor for ATPase assays. Perhaps the loss of a carboxyl group in acrylic acid-based polymers reduces the level of hydrogen interactions, therefore increasing membrane fluidity and the ability of BmrA to undergo full conformational change. This hypothesis indicates lateral pressure is more important for a lack of ABC transporter function in ATPase assays, stimulating an investigation into nanodisc fluidity.

6.8 Nanodisc Fluidity

In an attempt to ascertain if AASTY solubilised BmrA exhibits ATPase activity due to increased membrane fluidity, a laurdan assay was utilised. Laurdan is a lipophilic fluorescent dye that integrates into the hydrophobic core of membrane bilayers, where its emission spectra alternates based on exposure to polarity changes caused by an influx of water into highly curved membranes at higher temperatures.

All co-polymer nanodiscs displayed a higher degree of lipid packing and lower membrane fluidity when compared to DMPC liposomes in this research, similar to results reported in existing literature (Real Hernandez and Levental, 2023, Pardo, *et al.,* 2017). While DMPC liposomes display a sharp fluid-to-gel transition at ~37°C, a distinct shift is not witnessed for nanodiscs. Smaller nanodiscs have also been reported to exhibit higher degrees of membrane fluidity (Angelisová, *et al.,* 2019) but this relationship is not witnessed here with limited differences between SMA2000 and DIBMA.

There are also limited changes in laurdan GP values across the tested temperature range, with fluidity restricted in nanodiscs even at 60°C suggesting a loss of lipid co-operativity. While co-polymer solubilisation retains native phospholipids, they also appear to heavily perturb membrane fluidity bringing into question how representative these protein-lipid interactions truly are. However, these experiments were conducted using pure DMPC for both liposomes and lipid-only nanodiscs, which is a zwitterionic lipid known to be highly ordered with highly packed head groups due to reduced electrostatic interactions. It would be interesting to see

if the same relationship would be witnessed with protein-lipid nanodiscs and lipid-only nanodiscs of different lipid compositions.

6.9 Nanodisc Lipid Composition

One of the major benefits of co-polymer solubilisation is the ability to retain the native phospholipid environment surrounding solubilised membrane proteins. This stabilises protein structure and function and provides an interesting opportunity to study protein-lipid interactions and lipid composition. In an attempt to identify the lipid composition of nanodiscs produced with SMA, DIBMA, 6-50 and 11-50, MTBE lipid extraction and TLC was carried out.

While experiments were successful with phospholipids stained using molybdenum blue, densitometric analyses was difficult due to lane smearing and the presence of multiple contaminating bands. The smearing may be attributed to the intrinsic charge of co-polymers which interferes with lipid migration. While lipid extraction aims to isolate lipids, perhaps MTBE extraction resulted in the pull-through of co-polymers in samples, which when loaded onto TLC can results in 'blebs' forming close to the sample loading line. This hypothesis is further confirmed by the more pronounced 'blebbing' and smearing seen in SMA and DIBMA lanes when compared to 6-50 and 11-50 lanes – as the AASTY polymers were utilised at lower concentrations. It is clear that MTBE lipid extraction protocols require optimisation for further study.

While the total lipid composition was difficult to identify, the major lipid classes of bacterial and insect membranes PE, PG and PC were isolated and quantified to investigate differences between crude membrane lipids and co-solubilised lipids. While there does not appear to be lipid class preferences depending on the co-polymer produced, all nanodiscs tested appear to be slightly enriched in the zwitterionic phospholipid PE when compared to crude membranes.

This relationship has been previously reported using TLC (Pollock, *et al.,* 2018) and mass spectrometry (Teo, *et al.,* 2019). PE is a chemically reactive and poorly hydrated phospholipid that consists of a small headgroup and wide acyl chains. It is known to be a key structural component of both insect and bacterial membranes and has been linked to cytokinesis in mammalian cells (Emoto and Umeda, 2000), a process by which the cytoplasm and membrane

are split for cell division. PE has also been linked to protein translocation and integration into the plasma membrane (Den Uijl and Driessen, 2024). Considering this, perhaps PE plays a role in membrane pore formation during nanodisc production and as such more likely to appear within nanodiscs.

It is important to note that this experiment was conducted using pre-purified protein-lipid nanodiscs. While they provide a good model for the native lipid composition of insect and bacterial membranes, they are known to be rather heterogenous in regard to their size and composition. For future work, purified protein-lipid nanodiscs should be studied to elucidate if this enrichment is independent to the presence of membrane proteins This would help to define if enrichment is an artifact of co-polymer solubilisation or is linked to associations between membrane protein trafficking and the role of PE.

6.10 Mass photometry analysis of nanodisc size

As previously explored, nanodiscs can display highly heterogenous populations in regard to nanodisc size and composition. Nanodiscs produced with different co-polymers have been reported to display different diameters using techniques such as DLS. In this study, mass photometry was used to characterise single particle mass as a more accurate measure of single particle nanodisc size.

Purified protein-lipid nanodiscs were the first to be tested with interesting results found. First is the presence of a peak ~70kDa which represents a relatively high proportion of the sample. Previous studies using lipid-only SMALPs indicate that 'empty' nanodiscs are ~100kDa in mass (Olerinyova, *et al.,* 2021) suggesting that this population may represent empty nanodiscs. Owing to the fact that these samples were purified before analysis however – this is unlikely. Instead, this peak may represent excess polymer which is further evidenced by the more balanced profile witnessed in 6-50 and 11-50 attempts where a lower polymer concentration is used.

6-50 and 11-50 also displayed a third population of particles with a peak ~445kDa which was not found for SMA or DIBMA. While they have been reported to produce a more defined nanodisc size distribution compared to other co-polymers, perhaps they are able to solubilise

BmrA in a higher oligomeric order into larger nanodiscs resulting in a more heterogenous sample in this case. Recent studies have found that lower polymer concentrations result in the production of larger nanodiscs (Maier, *et al.,* 2023), lending credibility to this hypothesis.

The second peak between 231kDa and 280kDa was attributed to a population of protein-lipid nanodiscs with ~130 kDa mass contributed by BmrA homodimers (Dalmas, *et al.,* 2005) and ~100kDa mass contributed by polymer and lipids. Converse to existing literature, SMA appears to produce the largest nanodiscs in this experiment with 6-50, 11-50 and DIBMA nanodiscs all displaying similar masses. While more repeats would be necessary to confirm this, a high level of background stimulated the requirement for less complex membrane models.

Lipid-only nanodiscs were then investigated using mass spectrometry, with background signal successfully reduced when compared to protein-lipid study with each sample producing a single peak. While slightly smaller than previous attempts due to the removal of protein from nanodiscs, the average mass of this peak ~88kDa is similar to the weight reported for 'empty' nanodiscs. DIBMA nanodiscs also displayed the largest mass at 105kDa when compared to the other three co-polymers, which better aligns with existing literature. This is further evidenced in SEC traces with DIBMA nanodiscs displaying the largest nanodisc size, eluting at ~11ml which is earlier than SMA, 6-50 and 11-50 nanodiscs. While SEC is not a definitive measure of particle mass, the speed of elution gives a good indication of particle size based on the ability to travel though pores in the column matrix.
SEC and mass photometry data also correlates well for AASTY 6-50 and 11-50, with nanodiscs eluting between ~13-14ml and displaying masses of 92kDa and 75kDa. This is similar to SMALPs which elute at 13ml with a mass of 78kDa. 6-50 also appears to exhibit a wider distribution in both methods, suggesting a higher degree of heterogeneity providing more evidence for hypotheses formed in previous experiments.

To further probe sample homogeneity and if differences displayed are artifacts of sample preparation, samples of pooled or single SEC fractions from lipid-only SMALPs were analysed. While pooled samples appear to have a slightly lower concentration of particles - which can be attributed to the natural variance witnessed between biological repeats - the distribution was not too dissimilar to single fraction lipid-only SMALPs. It would be interesting to probe this using AASTY polymers to see if this relationship is any different.

As well as characterising single particle mass, mass photometry can be utilised to probe binding activity with negative and positive masses representing unbinding and binding events. SMA, DIBMA and 6-50 behaved similarly, with higher levels of binding events when compared to unbinding events. However, 11-50 stands out with an increase level of unbinding when compared to the other three co-polymers. While high unbinding events sometimes represent saturation of the glass slide used for analysis, this does not apply here as other samples that were more highly concentrated did not produce the same level of unbinding. It could however be an artifact of very large particles (>1MDa) or aggregates with 'wobbling' movement interpreted as unbinding events by the inbuilt analysis software. This provides more evidence to support hypotheses built regarding the heterogeneity of AASTY nanodiscs with particular reference to the significant reduction in BmrA purity for 11-50 nanodiscs.

6.12 BmrA reconstitution

It is clear that the application of different co-polymers results in the production of nanodiscs that can differ widely in size, composition and functionality, and while co-polymer solubilisation is beneficial for many different reasons some technical difficulties can arise. In order to retain the benefits of both co-polymer and detergent solubilisation, proteins can be switched in and out of different systems.

In order to reduce the difficulty experienced for functional study of ABC transporters in nanodiscs, attempts were made to reconstitute BmrA from SMALPs into proteoliposomes. While reconstitution from micelles is well defined, the transfer from SMALPs is less well known. Methods adapted from SMA and DIBMA reconstitution studies (Morrison, *et al.,* 2016, Dilworth, *et al.,* 2021) highlighted the requirement for magnesium to encourage reconstitution. In this project, reconstitution was attempted in the presence and absence of magnesium, with the utilisation of magnesium found to significantly increase the reconstitution efficiency of BmrA. While magnesium sensitivity is largely considered a disadvantage of nanodiscs, in this case it can be utilised to promote nanodisc disassociation.

The time of incubation was also tested as a factor for reconstitution efficiency, with shorter 5-minute incubation periods appearing to award slightly higher reconstitution efficiencies when compared to 30-minute incubations. Perhaps extended exposure to heat and/or magnesium results in protein aggregation and exclusion from proteoliposomes.

The transfer of membrane proteins from nanodiscs to micelles was also tested in this project. This may sound counterproductive, as co-polymer nanodiscs benefit from retaining native phospholipids with transfer to micelles resulting in the loss of these interactions. However, micelles are notoriously unstable with protein structure and function degrading even at 4°C while nanodiscs are much more thermostable with the ability to store samples in a functional state for longer periods of time. Reconstitution of BmrA from SMA, DIBMA, 6-50 and 11-50 nanodiscs was successfully conducted but displayed different efficiencies at different DDM concentrations. While reconstitution from SMA required higher concentrations of DDM (10%), the other polymers maintained higher efficiencies at lower concentrations of DDM (1% and 0.1%). On the other hand, 11-50 appears to be the least effected by DDM concentration, with above 90% efficiency at all three concentrations - suggesting BmrA is easily integrated into micelles following AASTY nanodisc disassociation.

Although DIBMA, 6-50 and 11-50 were found to be tolerant to magnesium at 10mM concentrations in protein-lipid and lipid-only sensitivity assays, the positive controls in this experiment showed disassociation of nanodiscs in the presence of 10mM magnesium. While the exact reason for this is undefined, external factors such as exposure to high temperatures during reconstitution may promote increased nanodisc sensitivity. It would be interesting to further probe this disparity by testing different magnesium concentrations in this assay.

BmrA was successfully solubilised, purified and reconstituted in this project using a wide range of solubilisation agents, with the resulting nanodiscs characterised based on size, composition and sensitivity. While results were mixed among co-polymer groups, AASTY 6-50 and 11-50 emerged as the optimal polymers for the functional study of BmrA with the first successful study of ABC transporter ATPase activity in AASTY nanodiscs. However, in the future it would be good to use reconstituted samples to try to measure transport via a vesicular uptake assay (Waeterschoot, *et al.,* 2024), rather than relying on ligand binding or ATPase activity as a proxy for transport function.

References

ABLA, N., CHINN, L. W., NAKAMURA, T., LIU, L., HUANG, C. C., JOHNS, S. J., KAWAMOTO, M., STRYKE, D., TAYLOR, T. R., FERRIN, T. E., GIACOMINI, K. M. & KROETZ, D. L. 2008. The human multidrug resistance protein 4 (MRP4, ABCC4): functional analysis of a highly polymorphic gene. J Pharmacol Exp Ther, 325, 859-68.

ALEXANDER, S. P. H., FABBRO, D., KELLY, E., MATHIE, A. A., PETERS, J. A., VEALE, E. L., ARMSTRONG, J. F., FACCENDA, E., HARDING, S. D., DAVIES, J. A., AMAROSI, L., ANDERSON, C. M. H., BEART, P. M., BROER, S., DAWSON, P. A., GYIMESI, G., HAGENBUCH, B., HAMMOND, J. R., HANCOX, J. C., HERSHFINKEL, M., INUI, K.-I., KANAI, Y., KEMP, S., KUNJI, E. R. S., STEWART, G., TAVOULARI, S., THWAITES, D. T. & VERRI, T. 2023. British Journal of Pharmacology, 180, S374-S469.

ALEXANDERSSON, E., SAALBACH, G., LARSSON, C. & KJELLBOM, P. 2004. Arabidopsis Plasma Membrane Proteomics Identifies Components of Transport, Signal Transduction and Membrane Trafficking. Plant and Cell Physiology, 45, 1543-1556.

ALLEN, K. N., ENTOVA, S., RAY, L. C. & IMPERIALI, B. 2019. Monotopic Membrane Proteins Join the Fold. Trends in Biochemical Sciences, 44, 7-20.

ALMéN, M. S., NORDSTRöM, K. J. V., FREDRIKSSON, R. & SCHIöTH, H. B. 2009. Mapping the human membrane proteome: a majority of the human membrane proteins can be classified according to function and evolutionary origin. BMC Biology, 7, 50.

ANGELISOVá, P., BALLEK, O., SýKORA, J., BENADA, O., ČAJKA, T., POKORNá, J., PINKAS, D. & HOřEJší, V. 2019. The use of styrene-maleic acid copolymer (SMA) for studies on T cell membrane rafts. Biochim Biophys Acta Biomembr, 1861, 130-141.

ARACHEA, B. T., SUN, Z., POTENTE, N., MALIK, R., ISAILOVIC, D. & VIOLA, R. E. 2012. Detergent selection for enhanced extraction of membrane proteins. Protein Expression and Purification, 86, 12-20.

ATURALIYA, R. N., KERR, M. C. & TEASDALE, R. D. 2012. A Novel Type III Endosome Transmembrane Protein, TEMP. Cells, 1, 1029-44.

AYUB, H., CLARE, M., MILIC, I., CHMEL, N. P., BöNING, H., DEVITT, A., KREY, T., BILL, R. M. & ROTHNIE, A. J. 2020. CD81 extracted in SMALP nanodiscs comprises two distinct protein populations within a lipid environment enriched with negatively charged headgroups. Biochimica et Biophysica Acta (BBA) - Biomembranes, 1862, 183419.

BALL, L. E., RILEY, L. J., HADASHA, W., PFUKWA, R., SMITH, C. J. I., DAFFORN, T. R. & KLUMPERMAN, B. 2021. Influence of DIBMA Polymer Length on Lipid Nanodisc Formation and Membrane Protein Extraction. Biomacromolecules, 22, 763-772.

BAYBURT, T. H., GRINKOVA, Y. V. & SLIGAR, S. G. 2002. Self-Assembly of Discoidal Phospholipid Bilayer Nanoparticles with Membrane Scaffold Proteins. Nano Letters, 2, 853-856.

BAYBURT, T. H., GRINKOVA, Y. V. & SLIGAR, S. G. 2006. Assembly of single bacteriorhodopsin trimers in bilayer nanodiscs. Archives of Biochemistry and Biophysics, 450, 215-222.

BOLDOG, T., GRIMME, S., LI, M., SLIGAR, S. G. & HAZELBAUER, G. L. 2006. Nanodiscs separate chemoreceptor oligomeric states and reveal their signaling properties. Proceedings of the National Academy of Sciences, 103, 11509-11514.

BORST, P., DE WOLF, C. & VAN DE WETERING, K. 2007. Multidrug resistance-associated proteins 3, 4, and 5. Pflügers Archiv - European Journal of Physiology, 453, 661-673.

BORTHS, E. L., POOLMAN, B., HVORUP, R. N., LOCHER, K. P. & REES, D. C. 2005. In Vitro Functional Characterization of BtuCD-F, the Escherichia coli ABC Transporter for Vitamin B12 Uptake. Biochemistry, 44, 16301-16309.

BOSVELD, F., BONNET, I., GUIRAO, B., TLILI, S., WANG, Z., PETITALOT, A., MARCHAND, R., BARDET, P.-L., MARCQ, P., GRANER, F. & BELLAïCHE, Y. 2012. Mechanical Control of Morphogenesis by Fat/Dachsous/Four-Jointed Planar Cell Polarity Pathway. Science, 336, 724-727.

BRADY, N. G., LI, M., MA, Y., GUMBART, J. C. & BRUCE, B. D. 2019. Non-detergent isolation of a cyanobacterial photosystem I using styrene maleic acid alternating copolymers. RSC Adv, 9, 31781-31796.

BROECKER, J., EGER, B. T. & ERNST, O. P. 2017. Crystallogenesis of Membrane Proteins Mediated by Polymer-Bounded Lipid Nanodiscs. Structure, 25, 384-392.

BROGDEN, R. N., HEEL, R. C., SPEIGHT, T. M. & AVERY, G. S. 1978. Cimetidine: a review of its pharmacological properties and therapeutic efficacy in peptic ulcer disease. Drugs, 15, 93-131.

BROUILLETTE, C. G., JONES, J. L., NG, T. C., KERCRET, H., CHUNG, B. H. & SEGREST, J. P. 1984. Structural studies of apolipoprotein A-I/phosphatidylcholine recombinants by high-field proton NMR, nondenaturing gradient gel electrophoresis, and electron microscopy. Biochemistry, 23, 359-367.

BRYANT, C. E., SPRING, D. R., GANGLOFF, M. & GAY, N. J. 2010. The molecular basis of the host response to lipopolysaccharide. Nature Reviews Microbiology, 8, 8-14.

CABRAL, H., MATSUMOTO, Y., MIZUNO, K., CHEN, Q., MURAKAMI, M., KIMURA, M., TERADA, Y., KANO, M. R., MIYAZONO, K., UESAKA, M., NISHIYAMA, N. & KATAOKA, K. 2011. Accumulation of sub-100 nm polymeric micelles in poorly permeable tumours depends on size. Nature Nanotechnology, 6, 815-823.

CANTOR, R. S. 1999. The influence of membrane lateral pressures on simple geometric models of protein conformational equilibria. Chemistry and Physics of Lipids, 101, 45-56.

CAO, Y., FANG, J., SHI, Y., WANG, H., CHEN, X., LIU, Y., ZHU, Z., CAO, Y., HONG, Z. & CHAI, Y. 2022. Screening potential P-glycoprotein inhibitors by combination of a detergent-free membrane protein extraction with surface plasmon resonance biosensor. Acta Pharm Sin B, 12, 3113-3123.

CHAMI, M., STEINFELS, E., ORELLE, C., JAULT, J. M., DI PIETRO, A., RIGAUD, J. L. & MARCO, S. 2002. Three-dimensional structure by cryo-electron microscopy of YvcC, an homodimeric ATP-binding cassette transporter from Bacillus subtilis. J Mol Biol, 315, 1075-85.

CHAPTAL, V., ZAMPIERI, V., WISEMAN, B., ORELLE, C., MARTIN, J., NGUYEN, K.-A., GOBET, A., DI CESARE, M., MAGNARD, S., JAVED, W., EID, J., KILBURG, A., PEUCHMAUR, M., MARCOUX, J., MONTICELLI, L., HOGBOM, M., SCHOEHN, G., JAULT, J.-M., BOUMENDJEL, A. & FALSON, P. 2022.

Substrate-bound and substrate-free outward-facing structures of a multidrug ABC exporter. Science Advances, 8, eabg9215.

CHEN, J. 2013. Molecular mechanism of the Escherichia coli maltose transporter. Current Opinion in Structural Biology, 23, 492-498.

CHENG, D., ZHAO, L., GUAN, G., LAI, H. & LUO, J. 2023. Synthesis of SMA by RAFT polymerization and its dispersion of TiO2 in aqueous solution. RSC Advances, 13, 7366-7371.

CHEREPANOV, D. A., BRADY, N. G., SHELAEV, I. V., NGUYEN, J., GOSTEV, F. E., MAMEDOV, M. D., NADTOCHENKO, V. A. & BRUCE, B. D. 2020. PSI-SMALP, a Detergent-free Cyanobacterial Photosystem I, Reveals Faster Femtosecond Photochemistry. Biophys J, 118, 337-351.

CHIFFLET, S., TORRIGLIA, A., CHIESA, R. & TOLOSA, S. 1988. A method for the determination of inorganic phosphate in the presence of labile organic phosphate and high concentrations of protein: Application to lens ATPases. Analytical Biochemistry, 168, 1-4.

CHOY, B. C., CATER, R. J., MANCIA, F. & PRYOR, E. E. 2021. A 10-year meta-analysis of membrane protein structural biology: Detergents, membrane mimetics, and structure determination techniques. Biochimica et Biophysica Acta (BBA) - Biomembranes, 1863, 183533.

COURNIA, Z. & CHATZIGOULAS, A. 2020. Allostery in membrane proteins. Current Opinion in Structural Biology, 62, 197-204.

CROOK, E., TREBBI, G. & FORDYCE, D. 1964. Thermodynamic properties of solutions of homogeneous p, t-octylphenoxyethoxyethanols (OPE1-10). The Journal of Physical Chemistry, 68, 3592-3599.

CROW, A., GREENE, N. P., KAPLAN, E. & KORONAKIS, V. 2017. Structure and mechanotransmission mechanism of the MacB ABC transporter superfamily. Proceedings of the National Academy of Sciences, 114, 12572-12577.

DALEY, D. O., RAPP, M., GRANSETH, E., MELéN, K., DREW, D. & VON HEIJNE, G. 2005. Global Topology Analysis of the Escherichia coli Inner Membrane Proteome. Science, 308, 1321-1323.

DALMAS, O., ORELLE, C., FOUCHER, A.-E., GEOURJON, C., CROUZY, S., DI PIETRO, A. & JAULT, J.-M. 2005. The Q-loop disengages from the first intracellular loop during the catalytic cycle of the multidrug ABC transporter BmrA. Journal of Biological Chemistry, 280, 36857-36864.

DANIELCZAK, B., RASCHE, M., LENZ, J., PéREZ PATALLO, E., WEYRAUCH, S., MAHLER, F., AGBADAOLA, M. T., MEISTER, A., BABALOLA, J. O., VARGAS, C., KOLAR, C. & KELLER, S. 2022. A bioinspired glycopolymer for capturing membrane proteins in native-like lipid-bilayer nanodiscs. Nanoscale, 14, 1855-1867.

DATE, S. S., FIORI, M. C., ALTENBERG, G. A. & JANSEN, M. 2017. Expression in Sf9 insect cells, purification and functional reconstitution of the human proton-coupled folate transporter (PCFT, SLC46A1). PLoS One, 12, e0177572.

DAVIDSON, A. L., DASSA, E., ORELLE, C. & CHEN, J. 2008. Structure, Function, and Evolution of Bacterial ATP-Binding Cassette Systems. Microbiology and Molecular Biology Reviews, 72, 317-364.

DAWSON, R. J. P. & LOCHER, K. P. 2006. Structure of a bacterial multidrug ABC transporter. Nature, 443, 180-185.

DE GRAAF, D., SHARMA, R. C., MECHETNER, E. B., SCHIMKE, R. T. & RONINSON, I. B. 1996. P-glycoprotein confers methotrexate resistance in 3T6 cells with deficient carrier-mediated methotrexate uptake. Proceedings of the National Academy of Sciences, 93, 1238-1242.

DEGNAN, PATRICK H., TAGA, MICHIKO E. & GOODMAN, ANDREW L. 2014. Vitamin B₁₂ as a Modulator of Gut Microbial Ecology. Cell Metabolism, 20, 769-778.

DEN UIJL, M. J. & DRIESSEN, A. J. M. 2024. Phospholipid dependency of membrane protein insertion by the Sec translocon. Biochimica et Biophysica Acta (BBA) - Biomembranes, 1866, 184232.

DENISOV, I. G., GRINKOVA, Y. V., LAZARIDES, A. A. & SLIGAR, S. G. 2004. Directed self-assembly of monodisperse phospholipid bilayer Nanodiscs with controlled size. J Am Chem Soc, 126, 3477-87.

DI CESARE, M., KAPLAN, E., RENDON, J., GERBAUD, G., VALIMEHR, S., GOBET, A., NGO, T. T., CHAPTAL, V., FALSON, P., MARTINHO, M., DORLET, P., HANSSEN, E., JAULT, J. M. & ORELLE, C. 2024. The transport activity of the multidrug ABC transporter BmrA does not require a wide separation of the nucleotide-binding domains. J Biol Chem, 300, 105546.

DILWORTH, M. V., FINDLAY, H. E. & BOOTH, P. J. 2021. Detergent-free purification and reconstitution of functional human serotonin transporter (SERT) using diisobutylene maleic acid (DIBMA) copolymer. Biochim Biophys Acta Biomembr, 1863, 183602.

DOEGE, H., BOCIANSKI, A., SCHEEPERS, A., AXER, H., ECKEL, J., JOOST, H. G. & SCHüRMANN, A. 2001. Characterization of human glucose transporter (GLUT) 11 (encoded by SLC2A11), a novel sugar-transport facilitator specifically expressed in heart and skeletal muscle. Biochem J, 359, 443-9.

DOMINGUEZ PARDO, J. J., DöRR, J. M., IYER, A., COX, R. C., SCHEIDELAAR, S., KOORENGEVEL, M. C., SUBRAMANIAM, V. & KILLIAN, J. A. 2017. Solubilization of lipids and lipid phases by the styrene–maleic acid copolymer. European Biophysics Journal, 46, 91-101.

DONG, H., ZHANG, Z., TANG, X., PATERSON, N. G. & DONG, C. 2017. Structural and functional insights into the lipopolysaccharide ABC transporter LptB2FG. Nature Communications, 8, 222.

DöRR, J. M., SCHEIDELAAR, S., KOORENGEVEL, M. C., DOMINGUEZ, J. J., SCHäFER, M., VAN WALREE, C. A. & KILLIAN, J. A. 2016. The styrene–maleic acid copolymer: a versatile tool in membrane research. European Biophysics Journal, 45, 3-21.

DUURKENS, R. H., TOL, M. B., GEERTSMA, E. R., PERMENTIER, H. P. & SLOTBOOM, D. J. 2007. Flavin Binding to the High Affinity Riboflavin Transporter RibU *. Journal of Biological Chemistry, 282, 10380-10386.

EFTINK, M. R. 1994. The use of fluorescence methods to monitor unfolding transitions in proteins. Biophys J, 66, 482-501.

EL-AWADY, R., SALEH, E., HASHIM, A., SOLIMAN, N., DALLAH, A., ELRASHEED, A. & ELAKRAA, G. 2016. The Role of Eukaryotic and Prokaryotic ABC Transporter Family in Failure of Chemotherapy. Front Pharmacol, 7, 535.

ELALI, A. & RIVEST, S. 2013. The role of ABCB1 and ABCA1 in beta-amyloid clearance at the neurovascular unit in Alzheimer's disease. Frontiers in Physiology, 4.

EMOTO, K. & UMEDA, M. 2000. An essential role for a membrane lipid in cytokinesis. Regulation of contractile ring disassembly by redistribution of phosphatidylethanolamine. J Cell Biol, 149, 1215-24.

FAUSTINO, I., ABDIZADEH, H., SOUZA, P. C. T., JEUCKEN, A., STANEK, W. K., GUSKOV, A., SLOTBOOM, D. J. & MARRINK, S. J. 2020. Membrane mediated toppling mechanism of the folate energy coupling factor transporter. Nat Commun, 11, 1763.

FLORY, J. & LIPSKA, K. 2019. Metformin in 2019. Jama, 321, 1926-1927.

FRALLICCIARDI, J., MELCR, J., SIGINOU, P., MARRINK, S. J. & POOLMAN, B. 2022. Membrane thickness, lipid phase and sterol type are determining factors in the permeability of membranes to small solutes. Nature Communications, 13, 1605.

FRANCIS, M. F., CRISTEA, M. & WINNIK, F. M. 2004. Polymeric micelles for oral drug delivery: Why and how. Pure and Applied Chemistry, 76, 1321-1335.

GAGNON, K. B. & DELPIRE, E. 2020. Sodium Transporters in Human Health and Disease. Front Physiol, 11, 588664.

GALDIERO, S., GALDIERO, M. & PEDONE, C. 2007. beta-Barrel membrane bacterial proteins: structure, function, assembly and interaction with lipids. Curr Protein Pept Sci, 8, 63-82.

GANCEDO, S. N., SAHORES, A., GóMEZ, N., DI SIERVI, N., MAY, M., YANEFF, A., DE SOUSA SERRO, M. G., FRAUNHOFFER, N., DUSETTI, N., IOVANNA, J., SHAYO, C., DAVIO, C. A. & GONZáLEZ, B. 2024. The xenobiotic transporter ABCC4/MRP4 promotes epithelial mesenchymal transition in pancreatic cancer. Front Pharmacol, 15, 1432851.

GASTER, M., HANDBERG, A., SCHüRMANN, A., JOOST, H. G., BECK-NIELSEN, H. & SCHRøDER, H. D. 2004. GLUT11, but not GLUT8 or GLUT12, is expressed in human skeletal muscle in a fibre type-specific pattern. Pflügers Archiv, 448, 105-113.

GIACOMINI, K. M., HUANG, S.-M., TWEEDIE, D. J., BENET, L. Z., BROUWER, K. L. R., CHU, X., DAHLIN, A., EVERS, R., FISCHER, V., HILLGREN, K. M., HOFFMASTER, K. A., ISHIKAWA, T., KEPPLER, D., KIM, R. B., LEE, C. A., NIEMI, M., POLLI, J. W., SUGIYAMA, Y., SWAAN, P. W., WARE, J. A., WRIGHT, S. H., WAH YEE, S., ZAMEK-GLISZCZYNSKI, M. J., ZHANG, L. & THE INTERNATIONAL TRANSPORTER, C. 2010. Membrane transporters in drug development. Nature Reviews Drug Discovery, 9, 215-236.

GRIME, R. L., LOGAN, R. T., NESTOROW, S. A., SRIDHAR, P., EDWARDS, P. C., TATE, C. G., KLUMPERMAN, B., DAFFORN, T. R., POYNER, D. R., REEVES, P. J. & WHEATLEY, M. 2021. Differences in SMA-like polymer architecture dictate the conformational changes exhibited by the membrane protein rhodopsin encapsulated in lipid nano-particles. Nanoscale, 13, 13519-13528.

GRINKOVA, Y. V., DENISOV, I. G. & SLIGAR, S. G. 2010. Engineering extended membrane scaffold proteins for self-assembly of soluble nanoscale lipid bilayers. Protein Eng Des Sel, 23, 843-8.

GUAN, S., ZHAO, L. & PENG, R. 2022. Mitochondrial Respiratory Chain Supercomplexes: From Structure to Function. Int J Mol Sci, 23.

GULAMHUSSEIN, A. A., MEAH, D., SOJA, D. D., FENNER, S., SAIDANI, Z., AKRAM, A., LALLIE, S., MATHEWS, A., PAINTER, C., LIDDAR, M. K., MOHAMMED, Z., CHIU, L. K., SUMAR, S. S., HEALY, H., HUSSAIN, N., PATEL, J. H., HALL, S. C. L., DAFFORN, T. R. & ROTHNIE, A. J. 2019. Examining the stability of membrane proteins within SMALPs. European Polymer Journal, 112, 120-125.

GULAMHUSSEIN, A. A., UDDIN, R., TIGHE, B. J., POYNER, D. R. & ROTHNIE, A. J. 2020. A comparison of SMA (styrene maleic acid) and DIBMA (di-isobutylene maleic acid) for membrane protein purification. Biochimica et Biophysica Acta (BBA) - Biomembranes, 1862, 183281.

GULATI, S., JAMSHAD, M., KNOWLES, TIMOTHY J., MORRISON, KERRIE A., DOWNING, R., CANT, N., COLLINS, R., KOENDERINK, JAN B., FORD, ROBERT C., OVERDUIN, M., KERR, IAN D., DAFFORN, TIMOTHY R. & ROTHNIE, ALICE J. 2014. Detergent-free purification of ABC (ATP-binding-cassette) transporters. Biochemical Journal, 461, 269-278.

HAGENBUCH, B. & STIEGER, B. 2013. The SLCO (former SLC21) superfamily of transporters. Mol Aspects Med, 34, 396-412.

HAWKINS, O. P., JAHROMI, C. P. T., GULAMHUSSEIN, A. A., NESTOROW, S., BAHRA, T., SHELTON, C., OWUSU-MENSAH, Q. K., MOHIDDIN, N., O'ROURKE, H., AJMAL, M., BYRNES, K., KHAN, M., NAHAR, N. N., LIM, A., HARRIS, C., HEALY, H., HASAN, S. W., AHMED, A., EVANS, L., VAITSOPOULOU, A., AKRAM, A., WILLIAMS, C., BINDING, J., THANDI, R. K., JOBY, A., GUEST, A., TARIQ, M. Z., RASOOL, F., CAVANAGH, L., KANG, S., ASPARUHOV, B., JESTIN, A., DAFFORN, T. R., SIMMS, J., BILL, R. M., GODDARD, A. D. & ROTHNIE, A. J. 2021. Membrane protein extraction and purification using partially-esterified SMA polymers. Biochim Biophys Acta Biomembr, 1863, 183758.

HE, L., VASILIOU, K. & NEBERT, D. W. 2009. Analysis and update of the human solute carrier (SLC) gene superfamily. Hum Genomics, 3, 195-206.

HENDERSON, G. B., ZEVELY, E. M. & HUENNEKENS, F. M. 1979. Mechanism of Folate Transport in Lactobacillus casei: Evidence for a Component Shared with the Thiamine and Biotin Transport Systems. Journal of Bacteriology, 137, 1308-1314.

HEROLD, K., XU, Z., GOLLMICK, F. A., GRäFE, U. & HERTWECK, C. 2004. Biosynthesis of cervimycin C, an aromatic polyketide antibiotic bearing an unusual dimethylmalonyl moiety. Organic & Biomolecular Chemistry, 2, 2411-2414.

HESKETH, S. J., KLEBL, D. P., HIGGINS, A. J., THOMSEN, M., PICKLES, I. B., SOBOTT, F., SIVAPRASADARAO, A., POSTIS, V. L. G. & MUENCH, S. P. 2020. Styrene maleic-acid lipid particles (SMALPs) into detergent or amphipols: An exchange protocol for membrane protein characterisation. Biochim Biophys Acta Biomembr, 1862, 183192.

HIGGINS, A. J., FLYNN, A. J., MARCONNET, A., MUSGROVE, L. J., POSTIS, V. L. G., LIPPIAT, J. D., CHUNG, C. W., CESKA, T., ZOONENS, M., SOBOTT, F. & MUENCH, S. P. 2021. Cycloalkane-modified amphiphilic polymers provide direct extraction of membrane proteins for CryoEM analysis. Commun Biol, 4, 1337.

HJELMELAND, L., M, 1980. A nondenaturing zwitterionic detergent for membrane biochemistry: Design and synthesis. Proc Natl Acad Sci U S A, 77, 6368 - 6370.

HOFFMANN, A., STEFFENS, U., MAčEK, B., FRANZ-WACHTEL, M., NIESELT, K., HARBIG, T. A., SCHERLACH, K., HERTWECK, C., SAHL, H.-G. & BIERBAUM, G. 2024. The unusual mode of action of the polyketide glycoside antibiotic cervimycin C. mSphere, 9, e00764-23.

HOLLENSTEIN, K., FREI, D. C. & LOCHER, K. P. 2007. Structure of an ABC transporter in complex with its binding protein. Nature, 446, 213-6.

HOU, W.-T., XU, D., WANG, L., CHEN, Y., CHEN, Z.-P., ZHOU, C.-Z. & CHEN, Y. 2022. Plastic structures for diverse substrates: A revisit of human ABC transporters. Proteins: Structure, Function, and Bioinformatics, 90, 1749-1765.

HOWARTH, P. H., STERN, M. A., ROI, L., REYNOLDS, R. & BOUSQUET, J. 1999. Double-blind, placebo-controlled study comparing the efficacy and safety of fexofenadine hydrochloride (120 and 180 mg once daily) and cetirizine in seasonal allergic rhinitis. Journal of Allergy and Clinical Immunology, 104, 927-933.

HUANG, Y., XUE, C., WANG, L., BU, R., MU, J., WANG, Y. & LIU, Z. 2023. Structural basis for substrate and inhibitor recognition of human multidrug transporter MRP4. Communications Biology, 6, 549.

ILGü, H., JECKELMANN, J.-M., GACHET, MARíA S., BOGGAVARAPU, R., UCURUM, Z., GERTSCH, J. & FOTIADIS, D. 2014. Variation of the Detergent-Binding Capacity and Phospholipid Content of Membrane Proteins When Purified in Different Detergents. Biophysical Journal, 106, 1660-1670.

IMMADISETTY, K., HETTIGE, J. & MORADI, M. 2019. Lipid-Dependent Alternating Access Mechanism of a Bacterial Multidrug ABC Exporter. ACS Central Science, 5, 43-56.

INFED, N., HANEKOP, N., DRIESSEN, A. J. M., SMITS, S. H. J. & SCHMITT, L. 2011. Influence of detergents on the activity of the ABC transporter LmrA. *Biochimica et Biophysica Acta (BBA) - Biomembranes,* 1808**,** 2313-2321.

JOOST, H.-G., BELL, G. I., BEST, J. D., BIRNBAUM, M. J., CHARRON, M. J., CHEN, Y. T., DOEGE, H., JAMES, D. E., LODISH, H. F., MOLEY, K. H., MOLEY, J. F., MUECKLER, M., ROGERS, S., SCHüRMANN, A., SEINO, S. & THORENS, B. 2002. Nomenclature of the GLUT/SLC2A family of sugar/polyol transport facilitators. *American Journal of Physiology-Endocrinology and Metabolism,* 282**,** E974-E976.

KAPSE, A., ANUP, N., PATEL, V., SARAOGI, G. K., MISHRA, D. K. & TEKADE, R. K. 2020. Chapter 6 - Polymeric micelles: a ray of hope among new drug delivery systems. *In:* TEKADE, R. K. (ed.) *Drug Delivery Systems.* Academic Press.

KELLEY, E., PHELPS, P., AKRE, M., WALLA, D., ROSS, J., SIMMONS, J., BULOK, E., AYRES, A. & SNYDER, E. 2019. The Influence of β1-Adrenergic Receptor Genotype of Renal Sodium Handling and Blood Pressure Response to Angiotensin Receptor Blockers in Hypertension Patients. *The FASEB Journal,* 33**,** 819.5-819.5.

KIM, Y. & CHEN, J. 2018. Molecular structure of human P-glycoprotein in the ATP-bound, outward-facing conformation. *Science,* 359**,** 915-919.

KISKER, C., SCHINDELIN, H. & REES, D. C. 1997. Molybdenum-cofactor-containing enzymes: structure and mechanism. *Annu Rev Biochem,* 66**,** 233-67.

KLUMPERMAN, B. 2010. Mechanistic considerations on styrene–maleic anhydride copolymerization reactions. *Polymer Chemistry,* 1**,** 558-562.

KNOWLES, T. J., FINKA, R., SMITH, C., LIN, Y.-P., DAFFORN, T. & OVERDUIN, M. 2009. Membrane Proteins Solubilized Intact in Lipid Containing Nanoparticles Bounded by Styrene Maleic Acid Copolymer. *Journal of the American Chemical Society,* 131**,** 7484-7485.

KOBAYASHI, N., NISHINO, K. & YAMAGUCHI, A. 2001. Novel Macrolide-Specific ABC-Type Efflux Transporter inEscherichia coli. *Journal of Bacteriology,* 183**,** 5639-5644.

KOK, D. E., STEEGENGA, W. T., SMID, E. J., ZOETENDAL, E. G., ULRICH, C. M. & KAMPMAN, E. 2020. Bacterial folate biosynthesis and colorectal cancer risk: more than just a gut feeling. *Critical Reviews in Food Science and Nutrition,* 60**,** 244-256.

KORONAKIS, V., ESWARAN, J. & HUGHES, C. 2004. Structure and function of TolC: the bacterial exit duct for proteins and drugs. *Annu Rev Biochem,* 73**,** 467-89.

KOTOV, V., BARTELS, K., VEITH, K., JOSTS, I., SUBHRAMANYAM, U. K. T., GüNTHER, C., LABAHN, J., MARLOVITS, T. C., MORAES, I., TIDOW, H., LöW, C. & GARCIA-ALAI, M. M. 2019. High-throughput stability screening for detergent-solubilized membrane proteins. *Scientific Reports,* 9**,** 10379.

KROGH, A., LARSSON, B., VON HEIJNE, G. & SONNHAMMER, E. L. L. 2001. Predicting transmembrane protein topology with a hidden markov model: application to complete genomes11Edited by F. Cohen. *Journal of Molecular Biology,* 305**,** 567-580.

KROLL, P., BENKE, J., ENDERS, S., BRANDENBUSCH, C. & SADOWSKI, G. 2022. Influence of Temperature and Concentration on the Self-Assembly of Nonionic C(i)E(j) Surfactants: A Light Scattering Study. *ACS Omega,* 7**,** 7057-7065.

KRüGEL, H., LICHT, A., BIEDERMANN, G., PETZOLD, A., LASSAK, J., HUPFER, Y., SCHLOTT, B., HERTWECK, C., PLATZER, M., BRANTL, S. & SALUZ, H. P. 2010. Cervimycin C resistance in Bacillus subtilis is due to a promoter up-mutation and increased mRNA stability of the constitutive ABC-transporter gene bmrA. *FEMS Microbiol Lett,* 313**,** 155-63.

KüHLBRANDT, W. 2015. Structure and function of mitochondrial membrane protein complexes. *BMC Biology,* 13**,** 89.

KUNST, F., OGASAWARA, N., MOSZER, I., ALBERTINI, A. M., ALLONI, G., AZEVEDO, V., BERTERO, M. G., BESSIèRES, P., BOLOTIN, A., BORCHERT, S., BORRISS, R., BOURSIER, L., BRANS, A., BRAUN, M., BRIGNELL, S. C., BRON, S., BROUILLET, S., BRUSCHI, C. V., CALDWELL, B., CAPUANO, V., CARTER, N. M., CHOI, S. K., CODANI, J. J., CONNERTON, I. F., CUMMINGS, N. J., DANIEL, R. A., DENIZOT, F., DEVINE, K. M., DüSTERHöFT, A., EHRLICH, S. D., EMMERSON, P. T., ENTIAN, K. D., ERRINGTON, J., FABRET, C., FERRARI, E., FOULGER, D., FRITZ, C., FUJITA, M., FUJITA, Y., FUMA, S., GALIZZI, A., GALLERON, N., GHIM, S. Y., GLASER, P., GOFFEAU, A., GOLIGHTLY, E. J., GRANDI, G., GUISEPPI, G., GUY, B. J., HAGA, K., HAIECH, J., HARWOOD, C. R., HéNAUT, A., HILBERT, H., HOLSAPPEL, S., HOSONO, S., HULLO, M. F., ITAYA, M., JONES, L., JORIS, B., KARAMATA, D., KASAHARA, Y., KLAERR-BLANCHARD, M., KLEIN, C., KOBAYASHI, Y., KOETTER, P., KONINGSTEIN, G., KROGH, S., KUMANO,

M., KURITA, K., LAPIDUS, A., LARDINOIS, S., LAUBER, J., LAZAREVIC, V., LEE, S. M., LEVINE, A., LIU, H., MASUDA, S., MAUëL, C., MéDIGUE, C., MEDINA, N., MELLADO, R. P., MIZUNO, M., MOESTL, D., NAKAI, S., NOBACK, M., NOONE, D., O'REILLY, M., OGAWA, K., OGIWARA, A., OUDEGA, B., PARK, S. H., PARRO, V., POHL, T. M., PORTETELLE, D., PORWOLLIK, S., PRESCOTT, A. M., PRESECAN, E., PUJIC, P., PURNELLE, B., et al. 1997. The complete genome sequence of the Gram-positive bacterium Bacillus subtilis. *Nature,* 390**,** 249-256.

LACROIX-PéPIN, N., DANYOD, G., KRISHNASWAMY, N., MONDAL, S., RONG, P.-M., CHAPDELAINE, P. & FORTIER, M. A. 2011. The Multidrug Resistance-Associated Protein 4 (MRP4) Appears as a Functional Carrier of Prostaglandins Regulated by Oxytocin in the Bovine Endometrium. *Endocrinology,* 152**,** 4993-5004.

LAGANOWSKY, A., READING, E., ALLISON, T. M., ULMSCHNEIDER, M. B., DEGIACOMI, M. T., BALDWIN, A. J. & ROBINSON, C. V. 2014. Membrane proteins bind lipids selectively to modulate their structure and function. *Nature,* 510**,** 172-175.

LEE, H. J., LEE, H. S., YOUN, T., BYRNE, B. & CHAE, P. S. 2022. Impact of novel detergents on membrane protein studies. *Chem,* 8**,** 980-1013.

LEE, K., KLEIN-SZANTO, A. J. P. & KRUH, G. D. 2000. Analysis of the MRP4 Drug Resistance Profile in Transfected NIH3T3 Cells. *JNCI: Journal of the National Cancer Institute,* 92**,** 1934-1940.

LEITZ, A. J., BAYBURT, T. H., BARNAKOV, A. N., SPRINGER, B. A. & SLIGAR, S. G. 2006. Functional reconstitution of Beta2-adrenergic receptors utilizing self-assembling Nanodisc technology. *Biotechniques,* 40**,** 601-2, 604, 606, passim.

LEWINSON, O., LEE, A. T., LOCHER, K. P. & REES, D. C. 2010. A distinct mechanism for the ABC transporter BtuCD-BtuF revealed by the dynamics of complex formation. *Nat Struct Mol Biol,* 17**,** 332-8.

LEWINSON, O., ORELLE, C. & SEEGER, M. A. 2020. Structures of ABC transporters: handle with care. *FEBS Letters,* 594**,** 3799-3814.

LI, T. T., AN, J. X., XU, J. Y. & TUO, B. G. 2019. Overview of organic anion transporters and organic anion transporter polypeptides and their roles in the liver. *World J Clin Cases,* 7**,** 3915-3933.

LI, Y., PUSTOVALOVA, Y., DOUKOV, T. I., HOCH, J. C., MAINS, R. E., EIPPER, B. A. & HAO, B. 2023. Structure of the Sec14 domain of Kalirin reveals a distinct class of lipid-binding module in RhoGEFs. *Nature Communications,* 14**,** 96.

LINDHOUD, S., CARVALHO, V., PRONK, J. W. & AUBIN-TAM, M.-E. 2016. SMA-SH: Modified Styrene–Maleic Acid Copolymer for Functionalization of Lipid Nanodiscs. *Biomacromolecules,* 17**,** 1516-1522.

LINKE, D. 2009. Chapter 34 Detergents: An Overview. *In:* BURGESS, R. R. & DEUTSCHER, M. P. (eds.) *Methods in Enzymology.* Academic Press.

LIOU, T. G. 2019. The Clinical Biology of Cystic Fibrosis Transmembrane Regulator Protein: Its Role and Function in Extrapulmonary Disease. *Chest,* 155**,** 605-616.

LOCHER, K. P. 2016. Mechanistic diversity in ATP-binding cassette (ABC) transporters. *Nature Structural & Molecular Biology,* 23**,** 487-493.

LU, S. & ZGURSKAYA, H. I. 2013. MacA, a periplasmic membrane fusion protein of the macrolide transporter MacAB-TolC, binds lipopolysaccharide core specifically and with high affinity. *J Bacteriol,* 195**,** 4865-72.

LYCZAK, J. B., CANNON, C. L. & PIER, G. B. 2002. Lung infections associated with cystic fibrosis. *Clin Microbiol Rev,* 15**,** 194-222.

MAIER, R., CUEVAS ARENAS, R., ZHANG, F., GARCíA-SáEZ, A. & SCHREIBER, F. 2023. Structural Insights into Polymer-Bounded Lipid Nanodiscs. *Langmuir,* 39**,** 2450-2459.

MAîTRE, J.-L., BERTHOUMIEUX, H., KRENS, S. F. G., SALBREUX, G., JüLICHER, F., PALUCH, E. & HEISENBERG, C.-P. 2012. Adhesion Functions in Cell Sorting by Mechanically Coupling the Cortices of Adhering Cells. *Science,* 338**,** 253-256.

MASCARENHAS, N. M. & GOSAVI, S. 2017. Understanding protein domain-swapping using structure-based models of protein folding. *Prog Biophys Mol Biol,* 128**,** 113-120.

MASUDA, S., TERADA, T., YONEZAWA, A., TANIHARA, Y., KISHIMOTO, K., KATSURA, T., OGAWA, O. & INUI, K.-I. 2006. Identification and Functional Characterization of a New Human Kidney–Specific H+/Organic Cation Antiporter, Kidney-Specific Multidrug and Toxin Extrusion 2. *Journal of the American Society of Nephrology,* 17.

MATTEVI, A. 2006. A Monotopic Membrane Protein Goes Solo. *Structure,* 14**,** 628-629.

MCKENZIE, B. J., WECHALEKAR, M. D., JOHNSTON, R. V., SCHLESINGER, N. & BUCHBINDER, R. 2021. Colchicine for acute gout. *Cochrane Database Syst Rev,* 8**,** Cd006190.

MOLINA-BOLíVAR, J. A. & RUIZ, C. C. 2012. Micellar size and phase behavior in n-octyl-β-d-thioglucoside/Triton X-100 mixtures: The effect of NaCl addition. *Fluid Phase Equilibria,* 327**,** 58-64.

MOLINA-BOLíVAR, J. A., HIERREZUELO, J. M. & CARNERO RUIZ, C. 2013. Energetics of clouding and size effects in non-ionic surfactant mixtures: The influence of alkyl chain length and NaCl addition. *The Journal of Chemical Thermodynamics,* 57**,** 59-66.

MOOSMANN, B. & BEHL, C. 2000. Cytoprotective antioxidant function of tyrosine and tryptophan residues in transmembrane proteins. *Eur J Biochem,* 267**,** 5687-92.

MORRISON, K. A., AKRAM, A., MATHEWS, A., KHAN, Z. A., PATEL, J. H., ZHOU, C., HARDY, D. J., MOORE-KELLY, C., PATEL, R., ODIBA, V., KNOWLES, T. J., JAVED, M.-U.-H., CHMEL, N. P., DAFFORN, T. R. & ROTHNIE, A. J. 2016. Membrane protein extraction and purification using styrene–maleic acid (SMA) copolymer: effect of variations in polymer structure. *Biochemical Journal,* 473**,** 4349-4360.

MORRISON, K. A., HEESOM, K. J., EDLER, K. J., DOUTCH, J., PRICE, G. J., KOUMANOV, F. & WHITLEY, P. 2021. Development of Methodology to Investigate the Surface SMALPome of Mammalian Cells. *Frontiers in Molecular Biosciences,* 8.

NAGAMORI, S., SMIRNOVA, I. N. & KABACK, H. R. 2004. Role of YidC in folding of polytopic membrane proteins. *J Cell Biol,* 165**,** 53-62.

NAGY, J. K., KUHN HOFFMANN, A., KEYES, M. H., GRAY, D. N., OXENOID, K. & SANDERS, C. R. 2001. Use of amphipathic polymers to deliver a membrane protein to lipid bilayers. *FEBS Lett,* 501**,** 115-20.

NAM, H. J., HAN, S. K., BOWIE, J. U. & KIM, S. 2013. Rampant exchange of the structure and function of extramembrane domains between membrane and water soluble proteins. *PLoS Comput Biol,* 9**,** e1002997.

NAOUS, M., MOLINA-BOLíVAR, J. A. & RUIZ, C. C. 2014. Micelle size modulation and phase behavior in MEGA-10/Triton X-100 mixtures. *Thermochimica Acta,* 598**,** 68-76.

NATH, A., ATKINS, W. M. & SLIGAR, S. G. 2007. Applications of Phospholipid Bilayer Nanodiscs in the Study of Membranes and Membrane Proteins. *Biochemistry,* 46**,** 2059-2069.

NELSON, C. M. & CHEN, C. S. 2003. VE-cadherin simultaneously stimulates and inhibits cell proliferation by altering cytoskeletal structure and tension. *Journal of Cell Science,* 116**,** 3571-3581.

NOWAKOWSKI, A. B., WOBIG, W. J. & PETERING, D. H. 2014. Native SDS-PAGE: high resolution electrophoretic separation of proteins with retention of native properties including bound metal ions. *Metallomics,* 6**,** 1068-78.

OEPEN, K., MATER, V. & SCHNEIDER, D. 2023. Unfolding Individual Domains of BmrA, a Bacterial ABC Transporter Involved in Multidrug Resistance. *Int J Mol Sci,* 24.

OEPEN, K., ÖZBEK, H., SCHüFFLER, A., LIERMANN, J. C., THINES, E. & SCHNEIDER, D. 2021. Myristic Acid Inhibits the Activity of the Bacterial ABC Transporter BmrA. *Int J Mol Sci,* 22.

OKADA, U., YAMASHITA, E., NEUBERGER, A., MORIMOTO, M., VAN VEEN, H. W. & MURAKAMI, S. 2017. Crystal structure of tripartite-type ABC transporter MacB from Acinetobacter baumannii. *Nature Communications,* 8**,** 1336.

OLERINYOVA, A., SONN-SEGEV, A., GAULT, J., EICHMANN, C., SCHIMPF, J., KOPF, A. H., RUDDEN, L. S. P., ASHKINADZE, D., BOMBA, R., FREY, L., GREENWALD, J., DEGIACOMI, M. T., STEINHILPER, R., KILLIAN, J. A., FRIEDRICH, T., RIEK, R., STRUWE, W. B. & KUKURA, P. 2021. Mass Photometry of Membrane Proteins. *Chem,* 7**,** 224-236.

OLUWOLE, A. O., DANIELCZAK, B., MEISTER, A., BABALOLA, J. O., VARGAS, C. & KELLER, S. 2017. Solubilization of Membrane Proteins into Functional Lipid-Bilayer Nanodiscs Using a Diisobutylene/Maleic Acid Copolymer. *Angew Chem Int Ed Engl,* 56**,** 1919-1924.

OTSUKA, M., MATSUMOTO, T., MORIMOTO, R., ARIOKA, S., OMOTE, H. & MORIYAMA, Y. 2005. A human transporter protein that mediates the final excretion step for toxic organic cations. *Proc Natl Acad Sci U S A,* 102**,** 17923-8.

PARIKH, R. R., PATEL, K. R., PERGOLIZZI, J. V., JR., BREVE, F. & MAGNUSSON, P. 2022. Effects of Digoxin in Heart Failure (HF) With Reduced Ejection Fraction (EF). *Cureus,* 14**,** e22778.

PAUTIER, P., ITALIANO, A., PIPERNO-NEUMANN, S., CHEVREAU, C., PENEL, N., FIRMIN, N., BOUDOU-ROUQUETTE, P., BERTUCCI, F., BALLEYGUIER, C., LEBRUN-LY, V., RAY-COQUARD, I., KALBACHER, E., BARDET, A., BOMPAS, E., COLLARD, O., ISAMBERT, N., GUILLEMET, C., RIOS, M., ARCHAMBAUD, B., DUFFAUD, F., ITALIANO, A., PAUTIER, P., LECESNE, A., PIPERNO-NEUMANN, S., CHEVREAU, C., CUPISSOL, D., PENEL, N., ALEXANDRE, J., BERTUCCI, F., RAY-COQUARD, I., LEBRUN-LY, V., KALBACHER, E., DUFFAUD, F., DELCAMBRE, C., BOMPAS, E., COLLARD, O., ISAMBERT, N., GUILLEMET, C., SOULIE, P., RIOS, M. & SAADA-BOUZID, E. 2022. Doxorubicin alone versus doxorubicin

with trabectedin followed by trabectedin alone as first-line therapy for metastatic or unresectable leiomyosarcoma (LMS-04): a randomised, multicentre, open-label phase 3 trial. *The Lancet Oncology,* 23**,** 1044-1054.

PERNIN, V., GLYDA, M., VIKLICKý, O., LõHMUS, A., WENNBERG, L., WITZKE, O., VON ZUR-MüHLEN, B., ANAOKAR, S., HURST, M., KAZEEM, G., UNDRE, N. & KUYPERS, D. R. J. 2023. Long-term Prolonged-release Tacrolimus-based Immunosuppression in De Novo Kidney Transplant Recipients: 5-Y Prospective Follow-up of Patients in the ADVANCE Study. *Transplant Direct,* 9**,** e1432.

PICCICA, M., LAGI, F., BARTOLONI, A. & ZAMMARCHI, L. 2021. Efficacy and safety of pentamidine isethionate for tegumentary and visceral human leishmaniasis: a systematic review. *J Travel Med,* 28.

POLLOCK, N. L., LEE, S. C., PATEL, J. H., GULAMHUSSEIN, A. A. & ROTHNIE, A. J. 2018. Structure and function of membrane proteins encapsulated in a polymer-bound lipid bilayer. *Biochim Biophys Acta Biomembr,* 1860**,** 809-817.

POPOT, J. L., BERRY, E. A., CHARVOLIN, D., CREUZENET, C., EBEL, C., ENGELMAN, D. M., FLöTENMEYER, M., GIUSTI, F., GOHON, Y., HONG, Q., LAKEY, J. H., LEONARD, K., SHUMAN, H. A., TIMMINS, P., WARSCHAWSKI, D. E., ZITO, F., ZOONENS, M., PUCCI, B. & TRIBET, C. 2003. Amphipols: polymeric surfactants for membrane biology research. *Cell Mol Life Sci,* 60**,** 1559-74.

POPOT, J.-L. 2010. Amphipols, Nanodiscs, and Fluorinated Surfactants: Three Nonconventional Approaches to Studying Membrane Proteins in Aqueous Solutions. *Annual Review of Biochemistry,* 79**,** 737-775.

POURMAL, S., GREEN, E., BAJAJ, R., CHEMMAMA, I. E., KNUDSEN, G. M., GUPTA, M., SALI, A., CHENG, Y., CRAIK, C. S., KROETZ, D. L. & STROUD, R. M. 2024. Structural basis of prostaglandin efflux by MRP4. *Nature Structural & Molecular Biology,* 31**,** 621-632.

POWL, A. M., EAST, J. M. & LEE, A. G. 2008. Anionic phospholipids affect the rate and extent of flux through the mechanosensitive channel of large conductance MscL. *Biochemistry,* 47**,** 4317-4328.

PRAGALLAPATI, S. & MANYAM, R. 2019. Glucose transporter 1 in health and disease. *J Oral Maxillofac Pathol,* 23**,** 443-449.

QUAZI, F., LENEVICH, S. & MOLDAY, R. S. 2012. ABCA4 is an N-retinylidene-phosphatidylethanolamine and phosphatidylethanolamine importer. *Nature Communications,* 3**,** 925.

QUIOCHO, F. A. & LEDVINA, P. S. 1996. Atomic structure and specificity of bacterial periplasmic receptors for active transport and chemotaxis: variation of common themes. *Molecular Microbiology,* 20**,** 17-25.

RAVAUD, S., DO CAO, M. A., JIDENKO, M., EBEL, C., LE MAIRE, M., JAULT, J. M., DI PIETRO, A., HASER, R. & AGHAJARI, N. 2006. The ABC transporter BmrA from Bacillus subtilis is a functional dimer when in a detergent-solubilized state. *Biochem J,* 395**,** 345-53.

RAVULA, T., HARDIN, N. Z., RAMADUGU, S. K. & RAMAMOORTHY, A. 2017. pH Tunable and Divalent Metal Ion Tolerant Polymer Lipid Nanodiscs. *Langmuir,* 33**,** 10655-10662.

RAVULA, T., HARDIN, N. Z., RAMADUGU, S. K., COX, S. J. & RAMAMOORTHY, A. 2018. Formation of pH-Resistant Monodispersed Polymer-Lipid Nanodiscs. *Angew Chem Int Ed Engl,* 57**,** 1342-1345.

RAVULA, T., RAMADUGU, S. K., DI MAURO, G. & RAMAMOORTHY, A. 2017. Bioinspired, Size-Tunable Self-Assembly of Polymer-Lipid Bilayer Nanodiscs. *Angew Chem Int Ed Engl,* 56**,** 11466-11470.

REAL HERNANDEZ, L. M. & LEVENTAL, I. 2023. Lipid packing is disrupted in copolymeric nanodiscs compared with intact membranes. *Biophysical Journal,* 122**,** 2256-2266.

REHAN, S., PAAVILAINEN, V. O. & JAAKOLA, V.-P. 2017. Functional reconstitution of human equilibrative nucleoside transporter-1 into styrene maleic acid co-polymer lipid particles. *Biochimica et Biophysica Acta (BBA) - Biomembranes,* 1859**,** 1059-1065.

REID, G., WIELINGA, P., ZELCER, N., VAN DER HEIJDEN, I., KUIL, A., DE HAAS, M., WIJNHOLDS, J. & BORST, P. 2003. The human multidrug resistance protein MRP4 functions as a prostaglandin efflux transporter and is inhibited by nonsteroidal antiinflammatory drugs. *Proceedings of the National Academy of Sciences,* 100**,** 9244-9249.

RICE, A. J., PARK, A. & PINKETT, H. W. 2014. Diversity in ABC transporters: type I, II and III importers. *Crit Rev Biochem Mol Biol,* 49**,** 426-37.

RITCHIE, T. K., GRINKOVA, Y. V., BAYBURT, T. H., DENISOV, I. G., ZOLNERCIKS, J. K., ATKINS, W. M. & SLIGAR, S. G. 2009. Chapter 11 - Reconstitution of membrane proteins in phospholipid bilayer nanodiscs. *Methods Enzymol,* 464**,** 211-31.

RITTER, C. A., JEDLITSCHKY, G., MEYER ZU SCHWABEDISSEN, H., GRUBE, M., KöCK, K. & KROEMER, H. K. 2005. Cellular export of drugs and signaling molecules by the ATP-binding cassette transporters MRP4 (ABCC4) and MRP5 (ABCC5). *Drug Metab Rev,* 37**,** 253-78.

SARPAL, R., PELLIKKA, M., PATEL, R. R., HUI, F. Y. W., GODT, D. & TEPASS, U. 2012. Mutational analysis supports a core role for Drosophila α-Catenin in adherens junction function. *Journal of Cell Science,* 125**,** 233-245.

SCHEIDELAAR, S., KOORENGEVEL, M. C., VAN WALREE, C. A., DOMINGUEZ, J. J., DöRR, J. M. & KILLIAN, J. A. 2016. Effect of Polymer Composition and pH on Membrane Solubilization by Styrene-Maleic Acid Copolymers. *Biophys J,* 111**,** 1974-1986.

SCHULER, M. A., DENISOV, I. G. & SLIGAR, S. G. 2013. Nanodiscs as a new tool to examine lipid-protein interactions. *Methods Mol Biol,* 974**,** 415-33.

SCHULTE, R. R. & HO, R. H. 2019. Organic Anion Transporting Polypeptides: Emerging Roles in Cancer Pharmacology. *Mol Pharmacol,* 95**,** 490-506.

SEDDON, A. M., CURNOW, P. & BOOTH, P. J. 2004. Membrane proteins, lipids and detergents: not just a soap opera. *Biochimica et Biophysica Acta (BBA) - Biomembranes,* 1666**,** 105-117.

SEJWAL, K., CHAMI, M., BAUMGARTNER, P., KOWAL, J., MüLLER, S. A. & STAHLBERG, H. 2017. Proteoliposomes – a system to study membrane proteins under buffer gradients by cryo-EM. *Nanotechnology Reviews,* 6**,** 57-74.

SHIMIZU, K., CAO, W., SAAD, G., SHOJI, M. & TERADA, T. 2018. Comparative analysis of membrane protein structure databases. *Biochimica et Biophysica Acta (BBA) - Biomembranes,* 1860**,** 1077-1091.

SMITH, A. A. A., AUTZEN, H. E., FAUST, B., MANN, J. L., MUIR, B. W., HOWARD, S., POSTMA, A., SPAKOWITZ, A. J., CHENG, Y. & APPEL, E. A. 2020. Lipid Nanodiscs via Ordered Copolymers. *Chem,* 6**,** 2782-2795.

STEIGENBERGER, J., MERGEN, C., DE ROO, V., GEUDENS, N., MARTINS, J. C. & HEERKLOTZ, H. 2022. The effect of membrane thickness on the membrane permeabilizing activity of the cyclic lipopeptide tolaasin II. *Front Mol Biosci,* 9**,** 1064742.

STEINFELS, E., ORELLE, C., DALMAS, O., PENIN, F., MIROUX, B., DI PIETRO, A. & JAULT, J.-M. 2002. Highly efficient over-production in E. coli of YvcC, a multidrug-like ATP-binding cassette transporter from Bacillus subtilis. *Biochimica et Biophysica Acta (BBA) - Biomembranes,* 1565**,** 1-5.

STEINFELS, E., ORELLE, C., FANTINO, J.-R., DALMAS, O., RIGAUD, J.-L., DENIZOT, F., DI PIETRO, A. & JAULT, J.-M. 2004. Characterization of YvcC (BmrA), a Multidrug ABC Transporter Constitutively Expressed in Bacillus subtilis. *Biochemistry,* 43**,** 7491-7502.

STETSENKO, A. & GUSKOV, A. 2017. An Overview of the Top Ten Detergents Used for Membrane Protein Crystallization. *Crystals,* 7**,** 197.

SULTANA, S., BRUNS, S., WILKES, H., SIMON, M. & WIENHAUSEN, G. 2023. Vitamin B12 is not shared by all marine prototrophic bacteria with their environment. *The ISME Journal,* 17**,** 836-845.

SUN, X., ZHOU, M., WEN, G., HUANG, Y., WU, J., PENG, L., JIANG, W., YUAN, H., LU, Y. & CAI, J. 2021. Paroxetine Attenuates Cardiac Hypertrophy Via Blocking GRK2 and ADRB1 Interaction in Hypertension. *J Am Heart Assoc,* 10**,** e016364.

SWAINSBURY, D. J. K., SCHEIDELAAR, S., FOSTER, N., VAN GRONDELLE, R., KILLIAN, J. A. & JONES, M. R. 2017. The effectiveness of styrene-maleic acid (SMA) copolymers for solubilisation of integral membrane proteins from SMA-accessible and SMA-resistant membranes. *Biochim Biophys Acta Biomembr,* 1859**,** 2133-2143.

SYCH, T., LEVENTAL, K. R. & SEZGIN, E. 2022. Lipid-Protein Interactions in Plasma Membrane Organization and Function. *Annu Rev Biophys,* 51**,** 135-156.

TADROS, T. 2013. Critical Micelle Concentration. *In:* TADROS, T. (ed.) *Encyclopedia of Colloid and Interface Science.* Berlin, Heidelberg: Springer Berlin Heidelberg.

TARLING, E. J., DE AGUIAR VALLIM, T. Q. & EDWARDS, P. A. 2013. Role of ABC transporters in lipid transport and human disease. *Trends Endocrinol Metab,* 24**,** 342-50.

TEO, A. C. K., LEE, S. C., POLLOCK, N. L., STROUD, Z., HALL, S., THAKKER, A., PITT, A. R., DAFFORN, T. R., SPICKETT, C. M. & ROPER, D. I. 2019. Analysis of SMALP co-extracted phospholipids shows distinct membrane environments for three classes of bacterial membrane protein. *Scientific Reports,* 9**,** 1813.

THOMAS, C. & TAMPé, R. 2020. Structural and Mechanistic Principles of ABC Transporters. *Annu Rev Biochem,* 89**,** 605-636.

THOMAS, C., ALLER, S. G., BEIS, K., CARPENTER, E. P., CHANG, G., CHEN, L., DASSA, E., DEAN, M., DUONG VAN HOA, F., EKIERT, D., FORD, R., GAUDET, R., GONG, X., HOLLAND, I. B., HUANG, Y., KAHNE, D. K., KATO, H., KORONAKIS, V., KOTH, C. M., LEE, Y., LEWINSON, O., LILL, R., MARTINOIA,

E., MURAKAMI, S., PINKETT, H. W., POOLMAN, B., ROSENBAUM, D., SARKADI, B., SCHMITT, L., SCHNEIDER, E., SHI, Y., SHYNG, S.-L., SLOTBOOM, D. J., TAJKHORSHID, E., TIELEMAN, D. P., UEDA, K., VáRADI, A., WEN, P.-C., YAN, N., ZHANG, P., ZHENG, H., ZIMMER, J. & TAMPé, R. 2020. Structural and functional diversity calls for a new classification of ABC transporters. *FEBS Letters,* 594**,** 3767-3775.

TIMCENKO, M., AUTZEN, A. A. A. & AUTZEN, H. E. 2022. Characterization of divalent cation interactions with AASTY native nanodiscs. *bioRxiv***,** 2021.10.07.463511.

TONIOLO, M., MUSER, D., GRILLI, G., BURELLI, M., REBELLATO, L., DALEFFE, E., FACCHIN, D. & IMAZIO, M. 2021. Oral procainamide as pharmacological treatment of recurrent and refractory ventricular tachyarrhythmias: A single-center experience. *Heart Rhythm O2,* 2**,** 840-847.

TRIBET, C., AUDEBERT, R. & POPOT, J. L. 1996. Amphipols: polymers that keep membrane proteins soluble in aqueous solutions. *Proc Natl Acad Sci U S A,* 93**,** 15047-50.

TRIBET, C., AUDEBERT, R. & POPOT, J. L. 1997. Stabilization of Hydrophobic Colloidal Dispersions in Water with Amphiphilic Polymers: Application to Integral Membrane Proteins. *Langmuir,* 13**,** 5570-5576.

VAN VEEN, H. W., CALLAGHAN, R., SOCENEANTU, L., SARDINI, A., KONINGS, W. N. & HIGGINS, C. F. 1998. A bacterial antibiotic-resistance gene that complements the human multidrug-resistance P-glycoprotein gene. *Nature,* 391**,** 291-5.

VAN VEEN, H. W., VENEMA, K., BOLHUIS, H., OUSSENKO, I., KOK, J., POOLMAN, B., DRIESSEN, A. J. & KONINGS, W. N. 1996. Multidrug resistance mediated by a bacterial homolog of the human multidrug transporter MDR1. *Proceedings of the National Academy of Sciences,* 93**,** 10668-10672.

VELAMAKANNI, S., YAO, Y., GUTMANN, D. A. & VAN VEEN, H. W. 2008. Multidrug transport by the ABC transporter Sav1866 from Staphylococcus aureus. *Biochemistry,* 47**,** 9300-8.

VITRAC, H., MACLEAN, D. M., JAYARAMAN, V., BOGDANOV, M. & DOWHAN, W. 2015. Dynamic membrane protein topological switching upon changes in phospholipid environment. *Proceedings of the National Academy of Sciences,* 112**,** 13874-13879.

VOGELGESANG, S. 2004. The role of P-glycoprotein in cerebral amyloid angiopathy; implications for the early pathogenesis of Alzheimer's disease. *Alzheimer Res,* 1**,** 121-125.

VOSKOBOYNIKOVA, N., MARGHERITIS, E. G., KODDE, F., RADEMACHER, M., SCHOWE, M., BUDKE-GIESEKING, A., PSATHAKI, O.-E., STEINHOFF, H.-J. & COSENTINO, K. 2021. Evaluation of DIBMA nanoparticles of variable size and anionic lipid content as tools for the structural and functional study of membrane proteins. *Biochimica et Biophysica Acta (BBA) - Biomembranes,* 1863**,** 183588.

WAETERSCHOOT, J., BARNIOL-XICOTA, M., VERHELST, S., BAATSEN, P., KOOS, E., LAMMERTYN, J. & CASADEVALL I SOLVAS, X. 2024. Lipid vesicle formation by encapsulation of SMALPs in surfactant-stabilised droplets. *Heliyon,* 10.

WARD, A. B., SZEWCZYK, P., GRIMARD, V., LEE, C. W., MARTINEZ, L., DOSHI, R., CAYA, A., VILLALUZ, M., PARDON, E., CREGGER, C., SWARTZ, D. J., FALSON, P. G., URBATSCH, I. L., GOVAERTS, C., STEYAERT, J. & CHANG, G. 2013. Structures of P-glycoprotein reveal its conformational flexibility and an epitope on the nucleotide-binding domain. *Proc Natl Acad Sci U S A,* 110**,** 13386-91.

WEBER, J. N., MINNER-MEINEN, R. & KAUFHOLDT, D. 2023. The Mechanisms of Molybdate Distribution and Homeostasis with Special Focus on the Model Plant Arabidopsis thaliana. *Molecules,* 29.

WOLF, B. A. 1985. Solubility of polymers. *Pure and Applied Chemistry,* 57**,** 323-336.

XU, K., ZHANG, M., ZHAO, Q., YU, F., GUO, H., WANG, C., HE, F., DING, J. & ZHANG, P. 2013. Crystal structure of a folate energy-coupling factor transporter from Lactobacillus brevis. *Nature,* 497**,** 268-271.

XUE, M., CHENG, L., FAUSTINO, I., GUO, W. & MARRINK, S. J. 2018. Molecular Mechanism of Lipid Nanodisk Formation by Styrene-Maleic Acid Copolymers. *Biophys J,* 115**,** 494-502.

YANG, N. J. & HINNER, M. J. 2015. Getting across the cell membrane: an overview for small molecules, peptides, and proteins. *Methods Mol Biol,* 1266**,** 29-53.

ZAHER, A., ELSAYGH, J., ELSORI, D., ELSAYGH, H. & SANNI, A. 2021. A Review of Trikafta: Triple Cystic Fibrosis Transmembrane Conductance Regulator (CFTR) Modulator Therapy. *Cureus,* 13**,** e16144.

ZHANG, H., HUANG, C.-S., YU, X., LEE, J., VAISH, A., CHEN, Q., ZHOU, M., WANG, Z. & MIN, X. 2021. Cryo-EM structure of ABCG5/G8 in complex with modulating antibodies. *Communications Biology,* 4**,** 526.

ZHENG, J. X., LIN, Z. W., SUN, X., LIN, W. H., CHEN, Z., WU, Y., QI, G. B., DENG, Q. W., QU, D. & YU, Z. J. 2018. Overexpression of OqxAB and MacAB efflux pumps contributes to eravacycline resistance and heteroresistance in clinical isolates of Klebsiella pneumoniae. *Emerg Microbes Infect,* 7**,** 139.

ZHOU, S., LV, P., LI, M., CHEN, Z., XIN, H., REILLY, S. & ZHANG, X. 2023. SARS-CoV-2 E protein: Pathogenesis and potential therapeutic development. *Biomed Pharmacother,* 159**,** 114242.

ZOONENS, M. & POPOT, J. L. 2014. Amphipols for each season. *J Membr Biol,* 247**,** 759-96.